Øyvind Borg

Role of Alumina Support in Cobalt Fischer-Tropsch Synthesis

Thesis for the degree of doktor ingeniør

Trondheim, April 2007

Norwegian University of
Science and Technology
Faculty of Natural Sciences and Technology
Department of Chemical Engineering

NTNU
Innovation and Creativity

NTNU
Norwegian University of Science and Technology

Thesis for the degree of doktor ingeniør

Faculty of Natural Sciences and Technology
Department of Chemical Engineering

ISBN 978-82-471-1237-3 (printed ver.)
ISBN 978-82-471-1240-3 (electronic ver.)
ISSN 1503-8181

Theses at NTNU, 2007:56

Printed by Tapir Uttrykk

Øyvind Borg

Role of Alumina Support in Cobalt Fischer-Tropsch Synthesis

Doctoral thesis
for the degree of philosophiae doctor

Trondheim, January 2007

Norwegian University of
Science and Technology
Faculty of Natural Sciences and Technology
Department of Chemical Engineering

Abstract

A large number of metal oxide supported cobalt Fischer-Tropsch catalysts were prepared applying one-step incipient wetness impregnation to give 12 or 20 wt% cobalt and 0 or 0.5 wt% rhenium. Cobalt nitrate hexahydrate and perrhenic acid were used as cobalt and rhenium precursor, respectively. Impregnation was followed by drying, calcination, *in situ* reduction, and Fischer-Tropsch synthesis.

The effect of calcination conditions on the properties of a γ-Al_2O_3 based cobalt catalyst was investigated. One common precursor for all the catalysts was exposed to four different calcination atmospheres and eight different calcination temperatures. Calcination decomposed the supported cobalt nitrate hydrate and gave supported Co_3O_4. Largest amounts of nitrate were decomposed at high calcination temperatures. In order to maximise the cobalt dispersion, it was necessary to minimise the concentration of the calcination products (NO_x, H_2O) in the calcination atmosphere and perform the calcination at low temperatures. One set of calcination conditions was chosen for all the other catalysts.

Co_3O_4 was found in aggregates of many individual crystallites on γ-Al_2O_3. Re_2O_7 was only found in these cobalt-rich areas. The average size of the aggregates ranged from 75 to 150 nm. Largest aggregates were found in the γ-Al_2O_3 materials of highest porosity. The particles in an aggregate tended to share an approximately common orientation.

The individual Co_3O_4 particle size was controlled by the support pore size. Large particles were formed in wide pores and small particles were formed in narrow pores. The calculated average Co_3O_4 particle diameter ranged from 14 to 53 nm. Presence of rhenium slightly decreased the γ-Al_2O_3 supported Co_3O_4 particle size.

Irrespective of support, Co_3O_4 was reduced to cobalt metal in two steps with CoO as the intermediate. The reduction of Co_3O_4 to CoO was complete and took place in the same temperature range for all catalysts. In contrast, the CoO particles had different reducibility. Small particles were more difficult to reduce than large particles. Presence of rhenium facilitated the second reduction step significantly.

In order to study the effect of support variables on the final support and Fischer-Tropsch synthesis performance, a large number of catalysts were prepared on γ-Al_2O_3 of different pore characteristics using exactly the same preparation method and amount of active components. Fischer-Tropsch synthesis was performed in a fixed-bed reactor at 483 K, 20 bar, and $H_2/CO = 2.1$. The γ-Al_2O_3 supports contained trace amounts of sodium (20-113 ppm), originating from the manufacture process. Sodium decreased both the cobalt-time yield and site-time yield. Positive correlations were found between the cobalt particle size and the C_{5+} selectivity and between the catalyst pore size and the C_{5+} selectivity. Since the olefin/paraffin ratios were constant for all samples, different extent of α-olefin re-adsorption could not explain the variations in C_{5+} selectivity. Thus, it seems difficult to explain the variations in selectivity with diffusion effects. Instead, it is suggested that the cobalt particle size or possibly also the particle shape and distribution control the product distribution.

Comparison of un-promoted and Re-promoted catalysts showed that Re increased the cobalt reducibility and cobalt-time yield, but did not modify the site-time yield. Presence of Re also increased the C_{5+} selectivity slightly.

Since oxygen mainly is rejected as water on cobalt-catalysed Fischer-Tropsch synthesis, water will always be present in the reactor system. In the absence of externally added water, the activity increased with increasing water concentration up to at least $P_{H_2O} = 3$ bar, irrespective of support nature. The amount of indigenous water was increased by increasing the reactant conversion. In order to simulate high water concentrations normally encountered during commercial operation, external water was added to the reactor. The catalysts behaved differently when exposed to moderate water concentrations ($P_{H_2O} \approx 6$ bar). For narrow pore γ-Al_2O_3 based catalysts, the activity decreased while for a catalyst supported on γ-Al_2O_3 with wider pores, the activity actually increased. The original activity was regained upon water feed termination. At higher water concentrations ($P_{H_2O} \approx 8$ bar), all catalysts were irreversibly deactivated. The C_{5+} selectivity increased with increasing water concentrations.

Acknowledgements

During the work with this thesis, I have received help and advice from a number of people. First, I would like to thank my supervisor Anders Holmen for all his help and support. Erling Rytter is greatly acknowledged for taking active part in all stages of this work.

I am most grateful to Sigrid Eri who has been of extremely valuable support throughout the last four years. Thank you!

Magnus Rønning, Nina Hammer, Torbjørn Vrålstad, and the staff at the Swiss-Norwegian Beam Lines at the European Synchrotron Radiation Facility are greatly acknowledged for their contribution to the X-ray absorption spectroscopy work.

I would also like to thank Edvard Bergene and Odd Asbjørn Lindvåg for keeping the gas chromatograph alive.

Thanks to Erlend Bjørgum, Sølvi Storsæter Bjørgum, Edd Anders Blekkan, Bjørn Christian Enger, Vidar Frøseth, Sara Lögdberg, Rune Myrstad, Magnus Rønning, Dag Schanke, and Torild Hulsund Skagseth for valuable discussions and comments on the manuscript.

There are also three people outside the catalysis environment who have contributed significantly with help with this thesis: Winter Borg, Ragnar Borg, and Bård Buttingsrud. Thank you!

I would further like to thank the Research Council of Norway for financial support. Statoil ASA is also greatly acknowledged for financial contribution.

Al fin quiero también agradecer a Esther. ¡Muchas gracias por estar ahí siempre!

List of selected papers and presentations

Papers and presentations related to this work are listed below. The author has also been involved in a number of additional papers and presentations. A summary is given in Appendix A.

Papers

A. ***Ø. Borg***, E. A. Blekkan, S. Eri, D. Akporiaye, B. Vigerust, E. Rytter, and A. Holmen. Effect of calcination atmosphere and temperature on γ-Al_2O_3 supported cobalt Fischer-Tropsch catalysts. *Top. Catal.*, DOI: 10.1007/s11244-002007-0237-1, 2007.

B. ***Ø. Borg***, J. C. Walmsley, R. Dehghan, B. S. Tanem, E. A. Blekkan, S. Eri, E. Rytter, and A. Holmen. Electron microscopy study of γ-Al_2O_3 supported cobalt Fischer-Tropsch catalysts. Submitted.

C. ***Ø. Borg***, M. Rønning, S. Storsæter, W. van Beek, and A. Holmen. Identification of cobalt species during temperature programmed reduction of Fischer-Tropsch catalysts. *Stud. Surf. Sci. Catal.*, 163:255-272, 2007.

D. ***Ø. Borg***, S. Eri, E. A. Blekkan, S. Storsæter, H. Wigum, E. Rytter, and A. Holmen. Fischer-Tropsch synthesis over γ-alumina-supported cobalt catalysts: Effect of support variables. *J. Catal.*, doi:10.1016/j.jcat.2007.03.008, 2007.

E. ***Ø. Borg***, S. Eri, E. Rytter, and A. Holmen. Fischer-Tropsch synthesis over different alumina supported cobalt catalysts. *Prepr. Pap. - Am. Chem. Soc., Div. Fuel Chem.*, 51:699-701, 2006.

F. ***Ø. Borg***, N. Hammer, S. Eri, O. A. Lindvåg, R. Myrstad, E. A. Blekkan, M. Rønning, E. Rytter, and A. Holmen. Fischer-Tropsch synthesis over un-promoted and Re-promoted γ-Al_2O_3 supported cobalt catalysts with different pore sizes. Submitted.

G. ***Ø. Borg***, S. Storsæter, S. Eri, H. Wigum, E. Rytter, and A. Holmen. The effect of water on the activity and selectivity for γ-alumina supported cobalt Fischer-Tropsch catalysts with different pore sizes. *Catal. Lett.*, 107:95-102, 2006.

H. ***Ø. Borg***, V. Frøseth, S. Storsæter, S. Eri, E. Rytter, and A. Holmen. Fischer-Tropsch synthesis. Recent studies on the relation between the properties of supported cobalt catalysts and the activity and the selectivity. Accepted *Stud. Surf. Sci. Catal.*

I. E. A. Blekkan, ***Ø. Borg***, V. Frøseth, and A. Holmen. Fischer-Tropsch synthesis on cobalt catalysts: the effect of water. *Catalysis, Royal Society of Chemistry*, 20, 2007.

Presentations

A list of oral and poster presentations is listed below. The presenter is typeset in bold face.

- Ø. Borg, V. Frøseth, S. Storsæter, E. Rytter, and ***A. Holmen***. Fischer-Tropsch synthesis: Recent studies on the relation between the properties of supported cobalt catalysts and the activity and the selectivity. Keynote lecture, 8th Natural Gas Conversion Symposium, Natal, Brazil, 27 - 31 May 2007.

- ***Ø. Borg***, S. Eri, E. A. Blekkan, S. Storsæter, H. Wigum, E. Rytter, and A. Holmen. Fischer-Tropsch synthesis over different alumina supported cobalt catalysts. Oral presentation, 232th ACS National Meeting, San Francisco, USA, 10 - 14 September 2006.

- Ø. Borg, S. Storsæter, V. Frøseth, R. Myrstad, O. A. Lindvåg, E. Bergene, E. Rytter, S. Eri, and ***A. Holmen***. Fischer-Tropsch synthesis on different alumina supported Co catalysts. Oral presentation, 229th ACS National Meeting, San Diego, USA, 13 - 17 March 2005.

- ***Ø. Borg***, S. Storsæter, S. Eri, E. Rytter, and A. Holmen. The effect of different γ-alumina supports on cobalt Fischer-Tropsch catalysts. Poster presentation, EuropaCat-VII, Sofia, Bulgaria, 28 August - 1 September 2005.

- ***Ø. Borg***, E. A. Blekkan, S. Eri, D. Akporiaye, B. Vigerust, E. Rytter, and A. Holmen. Effect of calcination atmosphere and temperature on γ-Al_2O_3 supported cobalt Fischer-Tropsch catalysts. Poster presentation, 12th Nordic Symposium on Catalysis, Trondheim, Norway, 28 - 30 May 2006.

- ***Ø. Borg***, S. Storsæter, S. Eri, E. Rytter, and A. Holmen. The effect of different γ-alumina supports on cobalt Fischer-Tropsch catalysts. Poster presentation, Catalysis and organic synthetic chemistry (KOSK) seminar, Oslo, Norway, 2 - 3 November 2006.

- ***Ø. Borg***, N. Hammer, S. Eri, O. A. Lindvåg, R. Myrstad, E. A. Blekkan, M. Rønning, E. Rytter, and A. Holmen. Fischer-Tropsch synthesis over un-promoted and Re-promoted γ-Al_2O_3 supported cobalt catalysts with different pore sizes. Abstract, EuropaCat-VIII, Turku, Finland, 26 - 31 August 2007.

- ***E. A. Blekkan***, Ø. Borg, V. Frøseth, and A. Holmen. The effect of water on the Fischer-Tropsch synthesis over supported cobalt catalysts. Poster presentation, 8th Natural Gas Conversion Symposium, Natal, Brazil, 27 - 31 May 2007.

Author's contribution

The author has had an active role in all stages of this thesis. All experimental work has been done by the author except for the following:

- Preparation and calcination of the catalyst precursor in Paper A were performed by SINTEF Materials and Chemistry.
- The electron microscopy pictures in Paper B were taken by John C. Walmsley.
- The catalytic measurements in Paper F were done in cooperation with SINTEF Materials and Chemistry.

The author has also analysed and interpreted all data in this thesis. One exception exists: The extended X-ray absorption fine structure (EXAFS) data analysis in Paper C was done by Magnus Rønning.

The author wrote Papers A to G and contributed to the writing of Papers H and I.

List of symbols and abbreviations

All variables and symbols used in this thesis are listed below. Some symbols have multiple definitions. It should, however, be apparent from the context which of the definitions to use.

Greek symbols

α	Chain growth probability
β	Peak width
θ	Angle
θ_M	Site density / m^{-2}
λ	X-ray wavelength / m
Φ	Pellet porosity
χ	EXAFS function / k^{-1}
χ	Structural parameter / m^{-1}

Symbols

B	Experimental line width
b	Instrumental line width
D	Dispersion
d	Particle diameter / m
$\Delta E/E$	Monochromator band pass
F	Flow rate / m^3/s
I_0	Intensity of incident X-rays
I_t	Intensity of transmitted X-rays
K	Constant

Symbols (continued)

k	Wave number / m^{-1}
N	Coordination number
n	Number of carbon atoms
n	Stoichiometric coefficient
P	Equilibrium pressure / Pa
P	Pressure / Pa
P_0	Saturated vapour pressure / Pa
P_i	Partial pressure of component i / Pa
R	Interatomic distance / m
R^2	Coefficient of determination
R_0	Catalyst pellet radius / m
r_p	Mean pore radius / m
S	Selectivity / %
T	Temperature / K
V_m	Monolayer capacity / m^3
W_n	Weight fraction of product containing n carbon atoms

Abbreviations

bbl	Barrell
BET	Brunauer-Emmett-Teller
BJH	Barrett-Joyner-Halenda
C	Catalyst
CTY	Cobalt-time yield
d	Day
EDS	Energy dispersive spectroscopy
EU	European Union
EXAFS	Extended X-ray absorption fine structure
FID	Flame ionisation detector
GC	Gas chromatograph
GTL	Gas-to-liquids
LNG	Liquefied natural gas
MPA	Medium pore alumina
NPA	Narrow pore alumina
S	Support
SSITKA	Steady-state isotopic transient kinetic analysis
STEM	Scanning tunneling electron microscopy
STY	Site-time yield

Abbreviations (continued)

TCD	Thermal conductivity detector
TEM	Transmission electron microscope
TPR	Temperature programmed reduction
US	United States
US$	United States dollar
WPA	Wide pore alumina
XANES	X-ray absorption near-edge structure
XAS	X-ray absorption spectroscopy
XRD	X-ray diffraction

Contents

Chapter 1

Introduction

Today, there is a growing interest in gas-to-liquids conversion (GTL) as a tool for monetising natural gas and production of premium quality products free of nitrogen, sulphur, aromatics, and metals. The Fischer-Tropsch synthesis is the chemical heart of the gas-to-liquids technology.

1.1 Gas-to-liquids

1.1.1 Drivers

Currently, the world's fuel and chemical production is based predominantly on crude oil. However, the proved reserves of natural gas are similar in size to that of oil and, therefore, represent a huge energy resource. In fact, at the end of 2005, the proved reserves of oil and natural gas were 1200 and 1130 $\cdot\ 10^9$ barrels oil equivalent, respectively [1]. The annual proved reserves of oil and natural gas from 1980 to 2005 are shown in Figure 1.1. While the proved reserves of crude oil appear to stagnate, the reserves of natural gas increase. For these reasons, the utilisation of natural gas will probably become of primary importance in the energy sector in the near future.

Even though the reserves of natural gas are plentiful, more than half of the reserves are located in remote areas lacking pipelines or other infrastructure for transportation to the market. Significant quantities of natural gas are also flared as an unwanted by-product in oil production.

The gas-to-liquids technology is one of several options for making these remote gas reserves commercially attractive. The liquids may be transportation

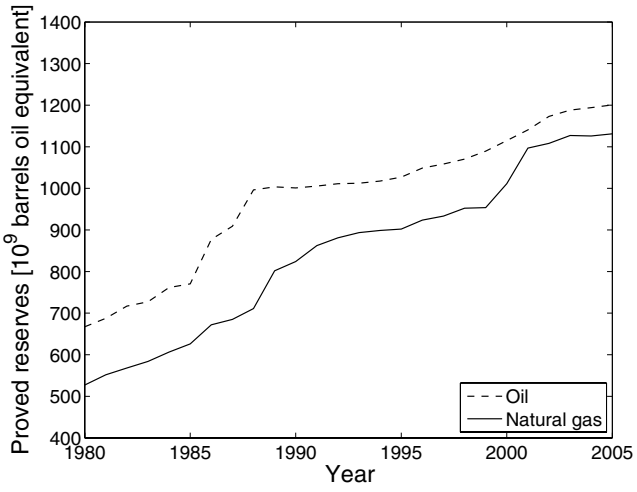

Figure 1.1: Proved reserves of oil and natural gas from 1980 to 2005 [1].

fuels produced via the Fischer-Tropsch synthesis, or alternative fuels such as methanol and dimethyl ether. These liquids are easily transportable. As shown in Figure 1.2, other ways to monetise the remote gas include pipelines, liquefied natural gas (LNG), and gas by wire.

Fischer-Tropsch synthesis based products include diesel and naphtha. These have a major advantage over liquefied natural gas, methanol, and dimethyl ether as they will be absorbed by a virtually unlimited distillate market. The high cost of gas pipelines limits the connection of gas resource and market to less than about 5,000 kilometers. Gas by wire has so far only found limited applications for similar distances.

The interest in gas-to-liquids technology has not just only come about as a result of the abundant supply of natural gas, but also because of a market demand for cleaner fuels. Diesel fuels produced from natural gas offer significant environmental benefits over transportation fuels derived from crude oil since they are essentially free of nitrogen, sulphur, aromatics, and metals. As shown in Table 1.1 [2], the diesel has properties that are well within current specifications. The liquid fuels can be used directly as fuels or blended with lower-quality crude oil derived fuels.

Until recently, natural gas derived fuels could not compete with the conventional fuels on price. However, rapid technological development has moved gas-to-liquids to the point of commercial operation, even if crude oil prices

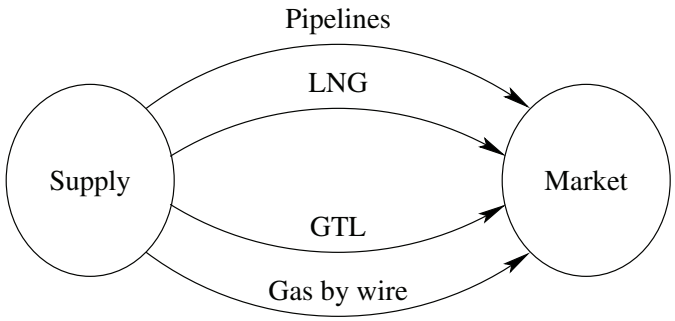

Figure 1.2: Options to bring the natural gas to the market.

drop below US$20 per barrel. For some time now, the oil price has been well above US$50 per barrel. A historical development of the oil price is given in Figure 1.3 [3].

1.1.2 History

The first synthesis of hydrocarbons from CO hydrogenation over transition metals dates back to 1902 when Sabatier and Senderens [4] formed methane over reduced nickel. About twenty years later, Fischer and Tropsch obtained liquid hydrocarbons from H_2 and CO on alkalised iron and other catalysts [5]. In 1925, Fischer and Tropsch announced the synthesis of higher hydrocarbons at atmospheric pressure over Group VIII metals [6]. A complete historical sketch until 1984 is given by Anderson [7].

The present number of large gas-to-liquids plants is low. In fact, only three plants produce more than 1,000 bbl/d [2]. The PetroSA plant in South Africa produces mainly gasoline and diesel fuel at an output rate of 25,000 bbl/d [2]. Shell operates a plant in Malaysia which has a capacity of approximately 14,000 bbl/d [2]. The main products are waxes, chemicals, and diesel. Sasol is cur-

Table 1.1: GTL diesel properties versus EU and US specifications [2].

Property	GTL diesel	EU (2005)	US (2006)
Maximum sulphur (ppm)	0	50/10	15
Minimum cetane number	70	51	40 (Index)
Maximum polyaromatics (wt%)	0	11	N.A.
Maximum aromatics (vol%)	0	N.A.	35
Maximum density (kg/l)	0.79	0.845	0.876

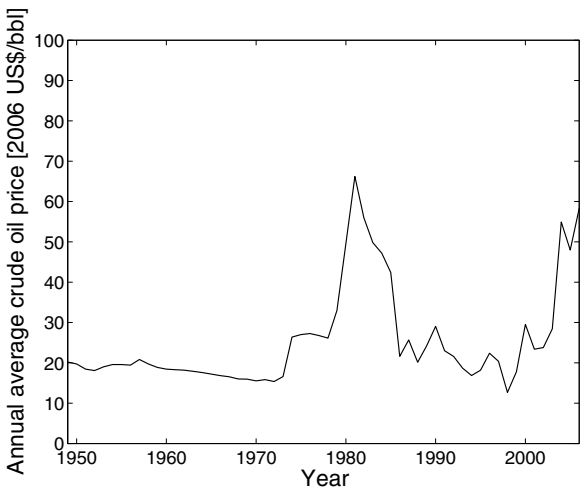

Figure 1.3: Historical development of the crude oil price. The numbers have been corrected for inflation to 2006 US$/bbl [3].

rently commissioning a plant in Qatar. The plant will manufacture 34,000 bbl/d of liquid fuels [2].

Although there are only three significant commercial operations based on natural gas, the interest is great. Licensers of GTL technology are many and include Blue Star Sustainable Technologies Corp., BP/Davy Process Technology, Chiyoda Corp., ConocoPhillips, Energy International, ExxonMobil, Foster Wheeler Energy, Hydrocarbon Technologies, Inc., National Petrochemical Co., Raytheon E&C, Rentech, Sasol, Shell, Statoil, Syncrude Technology, Synergy Technologies Corp./ECP, Synfuels International, Syntroleum Corp. An extensive overview of the companies that are involved in GTL commercialisation or process development is given by Hydrocarbon Publishing Company [2].

1.1.3 Technology

The gas-to-liquids process comprises three main elements: synthesis gas production, Fischer-Tropsch synthesis, and product upgrade as shown in Figure 1.4.

In the first stage, synthesis gas is produced from natural gas. Available technologies for synthesis gas production for gas-to-liquids plants include steam reforming, partial oxidation, and autothermal reforming. The most attractive and economical technology today is considered to be autothermal reforming [8].

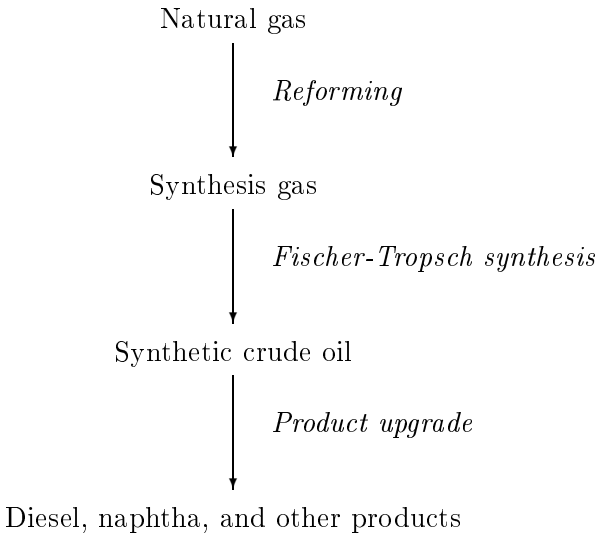

Figure 1.4: The three main steps in the gas-to-liquids technology.

The Fischer-Tropsch reaction is the chemical heart of the gas-to-liquids technology. In this step, synthesis gas is catalytically converted into paraffinic and olefinic hydrocarbons of varying chain lengths. The product distribution ranges from methane to hard waxes. A small fraction of oxygenates is also present in the product mixture.

In the last step, the products of the Fischer-Tropsch synthesis are upgraded. The cold flow properties of the product mixture are improved by hydrocracking and hydroisomerisation. In addition, olefins and oxygenates are hydrogenated. The treated compounds then go through a distillation column and are separated into fractions such as naphtha, diesel, kerosene, jet fuel, and residue. The residue fraction can either be recirculated to the hydrocracking/hydroisomerisation reactor or be used as a base oil precursor fraction. The chemical formulae of the gas-to-liquids products are presented in Table 1.2.

1.2 Fischer-Tropsch synthesis

Figure 1.4 illustrates that the gas-to-liquids technology consists of three steps. The remainder of this thesis, however, deals only with the second step, namely the Fischer-Tropsch synthesis.

Table 1.2: Gas-to-liquids products [9].

Name	Compound
Fuel gas	C_1-C_2
Liquefied petroleum gas	C_3-C_4
Gasoline	C_5-C_{12}
Naphtha	C_8-C_{12}
Kerosene (jet fuel)	C_{11}-C_{13}
Diesel (fuel oil)	C_{13}-C_{17}
Middle distillates (light gas oil)	C_{10}-C_{20}
Soft wax	C_{19}-C_{23}
Medium wax	C_{24}-C_{35}
Hard wax	C_{35+}

1.2.1 Reactions

Although the chemistry of the Fischer-Tropsch synthesis is complex, the fundamental aspects can be described by a few generalised equations (Table 1.3).

A characteristic of the Fischer-Trospch reactions is their high exothermicity. The formation of 1 mole of -CH_2- is accompanied by a heat release of 165 kJ/mol [10]. Typical industrial conditions are 483-513 K and 20-30 bar.

A typical product mixture using cobalt catalyst at low temperature is:

- *n*-paraffins (75-90%)
- 1-olefins (5-15%)
- *n*-alcohols (5%)
- Branched paraffins and olefins ($< 5\%$)
- Aldehydes, ketones, and acids ($< 1\%$)

However, it should be emphasised that Fischer-Tropsch synthesis run at other conditions and with other catalysts can give a very different product distribution.

The products are formed in a polymerisation reaction which comprises the following steps [11]:

Table 1.3: Major overall reactions in Fischer-Tropsch synthesis.

Main reactions	
Paraffins	$n\mathrm{CO} + (2n+1)\mathrm{H_2} \rightarrow \mathrm{C}_n\mathrm{H}_{2n+2} + n\mathrm{H_2O}$
Olefins	$n\mathrm{CO} + 2n\mathrm{H_2} \rightarrow \mathrm{C}_n\mathrm{H}_{2n} + n\mathrm{H_2O}$
Water-gas shift	$\mathrm{CO} + \mathrm{H_2O} \rightarrow \mathrm{CO_2} + \mathrm{H_2}$
Side reactions	
Oxygenates	$n\mathrm{CO} + 2n\mathrm{H_2} \rightarrow \mathrm{C}_n\mathrm{H}_{2n+2}\mathrm{O} + (n-1)\mathrm{H_2O}$
Boudouard reaction	$2\mathrm{CO} \rightarrow \mathrm{C} + \mathrm{CO_2}$

1. Reactant adsorption
2. Chain initiation
3. Chain growth
4. Chain termination
5. Product desorption
6. Readsorption and further reaction

Although the Fischer-Tropsch synthesis has been known since the 1920s, the exact mechanism is still a matter of debate. Over the years, various mechanisms have been proposed. The main difference is the monomer responsible for chain growth. In the original carbide mechanism proposed by Fischer and Tropsch [6], CH_x is the monomer, in the enol mechanism of Storch *et al.* [12], oxymethylene (HCOH) is the species responsible for chain growth, and in the CO insertion mechanism proposed by Pichler and Schulz [13], the chain growth occurs through the insertion of CO into the metal-methyl bond.

Although the carbide mechanism is supported by many studies [14, 15] and has been favoured for a long time, a recent study [16] points to the CO insertion mechanism as a more likely mechanism.

A discussion of the Fischer-Tropsch mechanism is beyond the scope of this thesis. However, for an understanding of the product distribution, it is sufficient to only consider the basics of the reaction mechanism. Growth of a hydrocarbon chain occurs, independent of the exact mechanism, by a stepwise addition of a one-carbon segment derived from CO at the end of an existing chain.

1.2.2 Catalyst candidates

Fischer and Tropsch [6] demonstrated early the activity of Group VIII metals. However, only iron, cobalt, nickel, and ruthenium based catalysts have sufficient activity to be considered for commercial application in the Fischer-Tropsch reaction.

The choice of catalyst for Fischer-Tropsch synthesis depends on a number of factors such as the price of the active metal, the desired end products, and the carbon source for synthesis gas production.

On a metal basis, the relative costs of Fe:Co:Ni:Ru are 1:1000:250:50000 [17]. The low availability and, accordingly, high price of ruthenium [17] makes the use of this element in large-scale industrial applications questionable.

Because of its powerful hydrogenation properties, nickel produces too much methane for viable operation [17]. In addition, when exposed to typical Fischer-Tropsch synthesis pressures, nickel forms volatile carbonyls [17]. These two properties make nickel unsuitable for Fischer-Tropsch synthesis. This leaves iron and cobalt as the most promising candidates.

Iron based catalysts possess high water-gas-shift activity. This makes them suitable for synthesis gas with low H_2/CO ratios, *e.g.* from coal or other heavy hydrocarbon feedstock, where the ratio is considerably lower than the consumption ratio of the Fischer-Tropsch reaction, $H_2/CO \approx 2.15$.

The water-gas-shift activity of cobalt catalysts is low. These catalysts can therefore be used when the synthesis gas is produced from natural gas. Synthesis gas produced from natural gas gives H_2/CO ratios close to the stoichiometric value 2.15. Only cobalt based catalysts will be considered in the remainder of this thesis.

In order to maximise the exposure of cobalt to gaseous reactants, the metal is normally dispersed on a catalyst support. The choice of support is important for the final Fischer-Tropsch synthesis catalyst. Common supports include Al_2O_3, SiO_2, and TiO_2. Typically, the cobalt metal loading ranges from 10 to 30 g per 100 g support.

1.2.3 Reactors

There are three different reactor concepts for Fischer-Tropsch synthesis; tubular fixed-bed reactor, fluidised bed reactor, and slurry bubble column reactor.

Key information and simple sketches of these reactors are given in Table 1.4 and Figure 1.5, respectively.

A major consideration in the design of suitable Fischer-Tropsch reactors is efficient removal of the heat of reaction. As shown in Figure 1.5, high rates of heat exchange are achieved by contact with water.

1.3 Scientific objective

Fischer-Tropsch synthesis is a popular topic in Academia. Although the catalytic performance of cobalt supported on a large number of supports has been thoroughly investigated, there are still many questions related to the role of the support material. For instance, major variations in selectivity to long-chain hydrocarbons between cobalt on different supports have been reported. An explanation does not exist. The purpose of this study is, therefore, to gain more knowledge about the role of the support material.

Some of the variations in selectivity may also be due to different conditions both in catalyst preparation, reduction, and Fischer-Tropsch synthesis. Accordingly, one of the main targets in this work is to investigate the role of support in a highly systematic and experimentally very careful way.

Previous investigations have been limited only to a few supports of the same chemical identity. In order to acquire a comprehensive and reliable data material, the catalytic performance of a large number of catalysts has been evaluated. The starting supports differed mainly in their pore characteristics.

1.4 Outline

The outline of this thesis is as follows: Chapter 2 is a literature review. Since the research on Fischer-Tropsch synthesis is enormous, only investigations that have direct relevance for this thesis are presented.

Chapter 3 gives all necessary information for reproduction of the experimental work.

The main results are discussed in Chapter 4.

Chapter 5 concludes the thesis and addresses unsolved issues and gives suggestions for further work.

Table 1.4: Alternative reactor designs for Fischer-Tropsch synthesis.

Tubular fixed-bed reactor	Fluidised bed reactor	Slurry bubble column reactor
Catalyst inside 1-2" tubes	Catalyst particles fluidised by gas	Catalyst particles suspended in liquid by gas
Steam generation on shell side	Steam generation on tube side	Steam generation on tube side
Catalyst: Co or Fe	Catalyst: Fe	Catalyst: Co or Fe
Particle size: > 1 mm	Particle size: 50-100 μm	Particle size: 50-100 μm
Temperature: 473-503 K (Co)	Temperature: 623 K	Temperature: 483-513 K (Co)
Product: liquid and wax	Product: liquid	Product: liquid and wax
Phases: 3	Phases: 2	Phases: 3

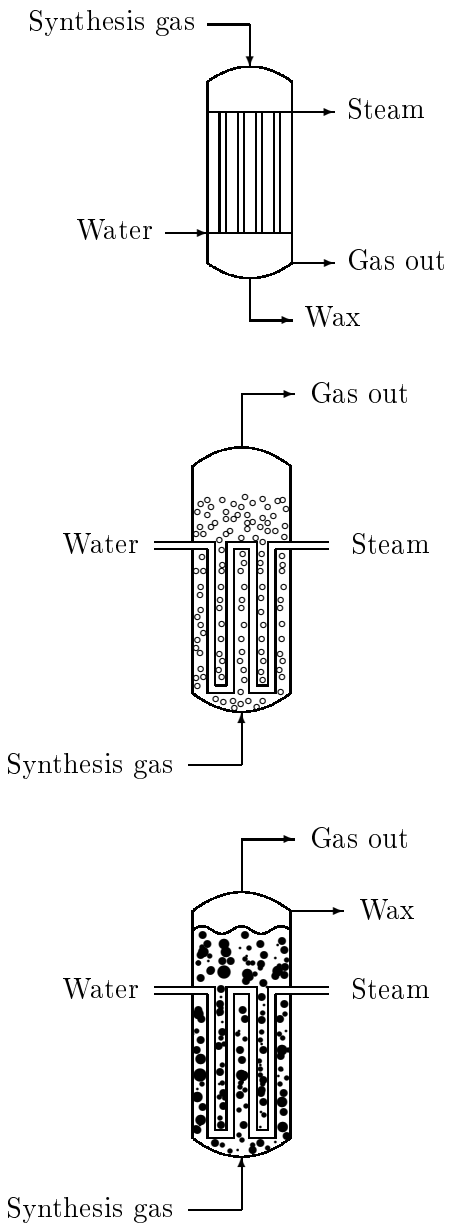

Figure 1.5: Alternative reactor designs for Fischer-Tropsch synthesis: tubular fixed-bed reactor (top), fluidised bed reactor (middle), and slurry bubble column reactor (bottom).

This thesis is based on a collection of nine publications that are provided as appendices. The effect of calcination atmosphere and temperature on the final Fischer-Tropsch catalyst and catalytic performance is the subject of Paper A.

Paper B gives transmission electron microscopy images of γ-Al_2O_3 catalysts with different pore sizes in their calcined state.

Reduction is an inevitable step in Fischer-Tropsch synthesis. The reduction scheme of Co_3O_4 to cobalt metal is investigated by X-ray absorption spectroscopy in Paper C. Different techniques for characterisation of the reducibility of cobalt catalysts are also compared.

In order to solely study the effect of support on the Fischer-Tropsch performance, a large number of supported cobalt catalysts were tested at exactly the same conditions. The only variables were the pore characteristics of the starting γ-Al_2O_3 material. Paper D gives the results of this investigation.

Fischer-Tropsch synthesis data of cobalt supported on different aluminas including the alumina precursor boehmite are given in Paper E.

Paper F investigates the influence of presence of rhenium for the catalytic performance of catalysts with different pore sizes.

A large fraction of the synthesis gas feed is converted during commercial operation. Because of high conversion, the water concentration in the reactors is significant. By addition of water to the feed in a conventional fixed-bed reactor, high conversions can be simulated without using long residence times. The effect of water on catalysts with different pore sizes is investigated in Paper G.

Paper H compares the Fischer-Tropsch synthesis data of cobalt supported on different metal oxides.

Paper I is a review paper. It gives an overview of the existing literature on the effect of water for cobalt supported catalysts.

Chapter 2

Literature review

Although the Fischer-Tropsch synthesis is an old process, the publication rate has never been as high as it is today (Figure 2.1). Since the amount of papers on this topic is so plentiful, this chapter only deals with the most important studies that have direct relevance for the present investigation.

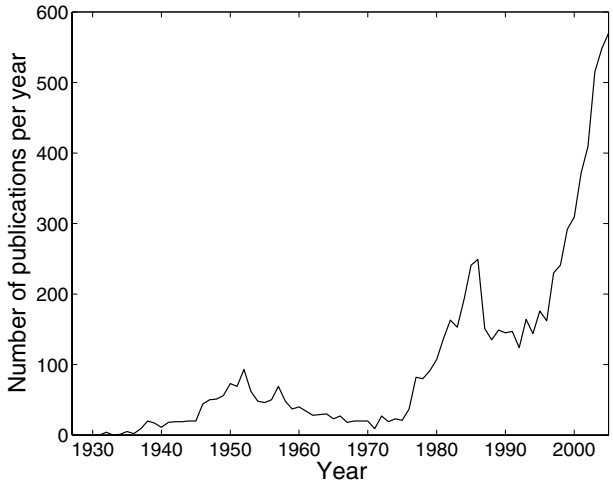

Figure 2.1: Number of publications registered in Chemical Abstracts on Fischer-Tropsch synthesis from 1927 to 2005. Title search string: "Fischer-Tropsch".

2.1 Preparation of Fischer-Tropsch catalysts

Incipient wetness impregnation of a metal oxide support with an aqueous solution of cobalt nitrate hexahydrate is a common way to produce Fischer-Tropsch catalysts. Impregnation is normally followed by drying and calcination in order to decompose the supported cobalt nitrate hydrate and obtain supported cobalt oxide. Reduction *in situ* transforms the inactive cobalt oxide to active metallic cobalt prior to Fischer-Tropsch synthesis. All the steps are schematically illustrated in Figure 2.2.

In spite of this inherently simple procedure, a number of factors in each step have a significant impact on the final metallic Fischer-Tropsch catalysts. Important investigations related to these steps are commented in the following sections.

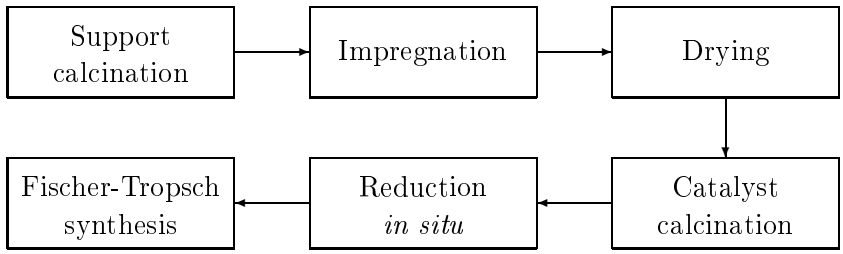

Figure 2.2: Catalyst preparation steps.

2.2 Impregnation

For catalysts prepared by incipient wetness impregnation of an oxide support with an aqueous solution of cobalt nitrate hexahydrate, the pore size distribution of the support plays a primary role for the Co_3O_4 particle size distribution as measured after drying and catalyst calcination [18–26]. For silica, it is well documented that small particles form in narrow pores and large particles form in wide pores [18–23, 26, 27]. The same scenario has been described for three γ-Al_2O_3 based catalysts [25]. Co_3O_4 particle size data of several investigations [18, 21, 22, 24–27] are given together in Figure 2.3.

As shown in Figure 2.3, the calculated Co_3O_4 crystallite or particle diameter in most cases exceeded the calculated pore width of the support. Khodakov *et al.* [20–22] speculated that since the diameters of the Co_3O_4 crystallites

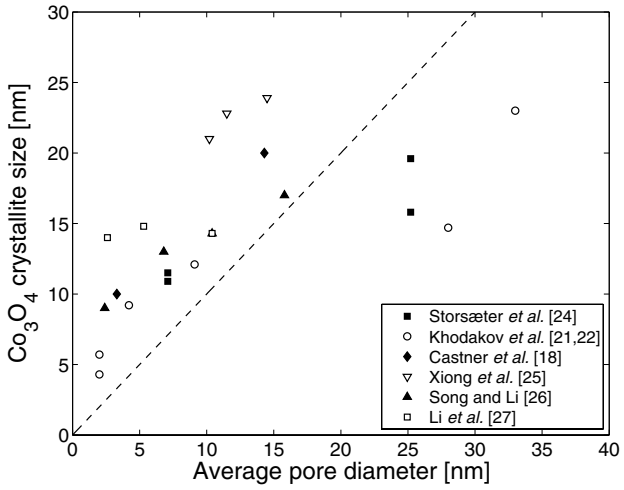

Figure 2.3: Cobalt oxide crystallite size data as determined from X-ray diffraction data. The crystallite size was in all cases calculated using the Scherrer equation, but different Co_3O_4 reflections were utilised.

were limited by the pore sizes of the supports, the crystallites were mainly encapsulated in the support pores rather than located on the outer surface of the supports. On the other hand, Dalai *et al.* [28] stated that since the average particle size was larger than the average pore diameter of the silica support, the cobalt particles were for the most part located on the exterior of the silica support.

The dependence between pore size and crystallite size can be circumvented by using other catalyst synthesis routes. For instance, in the so-called "High-Dispersion Cobalt" method, Lok [29] produced a uniform distribution of cobalt crystallites of 3-5 nm even at high cobalt loadings in a γ-Al_2O_3 support. The catalysts were made in a single deposition step by deposition-precipitation of cobalt compounds at high pH via a cobalt ammine complex.

2.3 Catalyst calcination

The conditions during calcination of impregnated cobalt precursors have a significant influence on the performance of the final catalyst [30, 31].

For instance, van de Loosdrecht *et al.* [31] observed that the catalyst performance is strongly dependent on the heating rate and the air-space velocity in fluidised bed calcination. Figure 2.4 shows that the catalyst activity increased

with an increase in the air-space velocity and a decrease in the heating rate. According to van de Loosdrecht *et al.* [31], both factors decrease the water and NO_x concentration at the catalyst during the calcination, with a positive effect on the catalytic performance during Fischer-Tropsch synthesis.

According to Reinalda and Kars [30], the activity (and selectivity to long-chain hydrocarbons) may be improved, if during calcination, the catalyst is exposed to an atmosphere containing large amounts of nitrogen oxides.

After calcination, the Co_3O_4 crystallites are usually not present one and one over the support, but in aggregates of many crystallites [19, 32–34]. Aggregate sizes between 30-700 nm have been reported [19, 32–34].

The pore size of the supports seems to be of particular importance for the size of the cobalt aggregate. For instance, Saib *et al.* [19] found the size of the aggregates to increase with increasing SiO_2 pore size. Storsæter *et al.* [33, 34] observed larger Co_3O_4 aggregates on silica than on γ-Al_2O_3, allegedly because of a wider pore diameter of the former. In contrast, on TiO_2 and α-Al_2O_3, Co_3O_4 existed as single crystals. It was concluded that the size of the aggregates increases with the pore size up to a certain limit. Above this limit, no aggregates of crystallites will occur.

Lok [29] found the structure of the "High-Dispersion Catalysts" to be markedly different from that of the traditional cobalt nitrate based catalysts. The latter contain cobalt crystallites in large aggregates while for the "High-Dispersion Catalysts", the crystallites are homogeneously distributed over the support.

2.4 Reduction

Reduction is an inevitable step in preparation of active Fischer-Tropsch catalysts. The general consensus is that Co_3O_4 is reduced to cobalt metal in two steps:

$$Co_3O_4 + H_2 \rightarrow 3CoO + H_2O \tag{2.1}$$

$$3CoO + 3H_2 \rightarrow 3Co^0 + 3H_2O \tag{2.2}$$

In some cases, the support interacts strongly with the active phase. Metal-support interactions may leave a fraction of the cobalt chemically inactive after reduction. Jacobs *et al.* [35] studied the reducibility of cobalt supported on several metal oxide supports, such as γ-Al_2O_3, TiO_2, SiO_2. The metal-support interactions increased in the order γ-$Al_2O_3 > TiO_2 > SiO_2$.

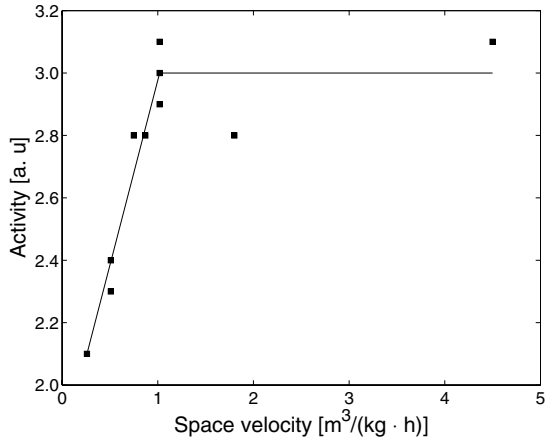

(a)

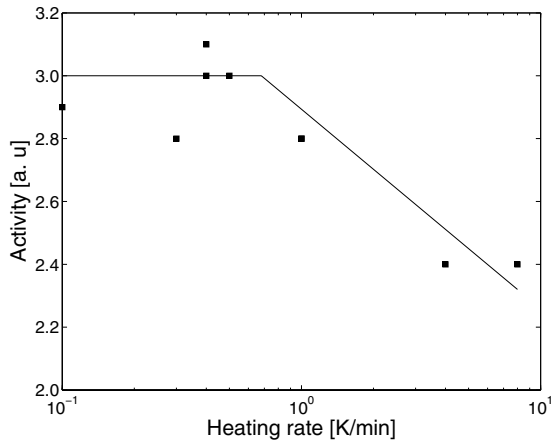

(b)

Figure 2.4: The influence of the air-space velocity (a) and heating rate (b) during fluidised bed calcination on the catalytic performance during Fischer-Tropsch synthesis.

Khodakov *et al.* [36] studied the reducibility of cobalt species in silica supported catalysts using *in situ* X-ray diffraction and *in situ* X-ray absorption spectroscopy. A series of catalysts with different particle sizes were the basis of the investigation. Independent of particle size, almost all Co_3O_4 particles could be reduced to the CoO phase. On the other hand, the CoO particles had different reducibility to metal species. The ease of reduction decreased from larger (20-70 nm) to smaller (6 nm) particles. Khodakov *et al.* [36] speculated that the interaction between metal and support is much stronger for smaller particles than for larger ones.

Khodakov *et al.* [20–22] also compared the reducibility of cobalt catalysts supported on silicas of varying pore size. Since the particle size followed the support pore diameter and the reducibility increased with increasing particle size, there was accordingly also a positive correlation between the support size and particle size. Similar results have been reported for silica supported cobalt catalysts [19, 28].

Castner *et al.* [37] suggested that the SiO_2 support porosity could influence the reducibility of supported cobalt oxide. While reduction of Co_3O_4 to CoO took place in the same temperature range for all catalysts, the difficulty of the second reduction step increased with decreasing cobalt oxide particle size. Castner *et al.* [37] discarded increased particle-support interaction as an explanation, and attributed the reducibility level to the ease of water removal during the CoO $\rightarrow Co^0$ reduction step.

In contrast to the investigations above, Song and Li [26] found lower degrees of reduction for large particles located in wide SiO_2 pores than for small particles in narrow SiO_2 pores. Xiong *et al.* [25] did the same observation for a series of three γ-Al_2O_3 supports.

The reducibility can also be changed by modification of the support. For instance, Zhang *et al.* [38] treated a γ-Al_2O_3 support in four types of media, namely ammonia, ammonium nitrate, acetic acid, and ethanol before cobalt impregnation. Although the cobalt oxide crystallite size of the oxidic catalyst precursor was almost unaffected by different support pre-treatment (11-15 nm), the reducibility of the catalysts varied greatly (12.5-51.6%).

The reducibility is also changed by other parameters such as cobalt precursor and solvent, cobalt loading, preparation method, and pre-treatment (*i.e.* conditions during drying, calcination, and reduction). The reader is referred to Storsæter *et al.* [33] for references.

2.5 Fischer-Tropsch synthesis

2.5.1 Site-time yield

Site-time yields (mol CO/(mol Co · s)) on supported cobalt catalysts are traditionally considered independent of cobalt dispersion and of support identity. Thus, the catalytic productivity can directly be predicted from the number of cobalt atoms deposited on the surface. For instance, Iglesia *et al.* [39–41] found constant site-time yield in the cobalt particle size range 10 to 210 nm which includes most of the typical low dispersion cobalt Fischer-Tropsch catalysts. Later publications have agreed with the conclusions drawn by Iglesia *et al.* [39–41].

As crystal structure depends only weakly on crystallite diameter over the dispersion range investigated by Iglesia *et al.* [39–41], it is not certain that the above conclusions can be extrapolated to higher dispersions. In fact, as shown in Figure 2.5, Bezemer *et al.* [42] recently showed for cobalt supported on carbon nanofibers that the site-time yield is lower for metallic particles smaller than 8 nm. The authors pointed out that the Fischer-Tropsch reaction comprises a large number of elementary steps, such as dissociation, hydrogenation, and insertion, and speculated that on small crystallites, the domains that combine these different active sites are not stable or they contain a non-optimum ratio of the different sites.

2.5.2 Selectivity

The products from the Fischer-Tropsch synthesis form a complex multicomponent mixture with significant variations in carbon number and type. Often it is assumed that the relative probability of chain growth and chain termination, denoted α and 1-α, respectively, is independent of the chain length and hence constant. In such a case, the carbon-number distribution of Fischer-Tropsch products can be represented by a simple statistical model, the Anderson-Schulz-Flory distribution [43]. A mathematical analysis gives:

$$\frac{W_n}{n} = (1-\alpha)^2\,\alpha^{n-1} \tag{2.3}$$

where W_n is the weight fraction of product containing n carbon atoms, and α is the chain growth probability.

Figure 2.6 shows how the theoretical product distribution of hydrocarbons depends on α. It is obvious that methane ($\alpha = 0$) and hard waxes ($\alpha = 1$)

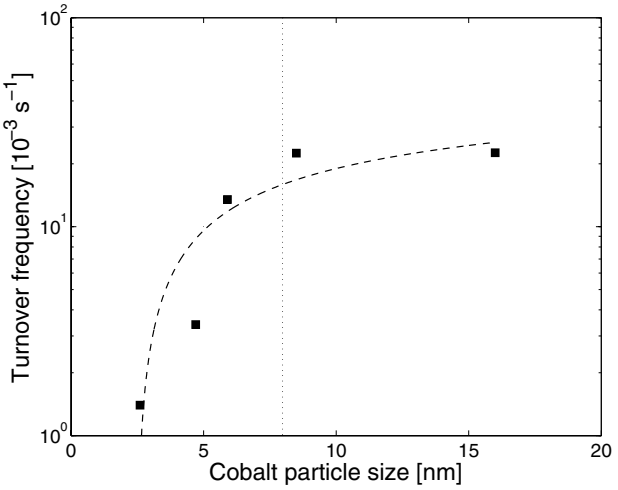

Figure 2.5: The influence of cobalt particle size on the site-time yield at 35 bar and 483 K [42]. The particle sizes were determined by X-ray photoelectron spectroscopy.

are the only products than can be produced to 100% selectivity. For all other values of α, a broad distribution of compounds exists.

Significant deviations from the Anderson-Schulz-Flory distribution have been observed in many studies. The usual deviations are a relatively high yield of methane, a relatively low selectivity to ethane, an increase in chain growth probability and an exponential decrease of the olefin to paraffin ratio with increasing chain length. References are given by van der Laan and Beenackers [9].

As illustrated in Figure 2.6, a mixture of hydrocarbons with various chain lengths is always formed. However, an appropriate choice of catalyst and reaction conditions enables the value of the chain growth probability to be shifted.

Mass transfer effects are very important in Fischer-Tropsch synthesis. Even though the reactants are in the gas phase, the pores will be filled with liquids, namely wax and water. Since diffusion in the liquid phase is almost three order of magnitude slower than in the gas phase, even slow reactions may become mass transfer limited. Limitations influence both the selectivity and activity.

There are predominantly two types of diffusion limitations; diffusion limited

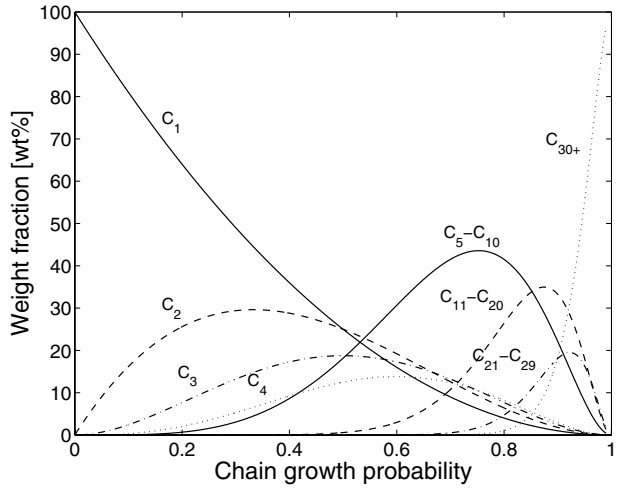

Figure 2.6: Selectivity of hydrocarbon fractions as a function of chain growth probability.

CO arrival and diffusion limited removal of the reactive products. The first type leads to shortage of CO at the catalytic sites and decreases the selectivity to long-chain hydrocarbons. The second type increases the role of the primary products in secondary reactions, and can lead to increased α-olefin re-adsorption or to α-olefin hydrogenation. A simplified network of primary and secondary reactions is given in Figure 2.7.

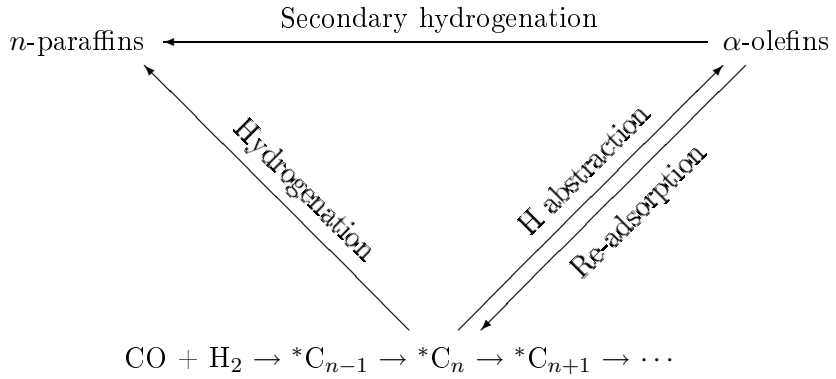

Figure 2.7: Simplified reaction network for the Fischer-Tropsch synthesis.

Iglesia *et al.* [39, 44, 45] contributed the observed differences in selectivity for cobalt on pure and modified Al_2O_3, SiO_2, and TiO_2 supports only to the variations in the extent of α-olefin re-adsorption. In other words, the dispersion and support were not considered to influence the intrinsic chain growth probability on cobalt surfaces, within the experimentally available dispersion (0.45-12%). According to Iglesia *et al.* [39, 44, 45], the selectivity solely depends on a structural parameter, χ, which is a measure of the intraparticle diffusion resistance at a given set of reaction conditions. It is defined as:

$$\chi = \frac{R_0^2 \Phi \theta_M}{r_p} \tag{2.4}$$

where R_0 is the catalyst pellet radius, Φ is the pellet porosity, θ_M is the density of surface metal atoms that act as catalytic sites, and r_p is the mean pore radius.

As shown in Figure 2.8, the optimum value of χ at typical Fischer-Tropsch synthesis conditions was found to be between 500-1000 $\cdot$ 10^{16} m^{-1}. At these values, the secondary chain building reactions of primary products are maximised without imposing significant diffusion limitations on the reactants.

Shi and Davis [46], on the other hand, reported that diffusion limitations for the α-olefin products and their subsequent re-incorporation as chain initiators do not have a major impact on the product distribution.

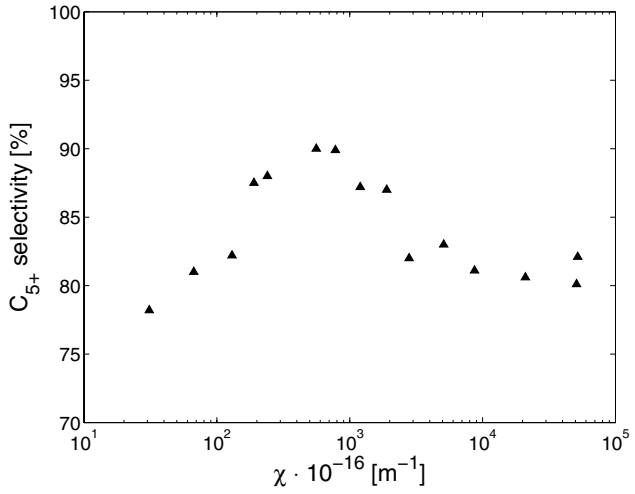

Figure 2.8: Volcano curve of Iglesia *et al.* [39, 44, 45].

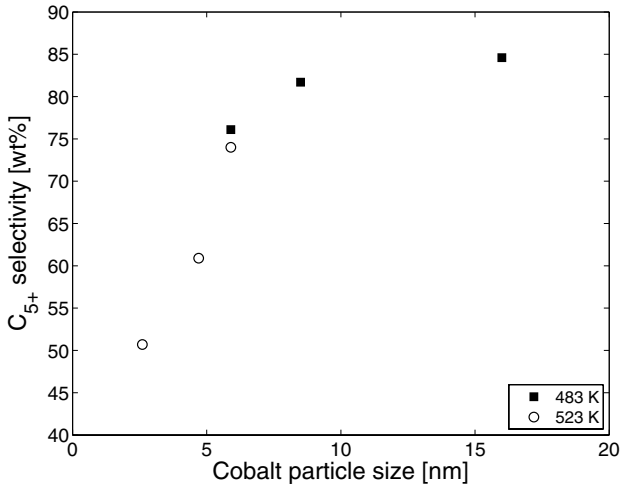

Figure 2.9: The influence of cobalt particle size on the C_{5+} selectivity at 35 bar and 483 K (■) and 523 K (○) [42].

Bezemer *et al.* [42] studied five catalysts with particle sizes ranging from 2.6 to 16 nm under industrially relevant conditions (35 bar). Figure 2.9 shows that the product distribution apparently is dependent on the cobalt particle size. The C_{5+} selectivity varied from 76 to 84% at 483 K and from 51 to 74% at 523 K. Bezemer *et al.* [42] ruled out that differences in cobalt site density could explain the data and ascribed the large variations in selectivity predominantly to the cobalt particle sizes of the catalysts. It must be mentioned that the catalysts were prepared using different solvents (nitrate, acetate, ethanol) during incipient wetness impregnation and contained very different cobalt amounts (1-22% Co). Furthermore, the selectivities were obtained at different CO conversions (13-84%) and temperatures (483 and 523 K). Thus, it is not unlikely that the particle size effect on the selectivity was confounded with other effects. In fact, it is known that both the solvent [47], cobalt loading [48], CO conversion level [44], and temperature [49] affect the catalyst or the product distribution directly.

The effect of particle size on C_{5+} selectivity for several other investigations [19, 24–26] is shown in Figure 2.10. A speculative trend line is included in the figure.

Saib *et al.* [19] investigated the effect of pore diameter of the silica on the performance in the Fischer-Tropsch synthesis. The C_{5+} and methane selectivity passed through a maximum at the 10 nm supported catalysts. It was explained

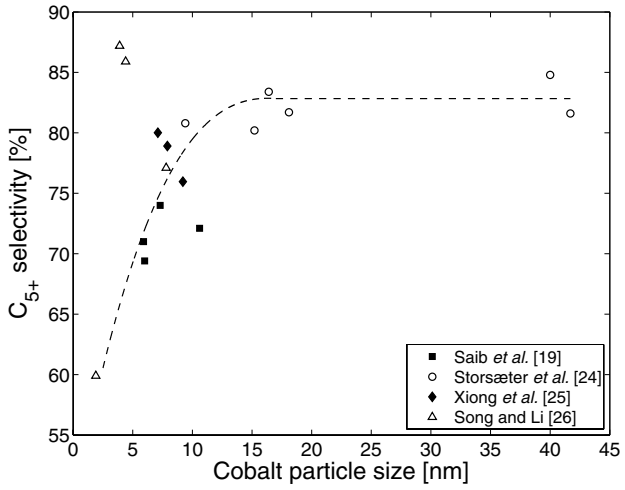

Figure 2.10: Effect of cobalt particle size on C_{5+} selectivity [19, 24–26].

quantitatively by the transport model by Iglesia *et al.* [39, 44, 45].

Storsæter *et al.* [24] obtained a positive, albeit weak correlation between the pore diameter and the C_{5+} selectivity. However, the work was done on different supports (γ-Al_2O_3, SiO_2, TiO_2) and may be a result of different chemical identity.

Schanke *et al.* [50] prepared aluminas with different surface areas by thermal treatment of γ-Al_2O_3. Improved C_{5+} selectivity was obtained for cobalt supported on low surface area alumina. The low surface area based catalysts had wide pores and low pore volumes.

In contrast to the investigations above, Xiong *et al.* [25] found a negative correlation between the pore size and the selectivity to C_{5+} hydrocarbons. Song and Li [26] observed that the C_{5+} selectivity passed through a maximum at 6.6 nm.

The results are summarised in Figure 2.11 [19, 24–26].

A closer look at the data sources gives the impression that it is more an exception than a rule that the C_{5+} selectivity of different catalysts is compared at the same water concentration. Most authors seem to be unaware that the amount of water is extremely important for the C_{5+} selectivity. To our best knowledge, among the investigations shown in Figures 2.10 and 2.11, only

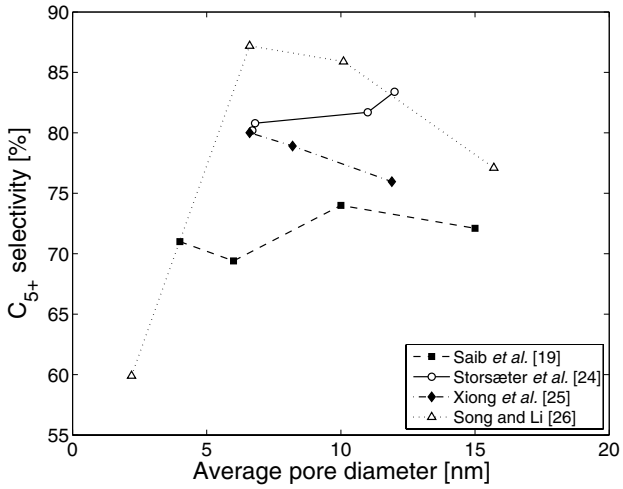

Figure 2.11: Effect of average catalyst pore diameter on C_{5+} selectivity [19, 24–26].

Storsæter *et al.* [24, 34] have compared the performance of different catalysts at the same CO conversion and, therefore, the same water concentration.

Bertole *et al.* [51] examined catalyst composition effects on methane selectivity using isotope $^{12}CO \rightarrow {}^{13}CO$ transients at reaction steady state. Cobalt supported on γ-Al_2O_3, SiO_2, and TiO_2 showed similar selectivity to C_{5+} hydrocarbons.

Zhang *et al.* [38] treated a γ-Al_2O_3 material in different media and evaluated the Fischer-Tropsch synthesis performance after cobalt impregnation. Significant variations in activity and C_{5+} selectivity were recorded. Cobalt supported on γ-Al_2O_3 treated in ammonia and ammonia nitrate gave high activity and C_{5+} selectivity. Low acidity γ-Al_2O_3 based catalysts also gave high activity and selectivity. Zhang *et al.* [38, 52] concluded that a high reducibility and a large fraction of bridged-form adsorbed CO were the main causes for high activity and high C_{5+} selectivity.

Bertole *et al.* [53] correlated the surface inventory of active carbon species with the product selectivity. Changes in carbon inventory caused proportional changes in the polymerisation probability at all carbon numbers. Most of the effects of changes in CO and water partial pressures on the chain growth probability appear to arise via an indirect effect on the active carbon inventory.

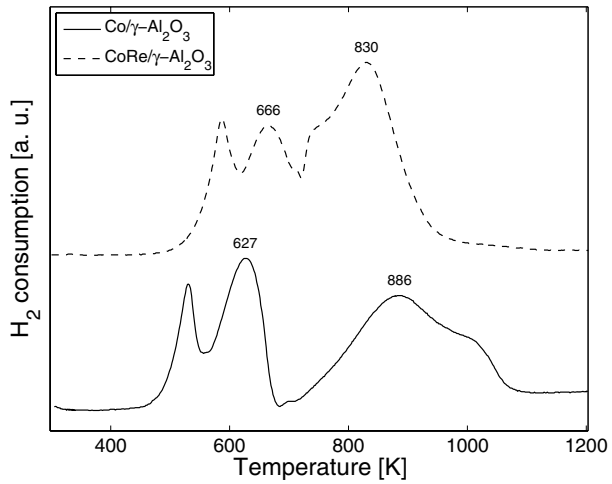

Figure 2.12: Temperature programmed reduction profiles of un-promoted and Re-promoted cobalt supported on γ-Al_2O_3 [24].

2.6 Promoter

A wide variety of promoters have been deliberately added to cobalt based catalysts in order to modify the catalyst properties. According to Morales and Weckhuysen [54], the following elements have been investigated: B, Mg, K, Ti, V, Cr, Mn, Ni, Cu, Zr, Nb, Mo, Ru, Rh, Pd, La, Re, Ir, Pt, Ce, Gd, and Th. This review focuses only on Re. The first application of Re in combination with cobalt for Fischer-Tropsch synthesis was reported in 1986 by Mauldin [55].

From literature, the prominent effect of Re seems to be its beneficial effect on the cobalt reducibility [54]. The promotion occurs via spillover of hydrogen to cobalt oxide and leads to catalysts with enhanced cobalt dispersion [54]. Re reduces at a slightly higher temperature than the temperature of reduction from Co_3O_4 to CoO. Thus, it does not facilitate the reduction of Co_3O_4 to CoO, but only from CoO to cobalt metal (peak 2 and 3 in Figure 2.12). Mauldin and Varnado [56] also reported that rhenium generates better cobalt oxide dispersion during decomposition of the nitrate salt in the catalyst preparation. It also maintained the cobalt oxide dispersion in air at high temperatures.

Mauldin and Varnado [56] incorporated small amounts of rhenium into a Co/TiO_2 catalyst and observed a dramatic improvement in Fischer-Tropsch activity. This activity improvement arose primarily from a significant increase in cobalt dispersion. During use, the catalysts performed with a turnover

number that was unaffected by the presence of rhenium. Also, there was no intrinsic activity difference between the type of cobalt produced, hexagonal close packed phase or face-centred cubic phase.

For cobalt supported on γ-Al_2O_3, Jacobs *et al.* [57] introduced different quantities of rhenium (0.2, 0.5, and 1.0 wt%) to the catalyst and tested the catalysts for Fischer-Tropsch synthesis under realistic conditions (493 K and 19.7 atm). Although presence of rhenium changed the initial CO conversion, the data were consistent with each surface cobalt atom having essentially equivalent activity.

Bertole *et al.* [51] examined the effect of Re on site-time yield using $^{12}CO \rightarrow {}^{13}CO$ isotope transients at reaction steady state. Re present at a Re/Co weight ratio of 0.1 did not affect the intrinsic Fischer-Tropsch synthesis activity. However, some modifications of SiO_2 and Al_2O_3 supports (with MgO, Y_2O_3, ZnO, and Ce_2O_3) reduced site-time yield by up to an order of magnitude.

Storsæter *et al.* [24] observed an increase in the reaction rate when rhenium was added to cobalt supported on γ-Al_2O_3, SiO_2, and TiO_2. For cobalt supported on γ-Al_2O_3 and SiO_2, the increase in activity was proportional to the increase in cobalt dispersion, making the site-time yield constant. However, for cobalt deposited on TiO_2, the cobalt dispersion was unchanged even though the activity of the Re based catalyst was higher. The deviation for TiO_2 supported catalysts is a well-known phenomenon [58].

While it is well known that Re facilitates the reduction of cobalt oxide, different effects on the C_{5+} selectivity have been reported. In some cases, Re has been reported to affect the C_{5+} positively. However, other investigations claim that it has no effect on the selectivity.

For instance, at a Re/Co weight ratio of 0.1, Bertole *et al.* [51] concluded that Re did not affect the Fischer-Tropsch synthesis selectivity. Mauldin and Varnado [56] found a strong effect of rhenium on activity, but concluded that the selectivity was largely unaffected. Das *et al.* [59] found virtually no difference in C_{5+} selectivity for un-promoted and a series of three Re-promoted catalysts (0.2-1.0% Re). The results are presented in Table 2.1.

Storsæter *et al.* [24] investigated the Fischer-Tropsch synthesis behaviour of un-promoted and Re-promoted cobalt supported on γ-Al_2O_3, SiO_2, and TiO_2. As shown in Table 2.1, presence of Re increased the C_{5+} selectivity of the SiO_2 and TiO_2 based catalysts. For cobalt supported on low (15 m^2/g) and high surface alumina (190 m^2/g), Schanke *et al.* [50] found Re to increase the

Table 2.1: Effect of Re on hydrocarbon selectivity.

Reference	Support	Metal loading (wt%)		Selectivity (%)	
		Co	Re	C_{5+}	CH_4
Storsæter *et al.* [24]	γ-Al_2O_3	12	0	80.2	9.7
Storsæter *et al.* [24]	γ-Al_2O_3	12	0.5	80.8	8.8
Storsæter *et al.* [24]	SiO_2	12	0	81.7	9.1
Storsæter *et al.* [24]	SiO_2	12	0.5	83.4	8.7
Storsæter *et al.* [24]	TiO_2	12	0	81.6	10.2
Storsæter *et al.* [24]	TiO_2	12	0.5	84.8	8.9
Schanke *et al.* [50]	γ-Al_2O_3	12	0	81.0	-
Schanke *et al.* [50]	γ-Al_2O_3	12	0.5	82.3	-
Schanke *et al.* [50]	α-Al_2O_3	12	0	85.0	-
Schanke *et al.* [50]	α-Al_2O_3	12	0.5	86.5	-
Das *et al.* [59]	γ-Al_2O_3	15	0	85.6	10.9
Das *et al.* [59]	γ-Al_2O_3	15	0.2	86.2	10.2
Das *et al.* [59]	γ-Al_2O_3	15	0.5	87.5	10.1
Das *et al.* [59]	γ-Al_2O_3	15	1.0	85.9	11.2

selectivity to long-chain hydrocarbons. The beneficial effects were similar in size to those of Storsæter *et al.* [24] (Table 2.1).

2.7 Effect of water

Water is an important product in the Fischer-Tropsch synthesis. The amount produced depends on several factors such as the conversion and the reactor system. Water may affect the catalyst activity, product distribution, and catalyst deactivation rates, which are governed by the choice of both catalyst and support.

An extensive review for the role of water on the performance of supported cobalt is given in Paper I. Only a short summary for cobalt supported on γ-Al_2O_3 will be given here.

2.7.1 Activity and kinetics

Since water forms on the surface during Fischer-Tropsch synthesis, it is not surprising that it influences the kinetics. However, the role of water is a highly complicated matter. Water is known to decrease [24, 34, 59–76] or increase the

catalytic activity [24, 28, 34, 40, 77–84]. In one instance, no effect was seen [85]. Although it is well documented that it influences the kinetics, almost no kinetic equations include a water-term [9]. van Steen and Schulz [86], however, suggested a common rate equation for Fe and Co based catalysts.

The influence of water on Fischer-Tropsch synthesis rates over γ-Al_2O_3 supported cobalt catalysts has been the subject of several studies. In nearly all cases, presence of water was unfortunate for reaction rates [24, 34, 59, 62–71]. Schanke *et al.* [62], on the other hand, observed an initial increase in the reaction rate during the first few hours after addition of water. However, the phenomenon and its magnitude were inconsistent from experiment to experiment.

2.7.2 Deactivation

Deactivation is an inevitable phenomenon in Fischer-Tropsch synthesis. The suggested mechanisms include oxidation, sintering, and solid state reactions rendering inactive cobalt.

Schanke *et al.* [62, 63] found that large amounts of water suppressed the activity of un-promoted and promoted cobalt supported on γ-Al_2O_3. Reoxidation of surface cobalt atoms or highly dispersed cobalt phases, and not bulk cobalt oxidation, was responsible for the loss in activity.

Hilmen *et al.* [64–66] also observed a loss in activity when water was introduced to unpromoted and promoted γ-Al_2O_3 based catalysts. It was observed by Schanke *et al.* [62], Hilmen *et al.* [64, 65], and Storsæter *et al.* [24] that the rhenium-promoted catalysts lost activity more rapidly than their unpromoted counterparts.

Deactivation of unpromoted and promoted cobalt was analysed by X-ray absorption spectroscopic techniques by Jacobs *et al.* [67]. X-ray absorption near edge structure analysis gave evidence of oxidation of a fraction of the cobalt clusters to cobalt aluminate-like species by water produced during reaction. Only the small clusters interacting with the support and clusters deviating from bulk-like behaviour were oxidised. However, extended X-ray absorption fine structure results also strongly suggested that a large part of the deactivation was caused by sintering. Sintering has also been proposed as an explanation for the deactivation of a CoRe/γ-Al_2O_3 catalyst [59].

Jacobs *et al.* [68] studied the effect of water on Co/γ-Al_2O_3 catalysts containing 15 and 25 wt% Co. These catalysts exhibited important differences

in the degree of cobalt interactions with the support surface. For the 15 wt% Co/γ-Al_2O_3 catalyst, which consisted of cobalt clusters between 5 and 6 nm, the oxidation likely included reaction with the support resulting in cobalt aluminate-like species. For the 25 wt% Co/γ-Al_2O_3 catalysts, the oxidation by water for the larger clusters (>10 nm) may be caused by surface oxidation to CoO. The catalysts with smaller cluster sizes were found to be more sensitive to permanent deactivation by water.

Li *et al.* [70] investigated the effect of water for a Pt-promoted Co/γ-Al_2O_3 catalyst in a continuously stirred tank reactor. It was found that small amounts of water (3-25 vol%) led to mild reversible deactivation, whereas larger amounts ($>$ 28 vol%) deactivated the catalyst permanently [71]. While the structure of cobalt remained intact after exposure of small amounts of water, X-ray absorption near edge structure scans indicated formation of species chemically resembling cobalt aluminate after exposure to larger amounts.

As illustrated above, there are three deactivation routes; oxidation of cobalt, sintering, or formation of metal-support compounds.

From a pure thermodynamic point of view, the oxidation of bulk phase metallic cobalt to either CoO or Co_3O_4 is unlikely, while the oxidation to $CoAl_2O_4$ is kinetically restricted [69]. Although bulk oxidation of cobalt metal is thermodynamically not favourable, a study by van Steen *et al.* [87] showed that oxidation of nano-sized cobalt crystallites seems to be thermodynamically possible. It was concluded that cobalt crystallites $<$ 4-5 nm will oxidise under realistic Fischer-Tropsch synthesis conditions. Similarly, Iglesia [40, 41] claimed that cobalt crystallites below 5-6 nm will oxidise and deactivate rapidly under realistic Fischer-Tropsch synthesis conditions.

Recently, Saib *et al.* [88] did X-ray absorption spectroscopy analyses of a Co/Pt/Al_2O_3 catalysts which consisted predominantly of cobalt crystallites of 6 nm in size. No oxidation of cobalt to cobalt oxide or cobalt aluminate took place during Fischer-Tropsch synthesis. Saib *et al.* [88] concluded that oxidation can be ruled out as a deactivation mechanism of cobalt crystallites larger or equal to 6 nm in diameter.

2.8 State of the art

There are many open questions related to cobalt catalysts and their performance in Fischer-Tropsch synthesis. This chapter has addressed a few. To summarise, some key questions are:

- How does presence of NO_x during calcination affect the catalyst and its catalytic performance?
- How is cobalt located in porous materials?
- Which factors determine the Fischer-Tropsch synthesis product selectivity?
- How does presence of rhenium influence the C_{5+} selectivity of cobalt supported catalysts?
- Why does the C_{5+} selectivity increase with increasing water concentration?
- What is the predominant cobalt deactivation route?

Chapter 3

Experimental

This chapter gives all information necessary to reproduce the experiments. Flow sheets are given only for custom-built apparatuses.

3.1 Catalyst preparation

All catalysts were prepared by one-step incipient wetness (co)-impregnation of different metal oxide supports (γ-Al_2O_3, α-Al_2O_3, SiO_2, TiO_2) with aqueous solutions of cobalt nitrate hexahydrate, $Co(NO_3)_2{\cdot}6H_2O$, and for the Re promoted catalysts, also perrhenic acid, $HReO_4$. The cobalt and rhenium loadings were 12 or 20 and 0 or 0.5 wt%, respectively.

All supports except one were pre-sieved to 53-90 μm and pre-calcined in air for 10 h at different temperatures prior to impregnation. The γ-Al_2O_3 and α-Al_2O_3 phases were produced by calcination at 773 and 1403 K, respectively. The SiO_2 support was calcined at 773 K. In order to obtain the rutile phase, the TiO_2 support was treated at 973 K. In all cases, a ramping rate of 1 K/min was used to heat the samples from ambient to the final calcination temperature. One support of boehmite nature was not calcined, but pre-sieved to 53-90 μm.

The point incipient wetness was determined by drop-wise addition of water to the pre-calcined supports until the pores were completely filled. The understanding of the end point may vary from laboratory to laboratory and, therefore, give different scenarios, from a completely dry appearance to a sticky snow-like. It should also be mentioned that in this work, free flowing liquid was never present.

After the water absorptivity was known (ml/g), the same specific volume of metal precursor(s) was added to the pre-treated supports. Approximately 30 g of support was used. The mixture was then thoroughly mixed to obtain homogeneity. It was subsequently placed in a furnace kept at 383 K. The total drying time was 3 h in which the sample was stirred gently every quarter the first hour, and every half-an-hour the last two hours.

The dried samples were calcined under air in a fixed-bed quartz reactor (inner diameter = 40 mm) at 573 K for 16 h. The gas was directed through the samples at a flow rate of 0.2 L/(g · h). A gradient of 2 K/min was used to heat the samples from ambient temperature to 573 K.

After calcination, the catalysts were sieved to 53-90 μm. Further treatment was done *in situ*.

For clarity, all the steps in catalyst preparation are shown in Figure 3.1.

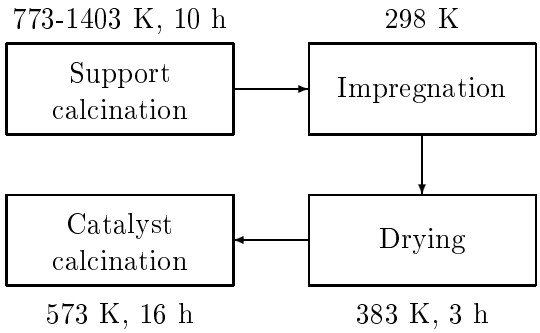

Figure 3.1: Catalyst preparation steps.

3.2 Support and catalyst characterisation

3.2.1 X-ray diffraction

X-ray diffraction patterns were recorded for all the supports and catalysts at ambient temperature on a Siemens D5005 X-ray diffractometer using CuKα radiation. The samples were finely ground and placed in a sample holder prior to measurement. The X-ray tube voltage was set to 40 kV and the current to 50 mA.

For phase identification of supports and catalysts, data were collected in the 2θ range between 10 and 90° using a step size of 0.04° and counting for 15 s at each step. Peaks were identified by comparison with standards in a database [89].

Table 3.1: Overview of the different X-ray diffraction experiments.

Sample	2θ range (°)	Step size (°)	Step time (s)
Support	10-90	0.04	15
Catalyst	10-90	0.04	15
Catalyst	32-43	0.04	150

New scans were recorded for the catalysts for determination of crystallite size. In order to obtain a high signal-to-noise ratio and, consequently, minimise the experimental error, the step time was increased to 150 s. The new scans were recorded in the 2θ range between 32 and 43°. The step size was still 0.04°.

An overview of the different X-ray diffraction experiments is presented in Table 3.1.

After data uptake, the contribution of CuKα_2 radiation to the diffractogram was stripped in the computer software "DIFFRAC^{plus}" by Bruker AXS Inc. [89].

In order to determine the instrumental line broadening, lanthanum hexaboride, LaB_6, was run as reference sample. LaB_6 exhibits instrumental broadening only.

The average Co_3O_4 crystallite thickness was calculated applying the Scherrer equation on the (311) diffraction peak located at $2\theta = 36.9°$. The shape factor, K, was set to 0.89. β in the Scherrer equation was calculated by:

$$\beta = \sqrt{B^2 - b^2} \tag{3.1}$$

where B is the experimental width of the Co_3O_4 reflection placed at $2\theta = 36.9°$ and b is the instrumental width of the LaB_6 peak located at $2\theta = 37.5°$.

The average spherical Co_3O_4 particle size was calculated multiplying the crystallite thickness by a factor of 4/3 [90].

3.2.2 Temperature programmed reduction

An in-house built equipment was used for temperature programmed reduction. It is described in detail by Blekkan *et al.* [91] and illustrated in Figure 3.2. Initially, the catalyst precursors were loaded into a U-shaped quartz reactor which in turn was placed inside an electrical furnace. A thermocouple was installed inside the reactor about one centimetre above the samples. The

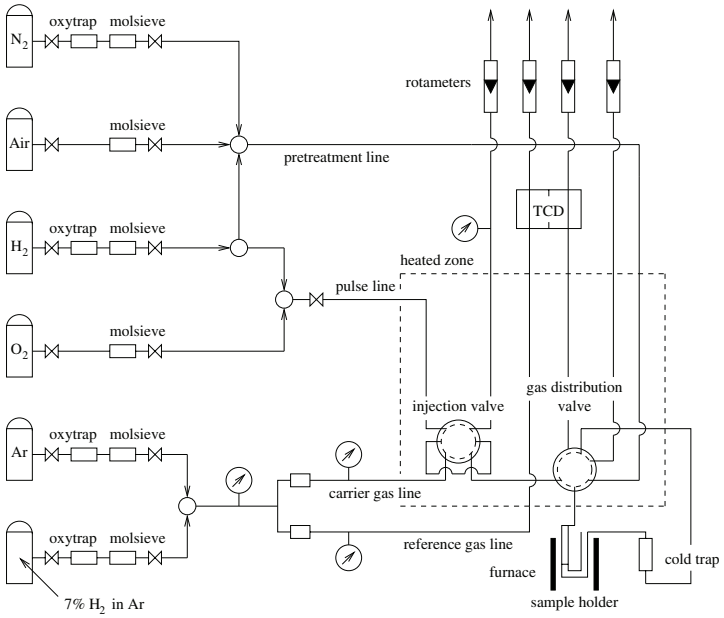

Figure 3.2: Apparatus used for temperature programmed reduction and oxygen titration (from Blekkan *et al.* [91]).

temperature in the furnace was controlled by a second thermocouple located outside the reactor, but in the same height as the first one.

The samples were exposed to a reducing gas mixture consisting of 7% H_2 in Ar while the temperature was increased from ambient to 1203 K at 10 K/min. The gas flow rate was 30 ml/min.

Reduction profiles were also recorded after *in situ* reduction. In this case, the calcined samples were reduced in a flow of pure hydrogen at 623 K. A ramp rate of 1 K/min was used to increase the temperature from ambient to the final reduction temperature. The samples were held at 623 K for 16 h before subsequently cooling to 298 K. The catalysts were flushed with He for 1 h, and finally heated at a rate of 10 K/min to 1203 K in 7% H_2 in Ar.

Water and other condensable components in the product mixtures were eliminated in a cold trap consisting of 2-propanol and dry ice. The consumption of hydrogen was measured by comparing the thermal conductivity of the reference and product gas. This was done by a Shimadzu GC-8A gas chromatograph. Calibration was done using Ag_2O.

3.2.3 Pulse oxidaton

Oxygen titration was performed in the equipment described in Section 3.2.2. The catalyst samples were reduced *in situ* under flowing hydrogen for 16 h at 623 K. The temperature was linearly ramped from ambient to the final reduction temperature at a rate of 1 K/min. After reduction, the samples were flushed in flowing He at 623 K for 1 h and subsequently heated to 673 K at 5 K/min under the same gaseous atmosphere.

A series of oxygen pulses were passed through the catalyst beds at 673 K [92]. One pulse of gas (50 μl, 373 K, 1.25 bar) corresponded to 2.04 μmol. The amount of oxygen consumed by the samples was calculated from the number of pulses and the known pulse volume. The degree of reduction was calculated assuming that all cobalt in metallic form was oxidised to Co_3O_4:

$$3Co^0 + 2O_2 \rightarrow Co_3O_4 \tag{3.2}$$

Any oxidation of Re was not considered in the calculations.

3.2.4 Hydrogen chemisorption

Hydrogen chemisorption was performed on a Micromeritics ASAP 2010C unit. The catalysts were loaded into a U-shaped quartz reactor and placed inside an electric furnace. A thermocouple located outside the reactor, but in the same height as the sample represented the sample temperature. The samples were initially evacuated at 313 K for one hour, and reduced *in situ* in flowing hydrogen at 623 K for 16 h. The temperature was increased by 1 K/min from 313 to 623 K. After reduction, the samples were evacuated for 1 h at 603 K, evacuated for 30 min at 373 K, and subsequently cooled to 313 K.

An adsorption isotherm was constructed at 313 K based on the adsorbed amount of hydrogen at 11 different pressures in the range 15-500 mmHg. The quantity of gas required to form a unimolecular coverage on the surface was calculated by intrapolating the straight-line portion of the isotherm, typically the eight last points, to zero pressure. Furthermore, in order to calculate the cobalt dispersion, it was assumed that two cobalt sites are covered by one hydrogen molecule, and that rhenium does not adsorb any hydrogen.

Cobalt particle sizes were estimated from the cobalt dispersion. For monodisperse spherical particles with site density of 14.6 atoms/nm^2 [93], the relation between cobalt dispersion and particle size is:

$$d(\mathrm{Co}^0)(\mathrm{nm}) = \frac{96}{D(\%)} \tag{3.3}$$

3.2.5 N_2 adsorption/desorption

Nitrogen adsorption/desorption isotherms for all supports and catalysts were measured on a Micromeritics TriStar 3000 instrument, and the data were collected at liquid nitrogen temperature, 77 K. The samples were outgassed at 573 K overnight prior to measurement.

The surface area was calculated from the Brunauer-Emmett-Teller (BET) equation. The monolayer capacity, V_m, was obtained from a plot of $P/V(P_0 - P)$ versus P/P_0 in the pressure range $0 < P/P_0 < 0.30$.

The total pore volume and pore size distribution were found applying the Barrett-Joyner-Halenda (BJH) method [94]. The nitrogen desorption branch was chosen for pore size analysis [95].

3.2.6 Mercury porosimetry

Pore size measurements were performed using a Carlo Erba Porosimeter 2000 by mercury intrusion. The samples were evacuated and dried at 423 K prior to analysis. A cylindrical pore model was assumed.

3.2.7 X-ray absorption spectroscopy

Transmission XAS data were collected at the Swiss-Norwegian Beamline at the European Synchrotron Radiation Facility (ESRF), France. Spectra were obtained at the cobalt K edge (7,709 eV) using a channel-cut Si(111) monochromator. Higher order harmonics were rejected by means of a chromium-coated mirror angled at 3.5 mrad with respect to the beam to give a cut-off energy of approximately 14 keV. The beam currents ranged from 130 - 200 mA at 6.0 GeV. The maximum resolution ($\Delta E/E$) of the Si(111) bandpass is $1.4 \cdot 10^{-4}$ using a beam of size $0.6 \cdot 7.2$ mm. Ion chamber detectors with their gases at ambient temperature and pressure were used for measuring the intensities of the incident (I_0) and transmitted (I_t) X-rays.

The amounts of material in the samples were calculated from element mass fractions and the absorption coefficients of the constituent elements just above the absorption edge to give an absorber optical thickness close to 2.0 absorption lengths. The samples were loaded into a Lytle *in situ* reactor-cell [96]

and reduced in a mixture of H_2 (5%) in He (purity: 99.995%: flow rate 30 ml/min) by heating at a rate of 5 K/min from ambient temperature to 673 K. The samples were kept at 673 K for 3 h. Two EXAFS scans were recorded and summed at room temperature for each sample before and after reduction. XANES scans were taken continuously during reduction.

The energy calibration was checked by measuring the spectrum of a cobalt foil (thickness 0.0125 mm) with the energy of the first inflection point being defined as the edge energy.

The XAS data analysis program WinXAS v. 3.1 [97] was used for examining the Co K absorption edge XANES data. The identification of the number of phases present during *in situ* reduction was done by a principal component analysis (PCA) of the experimental spectra [98]. Reference spectra were then used in a linear combination fitting procedure to determine the quantity of each phase present. The algorithm uses a least squares procedure to refine the sum of a given number of reference spectra to an experimental spectrum.

The XAS data were converted to k-space, summed and background subtracted to yield the EXAFS function $\chi(k)$ using WinXAS v. 3.1 [97]. Model fitting was carried out with *EXCURV98* using curved-wave theory and *ab initio* phase shifts [99, 100]. A cobalt metal foil (0.0125 mm), CoO, Co_3O_4, and $CoAl_2O_4$ were used as model compounds to check the validity of the *ab initio* phase shifts and establish the general amplitude reduction factor. Cobalt K-edge EXAFS data were fitted in the range Δk = 3.0 - 14.0 Å^{-1} using a Fourier filtering window ΔR = 1.0 - 3.2 Å.

The extent of reduction from EXAFS was obtained by looking at the fractional coordination number of the nearest Co-O coordination shell. The bulk cobalt oxides have Co-O coordination of 6 (N_{ox}). The Co-O coordination number for the reduced catalysts (N_{red}) will be lower, depending on the extent of reduction. For a completely reduced catalyst, N_{red} will be zero. The degree of reduction is thus given by the expression 1 - $N_{\mathrm{red}}/N_{\mathrm{ox}}$.

3.2.8 Electron microscopy

For ultramicrotomy, small amounts of the catalysts were embedded in a two component epoxy resin and stored overnight at room temperature. Thin slices (nominally approximately 40 nm) were obtained by cutting the embedded catalyst with a diamond knife using a Reichert-Jung ultramicrotome and collected on a standard perforated carbon support Cu mesh grid.

Transmission electron microscope (TEM) and scanning transmission electron microscope (STEM) analysis was performed using a JEOL 2010F instrument operating at 200 kV equipped with an Oxford Instruments X-ray detector for energy dispersive spectroscopy (EDS) composition analysis. For EDS, the microscope was operated in scanning transmission electron microscope mode with a nominal probe diameter of approximately 0.7 nm.

STEM images were acquired using an annular dark field detector which provides contrast that has a strong dependence on atomic number. This is particularly useful for distinguishing higher atomic number catalyst particles, which appear bright relative to a lower atomic number support.

Conventional TEM was performed under bright-field diffraction contrast conditions. Dark-field imaging and selected area diffraction were performed in a Philips CM30 instrument operated at 200 kV.

3.3 Fischer-Tropsch synthesis

Fischer-Tropsch synthesis was run in two parallel fixed-bed reactors (inner diameter 10 mm) made of stainless steel. A detailed illustration of the apparatus is given in Figure 3.3.

Available reactant gases included synthesis gas, hydrogen, and helium. All gases were purified and dried before use by Alltech oxytraps and Alltech gas driers. CO in the synthesis gas can react with iron in the gas bottle material and form iron carbonyl. To remove this poison, the synthesis gas was sent through a Pb(II)O trap.

Initially, the catalyst samples were diluted with inert SiC particles in order to ensure isothermal conditions in the catalytic zone. The weight ratio between catalyst and SiC was 1:5. After the catalysts were loaded in the reactor, the reactor was surrounded by aluminium blocks to further minimise temperature gradients in the catalytic bed. The system was then flushed with He for one hour.

To ensure safe operation, the system was leak tested in 20 bar of helium overnight. After passed leak test, the pressure was relieved to atmospheric. The catalysts were then reduced at 1 bar and 623 K for 16 h in flowing hydrogen (250 ml/min). A temperature gradient of 1 K/min was used to ramp the temperature from ambient to 623 K. After reduction, the samples were cooled to 443 K under hydrogen.

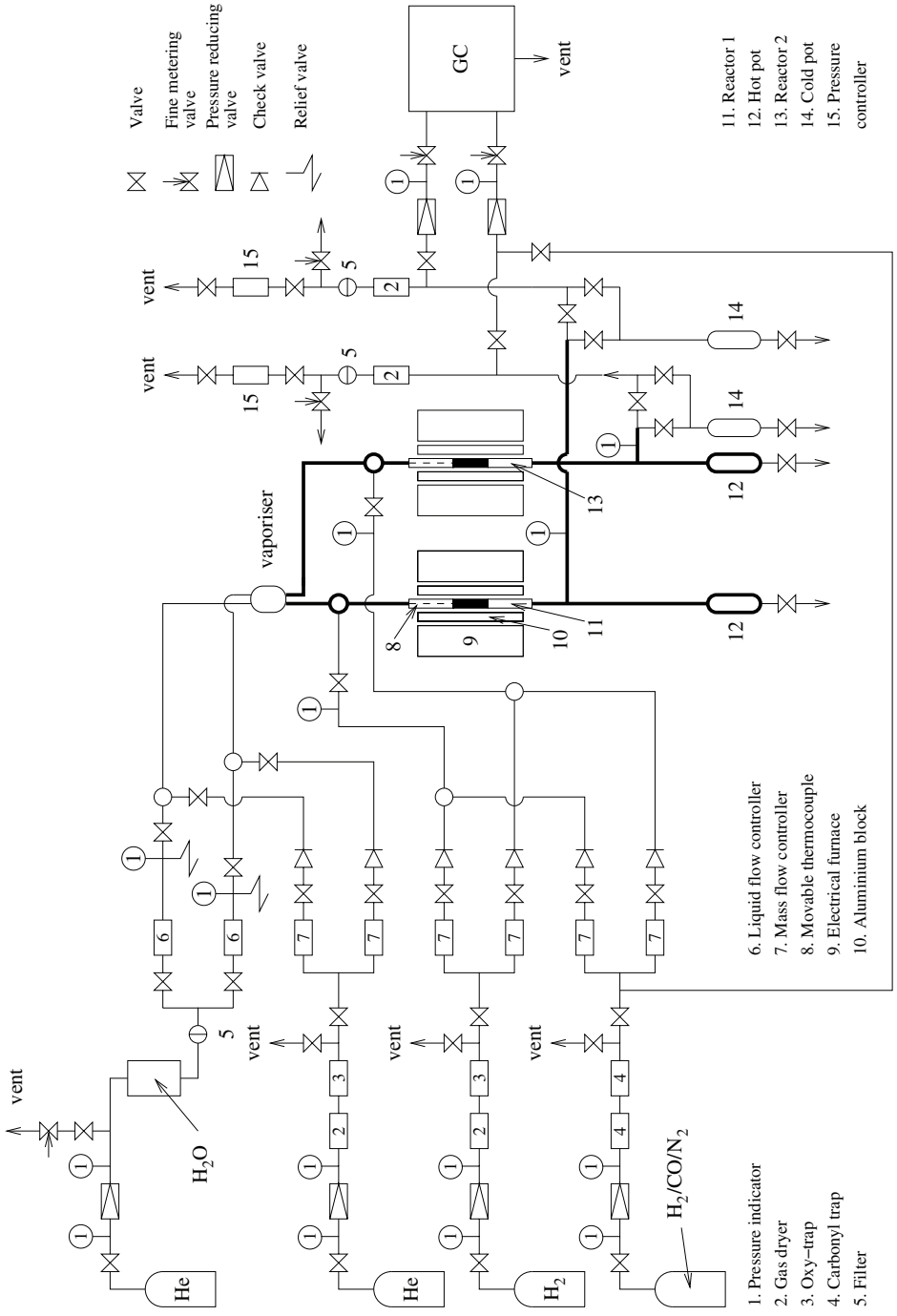

Figure 3.3: Fischer-Tropsch synthesis setup.

The system was then pressurised to 20 bar at 443 K under equal flow rates of hydrogen and helium (125 ml/min). At 20 bar, the hydrogen flow was stopped and the helium flow increased to 250 ml/min in order to flush the reactor system. After 1 h, the helium flow was replaced by synthesis gas. The composition of the synthesis gas was approximately 65 mol% H_2, 32 mol% CO, and 3 mol% N_2 (internal standard). To avoid run-away and catalyst deactivation, the catalysts were heated slowly to the reaction temperature 483 K. Movable thermocouples were installed into the reactor in order to measure the average temperature in the catalytic beds.

The effect of water on the Fischer-Tropsch synthesis performance was evaluated for all catalysts. In order to generate water vapour, liquid water was sent into a vaporiser kept at 623 K. The water flow rates were adjusted by Hi-Tec liquid flow controllers. Helium was passed through the water tank in order to degas and pressurise the deionised water prior to experiment start-up. The total pressure and the flow rate of synthesis gas were kept constant during external water addition. Thus, the CO and H_2 partial pressures were reduced as water was introduced to the reactor.

The experiments were divided into five periods, each of 26 or 28 h. The following conditions were used:

Period 1: Synthesis gas at flow rate 250 ml/min, F_1.

Period 2: Synthesis gas at adjusted flow rate, F_2, to give a target value of 50% CO conversion.

Period 3: Synthesis gas at flow rate F_2 and 20 mol% water vapour at reactor inlet.

Period 4: Synthesis gas at flow rate F_2 and 33 mol% water vapour at reactor inlet.

Period 5: Synthesis gas at flow rate F_2.

Experiments were also done without any water addition. For the "dry" experiments, period 1 was identical to the first period of the "wet experiment". The conditions during period 2 were also identical, but extended by 78 h.

Heavy products were removed in a hot trap (358-368 K) while lighter compounds were collected in a cold trap (298 K). The light gases were analysed

on an HP5890 gas chromatograph. H_2, N_2 (internal standard), CO, CH_4, and CO_2 were separated in a 10 ft · 1/8" inner diameter Carbosieve SII packed column and analysed on the TCD. Hydrocarbon products were separated in a 30 m · 0.53 mm inner diameter GS-Q capillary column and detected on the FID. CH_4 was used to combine the TCD and FID analyses.

Activity is reported as cobalt-time yield (mol CO/(mol Co · s)). The C_{5+} selectivity was calculated by subtracting the amount of C_1-C_4 hydrocarbons and CO_2 in the product gas mixture from the total mass balance.

Chapter 4

Results and discussion

This chapter briefly summarises the results from this work. Complete results and more detailed discussions are given in Papers A to H. Paper I is a review article and the reader is referred to the complete article.

4.1 *Paper A: Effect of calcination atmosphere and temperature on γ-Al_2O_3 supported cobalt Fischer-Tropsch catalysts*

A systematic study of the effect of calcination temperature and atmosphere on γ-Al_2O_3 supported cobalt Fischer-Tropsch catalysts was carried out. One common precursor for all the catalysts was prepared by incipient wetness impregnation of γ-Al_2O_3 with an aqueous solution containing the required amounts of cobalt precursor to give a loading of 20 wt%. Cobalt nitrate hexahydrate was used as cobalt source. The calcination parameters are given in Table 4.1.

As shown in Figure 4.1, X-ray diffraction patterns of the dried, but uncalcined precursor sample confirmed the presence of γ-Al_2O_3 and cobalt nitrate hydrate, $Co(NO_3)_2{\cdot}4H_2O$ [89]. Reflections of Co_3O_4 were also present [89], although of modest intensity. For all the 32 calcined catalysts, X-ray diffraction patterns showed presence of γ-Al_2O_3 and Co_3O_4 [89]. One example (catalyst B7) is given in Figure 4.1. Although all $Co(NO_3)_2{\cdot}4H_2O$ had not been decomposed, the concentration was too low to give detectable diffraction peaks.

The average Co_3O_4 crystallite size was calculated from the Scherrer equation [101] using the (311) diffraction peak located at $2\theta = 36.9°$. For series B, C, and D, the crystallite size increased slightly (approximately from 10 to 12 nm) with increasing temperature of calcination. In contrast, for series A, there

Table 4.1: Calcination parameters.

Series	Gas mixture	Flow (Nml/min)	Temperature (K)							
			1	2	3	4	5	6	7	8
A	Air/50% steam	30	473	523	548	573	598	623	673	723
B	Air	30	473	523	548	573	598	623	673	723
C	Air	50	473	523	548	573	598	623	673	723
D	N_2	30	473	523	548	573	598	623	673	723

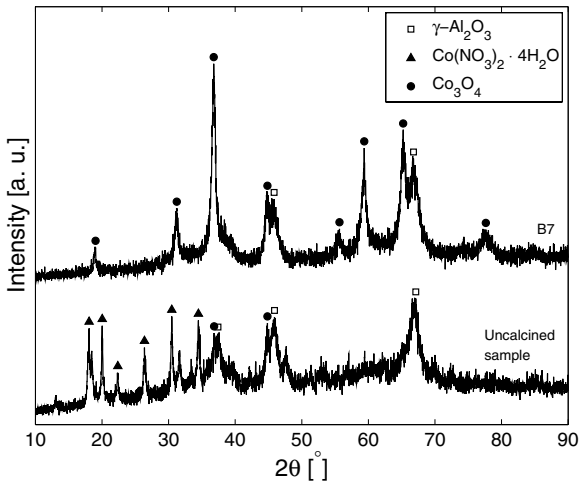

Figure 4.1: X-ray diffraction patterns.

was no difference in the crystallite size for the eight samples. The crystallite size for the samples calcined at 523 K increased in the series order C $\leq$ D $\leq$ B $<$ A. No significant variation in crystallite size was observed after calcination at 673 K.

As shown in Figure 4.2, temperature programmed reduction profiles contained three main reduction peaks. The first reduction peak represents reduction of residual cobalt nitrate remaining after calcination [102]. The peak area decreased with increasing temperature of calcination. The two last reduction peaks can be assigned to a two-step reduction of Co_3O_4 to Co^0 via CoO as an intermediate species.

While the nitrogen content of the uncalcined sample was 6.3 wt%, Figure 4.3 shows that the amount of nitrogen in the calcined samples varied between 0.1 and 1.2 wt%. Thus, between 81 and 98% of the supported cobalt nitrate was decomposed into water and nitrogen oxides during calcination. Larger amounts of cobalt nitrate were decomposed at high temperatures. Thus, Figure 4.3 essentially proves that the low temperature reduction peak represents reduction of supported cobalt nitrate.

At intermediate calcination temperatures, the amount of residual nitrate increased in the following series order D $<$ C $<$ B $<$ A (Figure 4.3). The difference can probably be related to the water amount and flow rate of the calcination agent. A dry gas in combination with a high flow rate minimises

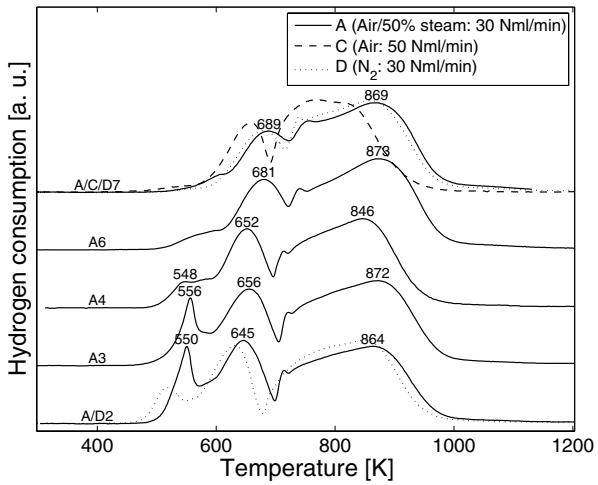

Figure 4.2: Temperature programmed reduction profiles.

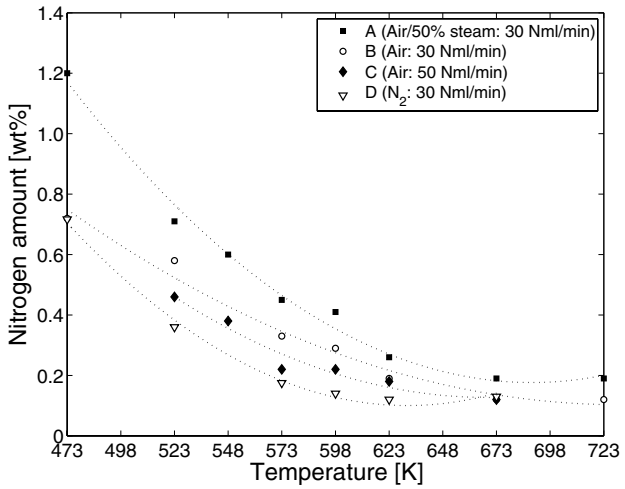

Figure 4.3: Effect of calcination temperature and atmosphere on the nitrogen amount.

the amount of nitrogen oxides and water in the calcination atmosphere. This allows the decomposition process to occur to a greater extent, in agreement with Le Châtelier's principle.

Due to the large number of samples, cobalt dispersion values were collected only for a selection of catalysts. The results are presented in Figure 4.4. Three main conclusions can be drawn. First, with the exception of series A, the cobalt dispersion decreased with increasing temperature of calcination. Two possible explanations exist: crystallite growth or lower reducibility of cobalt. Second, the cobalt dispersion was similar for all the catalysts calcined at 673 K. X-ray diffraction data also showed similar crystallite size for the high-temperature calcined catalysts. Third, the effect of calcination atmosphere came into play at lower temperatures. At 523 K, the cobalt dispersion increased in the series order A $<$ D $\approx$ B $<$ C. The difference is probably related to how efficiently water and nitrogen oxides were removed from the calcination atmosphere.

To conclude, in order to maximise the cobalt dispersion, it is necessary to remove the cobalt precursor decomposition products (NO_x and H_2O) efficiently and perform the calcination at low temperatures. However, it is not necessarily always desirable to maximise the cobalt dispersion. As will be demonstrated in Section 4.4, small particles seem to give lower C_{5+} selectivity than large particles.

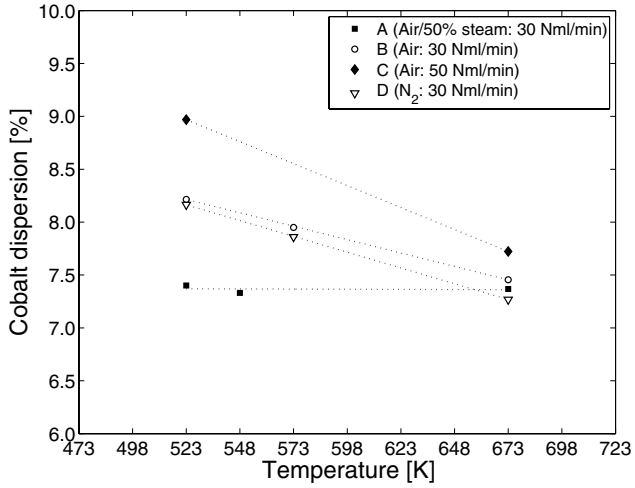

Figure 4.4: Effect of calcination temperature and atmosphere on the cobalt dispersion.

The Fischer-Tropsch performance of two catalysts calcined at the same temperature, but at different air flow rates was evaluated. No significant effect of the air flow rate was found on the site-time yield or C_{5+} selectivity, but a high flow rate resulted in 30% higher activity per gram catalyst.

4.2 *Paper B: Electron microscopy study of γ-Al_2O_3 supported cobalt Fischer-Tropsch catalysts*

An electron microscopy study of γ-Al_2O_3 supported cobalt Fischer-Tropsch synthesis catalysts with different pore sizes was done. It is important to bear in mind that the catalysts subjected to electron microscopy were in their calcined state. The results may, therefore, not be exactly representative of the catalysts after reduction. The catalysts were prepared by incipient wetness impregnation to give 20 wt% cobalt and 0.5 wt% rhenium. The support and catalyst nomenclature is based on the γ-Al_2O_3 pore sizes: "NPA" (narrow pore alumina), "MPA" (medium pore alumina), and "WPA" (wide pore alumina). After cobalt and rhenium impregnation, the catalyst nomenclature was "CoRe/NPA", "CoRe/MPA", and "CoRe/WPA".

Adsorption/desorption isotherms are given in Figure 4.5. Three types of hysteresis loop and, therefore, three types of pore geometry were represented by the three supports. In the absence of a universal model, the Barrett-Joyner-Halenda model was chosen for calculation of pore sizes. Figure 4.6 gives the pore size distributions of the γ-Al_2O_3 supports and the corresponding impregnated samples. Although the starting support in all cases was γ-Al_2O_3, the physical parameters varied significantly. Impregnation, drying, and calcination did not significantly modify the pore size distributions, but merely reduced the nitrogen uptake.

X-ray diffraction patterns of the calcined catalysts confirmed the presence of γ-Al_2O_3 and Co_3O_4 [89]. Figure 4.7 (filled squares) shows relatively large variations in Co_3O_4 particle size. The size could be correlated with the support pore diameter. According to Figure 4.7, the average Co_3O_4 particle size was larger than the average support pore diameter. Thus, the majority of the particles were apparently located on the exterior of the supports. Comparison of pore diameter and particle size for location of the particles should, however, be done with care. In fact, the particles are probably located inside the pore system. The conflicting results in Figure 4.7 can be related to the choice of pore geometry model. In reality, no simple pore geometry exists.

Rytter *et al.* [103] used transmission electron microscopy to visualise the pores

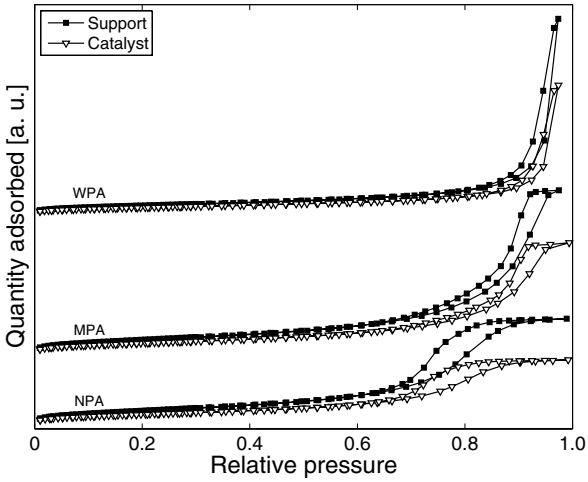

Figure 4.5: Nitrogen adsorption/desorption isotherms.

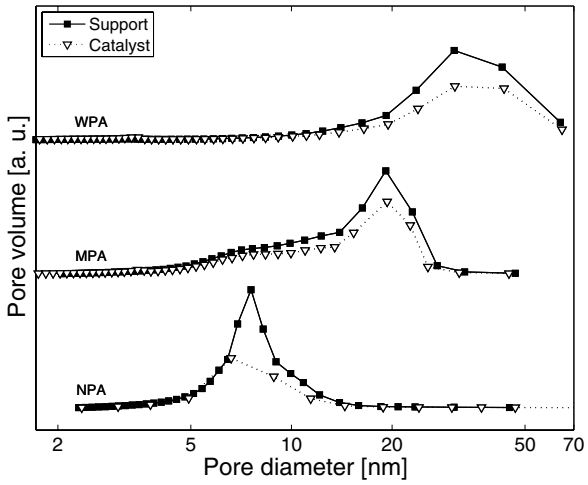

Figure 4.6: Pore size distribution calculated from the Barrett-Joyner-Halenda method.

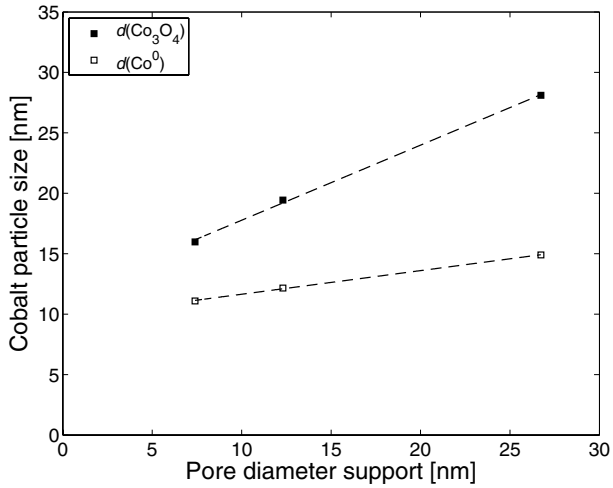

Figure 4.7: Cobalt particle size data.

and the Co/γ-Al_2O_3 interphase. Indeed, a simple pore structure with the metal oxide impregnated to the walls of the pores did not exist. Instead, the alumina crystals were entangled into each other in what appeared to be a chaotic fashion. Furthermore, the cobalt agglomerates stretched over a number of alumina crystals and so-called pores.

To conclude, the calculated Co_3O_4 particle size can very well be larger than calculated pore size even though the particles actually are located inside the pores. However, it is important to stress out that the pore size distributions in Figure 4.6 most likely represent real differences, but that the actual numbers may be biased.

As shown in Figure 4.7 (open squares), the cobalt metal particle sizes measured by hydrogen chemisorption also followed the pore size of the supports. The difference between the Co_3O_4 particle size and Co^0 particle size increased with increasing support pore diameter.

Figure 4.8 shows a dark-field STEM micrograph (a) and complementary mapping (b)-(e) of catalyst CoRe/MPA. In (a), Co_3O_4 appears as bright, spherical aggregates embedded in the surrounding amorphous γ-Al_2O_3 support. The support appears grey relative to the Co_3O_4 because of its lower average atomic number. The distribution of the phases in the STEM image was confirmed by EDS mapping of Co, Re, Al and O in the same field of view ((b)-(e)). The results indicate that most or all of the Re was associated with the Co_3O_4.

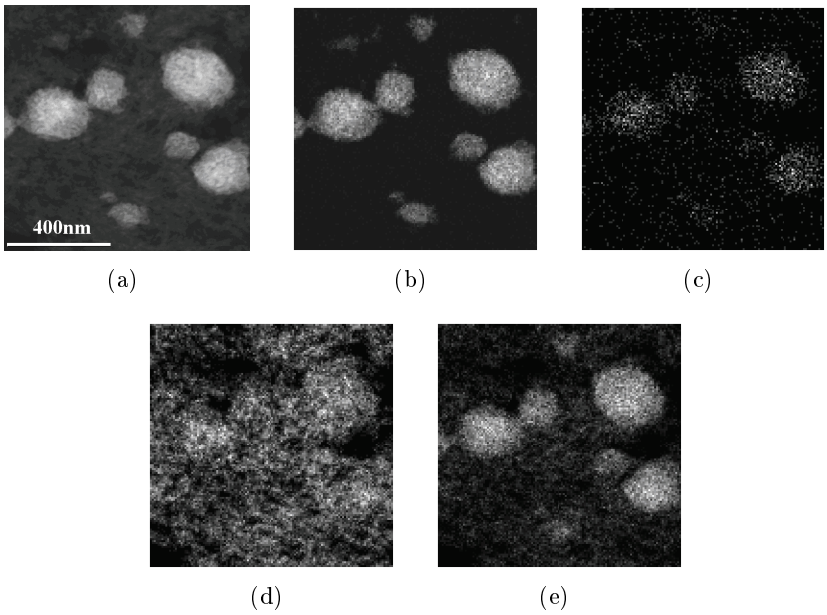

Figure 4.8: Dark-field STEM micrograph and complementary EDS mapping of catalyst CoRe/MPA (a), Co map (b), Re map (c), Al map (d), O map (e).

Bright-field TEM micrographs of the catalysts indicated significant variations in average aggregate size. One image is shown in Figure 4.9. While the average aggregate size of CoRe/NPA was 77 nm, the corresponding sizes of catalysts CoRe/MPA and CoRe/WPA were similar and close to 150 nm. Due to the higher density and stronger diffraction from the more crystalline Co_3O_4 particles relative to the γ-Al_2O_3 support, the Co_3O_4 aggregates are dark relative to the alumina support.

More detailed analysis of aggregates shows that these can tend to grow with particles roughly aligned in a common crystallographic orientation. This is illustrated in Figure 4.10. The dark-field image shows bright contrast over the whole aggregate, suggesting a common diffraction condition for most of the particles in the aggregate. This is confirmed by the diffraction pattern that was recorded from an area in the sample including the entire aggregate. It shows a clean systematic row based on the (220) Co_3O_4 reflection. This is consistent with cobalt having crystallised not as independent particles, but as an interconnected network, with a roughly common crystallographic orientation, within the matrix pore structure. Other diffraction is from discrete, randomly oriented Co_3O_4 particles from the aggregate and the alumina support.

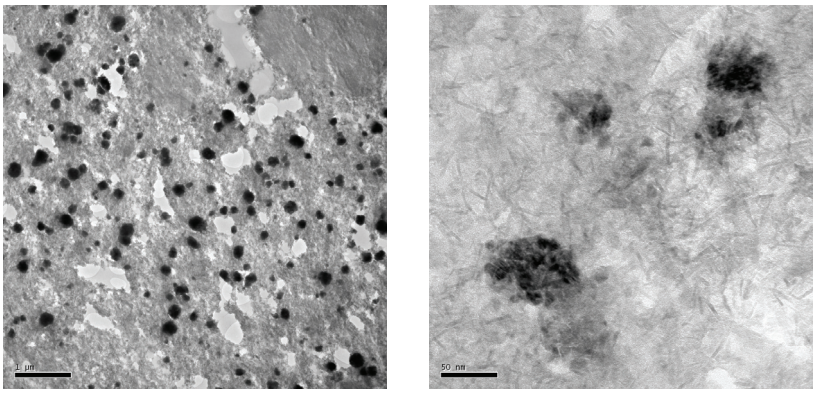

(a) (b)

Figure 4.9: Bright-field TEM micrographs of catalyst CoRe/MPA (low magnification (a), higher magnification (b)).

Although the cobalt-time yields varied substantially (4.6-6.7 $\cdot$ 10^{-3} mol CO/ (mol Co $\cdot$ s)) for the three catalysts, the site-time yields were constant (58-64 $\cdot$ 10^{-3} s^{-1}). Variations in C_{5+} selectivity were also observed. The numbers were 80.6, 82.1, and 84.1% for catalysts CoRe/NPA, CoRe/MPA, and CoRe/WPA. These variations cannot be directly ascribed to variations in aggregate size or particle appearance. Exactly how these parameters influence the catalytic performance remain unknown. Nevertheless, Storsæter *et al.* [33] observed that when Co_3O_4 appeared as single crystals as on α-Al_2O_3 and TiO_2, the C_{5+} selectivity was high. For γ-Al_2O_3, Co_3O_4 was located in aggregates and the selectivity was lower.

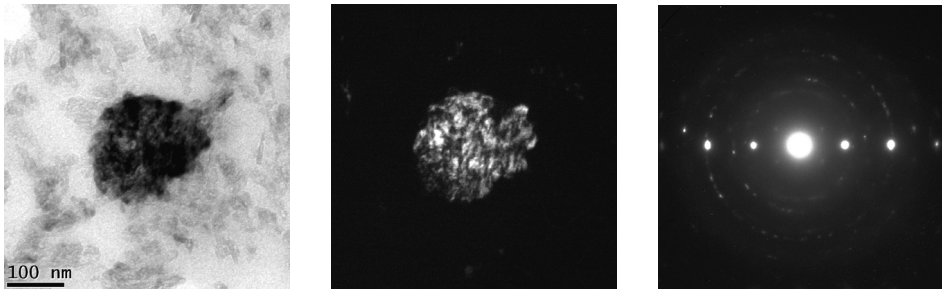

(a) (b) (c)

Figure 4.10: Bright-field (a) and dark-field image (b), and a diffraction pattern (c) recorded from an aggregate in CoRe/MPA.

The activity and selectivity results confirm the significant influence that the pore sizes of the starting γ-Al_2O_3 has on the catalytic properties. While the activity of narrow-pore catalysts is high because of high cobalt dispersion, the C_{5+} selectivity is low most likely because of small cobalt particles [104] or possibly small cobalt aggregates. The wide-pore based catalysts have the opposite properties. These catalysts have large cobalt particles and large cobalt aggregates.

4.3 *Paper C: Identification of cobalt species during temperature programmed reduction of Fischer-Tropsch catalysts*

An *in situ* X-ray absorption spectroscopic (XAS) study of the reduction behaviour of a series rhenium-promoted supported cobalt Fischer-Tropsch catalysts was performed at the cobalt K absorption edge. The catalysts were prepared by incipient wetness impregnation to give 12 or 20 wt% cobalt and 0.5 wt% rhenium. Information about supports and catalysts is given in Table 4.2.

Apart from the peaks indicative of the various supports, X-ray diffraction patterns of the calcined catalysts confirmed the presence of Co_3O_4 [89]. The average Co_3O_4 particle size is given in Table 4.3.

Temperature programmed reduction profiles are given in Figure 4.11. For the γ-Al_2O_3 based samples, reduction peaks appeared at 506 and 558 K. These can be ascribed to reduction of supported cobalt nitrate remaining after cal-

Table 4.2: Surface area and pore characteristics.

Sample	Surface area (m^2/g)	Pore diameter (nm)	Pore volume (cm^3/g)
SiO_2	333	25.2	2.28
12CoRe/SiO_2	302	12.0	1.10
TiO_2	9.3	844	1.41
12CoRe/TiO_2	12	790	0.90
α-Al_2O_3	17	150	0.38
20CoRe/α-Al_2O_3	23	150	0.27
γ-Al_2O_3[§]	186	12.3	0.73
20CoRe/γ-Al_2O_3[§]	148	11.6	0.50
γ-Al_2O_3	196	7.1	0.49
12CoRe/γ-Al_2O_3	155	6.8	0.36

Table 4.3: Co_3O_4 particle size as calculated from X-ray diffraction data.

Catalyst	Co_3O_4 particle size (nm)
12CoRe/SiO_2	20
12CoRe/TiO_2	51
20CoRe/α-Al_2O_3	25
20CoRe/γ-Al_2O_3[§]	14
12CoRe/γ-Al_2O_3	15

cination [102]. All catalysts showed a reduction peak in a relatively narrow temperature interval, 581 to 632 K, which represents reduction of Co_3O_4 to CoO. Similarly, Castner *et al.* [37] showed for a series of SiO_2 supported catalysts that the temperature of this step is independent of particle size, pore size, and surface area.

Most likely, the last reduction process in Figure 4.11 represents reduction of CoO to Co^0. The reduction feature was relatively narrow for the α-Al_2O_3 based catalyst and particularly narrow for cobalt supported on SiO_2 and TiO_2, most likely because of weak metal-support interactions. For the γ-Al_2O_3 supported

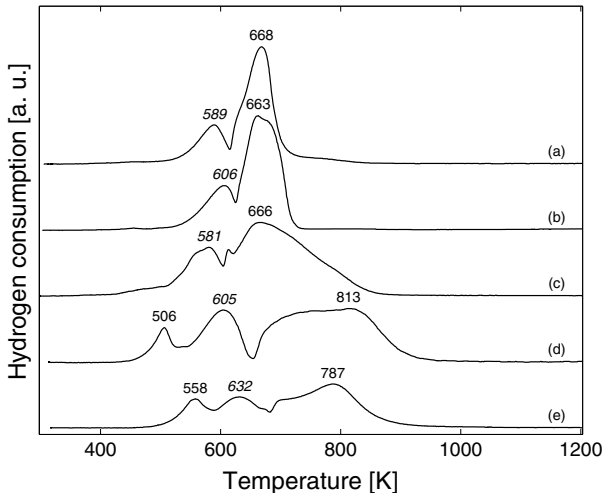

Figure 4.11: Temperature programmed reduction of 12CoRe/SiO_2 (a), 12CoRe/TiO_2 (b), 20CoRe/α-Al_2O_3 (c), 20CoRe/γ-Al_2O_3[§] (d), 12CoRe/γ-Al_2O_3 (e) after calcination. The temperatures typeset in italic font represent the temperatures for maximum reduction rate for transformation of Co_3O_4 to CoO.

catalysts, the interactions are stronger which resulted in broader reduction peaks. The reason for the strong interactions is the presence of small cobalt particles.

For all catalysts, the area ratio between the two last reduction peaks in Figure 4.11 was close to 1/3. This further indicates that irrespective of the nature of the support, reduction of supported Co_3O_4 to Co^0 takes place according to the following scheme:

$$Co_3O_4 + H_2 \rightarrow 3CoO + H_2O \tag{4.1}$$

$$3CoO + 3H_2 \rightarrow 3Co^0 + 3H_2O \tag{4.2}$$

The reduction sequence was also investigated by X-ray absorption spectroscopy experiments at the Co K absorption edge. Specifically, X-ray absorption near-edge spectroscopy spectra were collected during *in situ* reduction. These were compared with reference spectra of Co_3O_4, CoO, and a Co^0 foil. A linear combination fitting procedure gave the quantity of each phase present. Figure 4.12 displays changes in Co_3O_4, CoO, and Co^0 metal fraction during reduction of a γ-Al_2O_3 and an α-Al_2O_3 based catalyst. The shape of the component fraction plots for all the other catalysts was similar to the catalysts presented in Figure 4.12. Thus, in agreement with the temperature programmed reduction profiles, Co_3O_4 was reduced to Co^0 in two steps with CoO as intermediate.

Table 4.4 compares the measured reducibility by oxygen titration with values obtained by X-ray absorption spectroscopy. Oxygen titration gave degrees of reduction between 59 and 69 percent. The lowest and highest value was obtained for cobalt supported on γ-Al_2O_3 and TiO_2, respectively. The degree of reduction ranged from 63 to 85 percent using XANES data, while EXAFS analysis yielded values from 65 to 79 percent. The consistency between values obtained from X-ray absorption spectroscopy was good and within experimental errors.

Two conclusions can be drawn from Table 4.4. First, the degree of reduction obtained for cobalt by X-ray absorption spectroscopy followed the support order $SiO_2 > TiO_2 > \alpha$-$Al_2O_3 > \gamma$-Al_2O_3. For cobalt supported on SiO_2, TiO_2 and γ-Al_2O_3, the same order with respect to percentage reduction was observed by Jacobs *et al.* [35]. Second, the degree of reduction measured by oxygen titration were systematically lower than the values from X-ray absorption spectroscopy. However, roughly the same order between the supports was found.

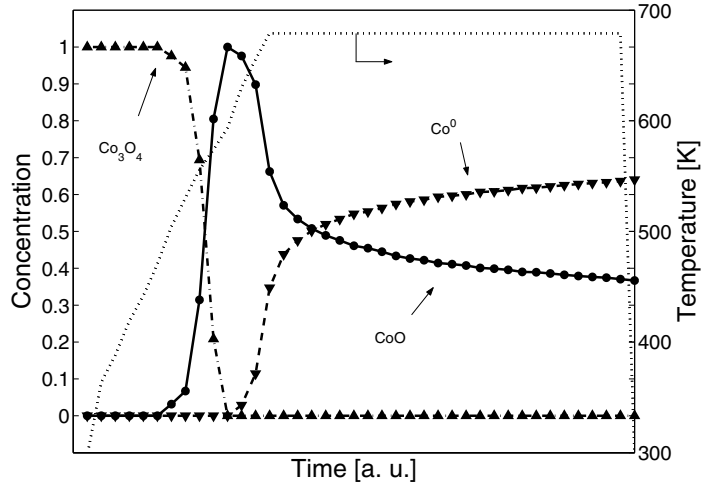

(a) 12CoRe/γ-Al_2O_3

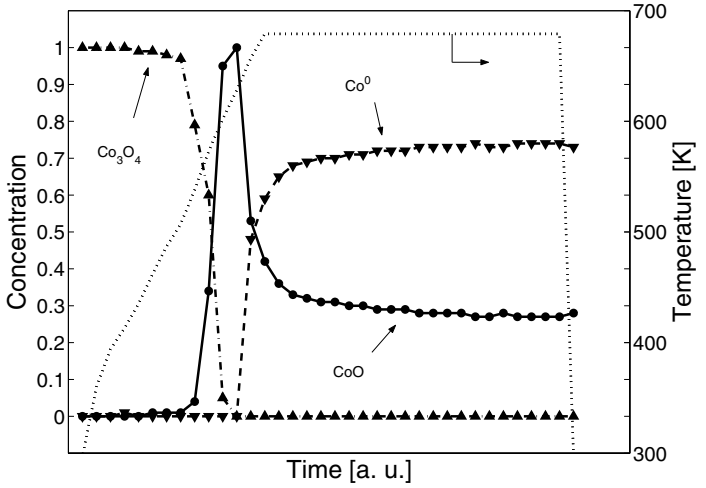

(b) 20CoRe/α-Al_2O_3

Figure 4.12: Component fraction plot during *in situ* reduction (▲ = Co_3O_4, • = CoO, ▼ = cobalt metal, ⋯ = temperature).

Table 4.4: The degree of reduction as determined by oxygen titration and X-ray absorption spectroscopy measurements.

Catalyst	Degree of reduction (%)		
	Oxygen titration	XANES	EXAFS
12CoRe/SiO_2	67	85	79
12CoRe/TiO_2	69	75	75
20CoRe/α-Al_2O_3	63	74	71
20CoRe/γ-Al_2O_3[§]	60	71	70
12CoRe/γ-Al_2O_3	59	63	65

Calculation of the degree of reduction from oxygen titration data assumes stoichiometric oxidation of Co^0 to Co_3O_4. To check this assumption, a separate reduction study was done as shown in Figure 4.13. Temperature programmed reduction profiles of one γ-Al_2O_3 supported catalyst were recorded after calcination, after reduction and pulse oxidation, and, finally, after reduction and recalcination. Figure 4.13 shows that reoxidation of the reduced catalyst with pulses of oxygen did not completely oxidise the sample. The H:Co ratio was significantly less than the ratio for the calcined catalyst (2.2 mol H/mol Co vs. 2.6 mol H/mol Co), indicating that oxygen titration underestimated the degree of reduction.

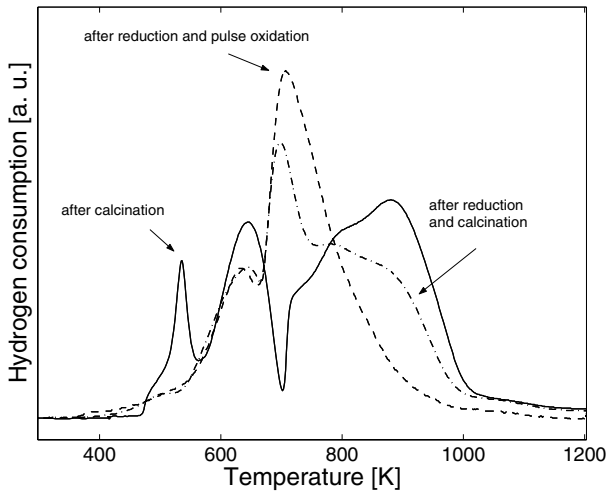

Figure 4.13: Temperature programmed reduction profile of 20CoRe/γ-Al_2O_3* after calcination (573 K, 16 h), after reduction (623 K, 16 h) and pulse oxidation (673 K), after reduction (623 K, 16 h) and calcination (573 K, 16 h).

The reduction profile after reduction and subsequent recalcination closely resembled the profile of the calcined sample. Calcination, therefore, oxidised the reduced sample more completely than the pulse oxidation treatment. However, the H:Co ratio was still lower than the ratio for the original calcined sample (2.4 mol H/mol Co vs. 2.6 mol H/mol Co).

4.4 *Paper D: Fischer-Tropsch synthesis over γ-alumina-supported cobalt catalysts: Effect of support variables*

A systematic study of the effect of γ-Al_2O_3 support variables on the Fischer-Tropsch synthesis activity and selectivity was carried out under industrially relevant conditions (T = 483 K, P = 20 bar, H_2/CO = 2.1). A total of 13 catalysts were produced by incipient wetness impregnation and consisted of 20 wt% cobalt and 0.5 wt% rhenium deposited on γ-Al_2O_3 supports of different pore characteristics and chemical purities.

The 13 alumina supports came from different suppliers and contained varying amounts of trace elements. With respect to Fischer-Tropsch synthesis performance, the most important trace element is probably sodium [105]. The amount of sodium in the calcined catalysts ranged from 20-113 parts per million.

Several different types of nitrogen adsorption/desorption isotherms were obtained for the different samples. In the absence of a universal model, the Barrett-Joyner-Halenda method was chosen for pore size calculations. Pore size distributions are presented in Figure 4.14. Most of the samples had a narrow Gaussian-like unimodal pore size distribution. However, some sets of samples showed broad or bimodal distributions. Deposition of metal precursors on the supports did not influence the shape of the pore size distribution, but merely reduced the nitrogen uptake. Physical properties of all samples are given in Table 4.5.

X-ray diffraction patterns of all supports confirmed the presence of only γ-Al_2O_3 [89]. The patterns of the corresponding impregnated samples exhibited reflections identical to γ-Al_2O_3 and Co_3O_4 [89]. The only difference between the X-ray diffraction patterns of the calcined samples was the width of the Co_3O_4 peaks. Thus, the average Co_3O_4 particle size was dependent on the γ-Al_2O_3 support. Figure 4.15 (filled squares) shows that the Co_3O_4 particle size clearly increased with increasing support pore size. It should also be mentioned that no noticeable correlation was found between the surface areas of the supports and the Co_3O_4 particle sizes.

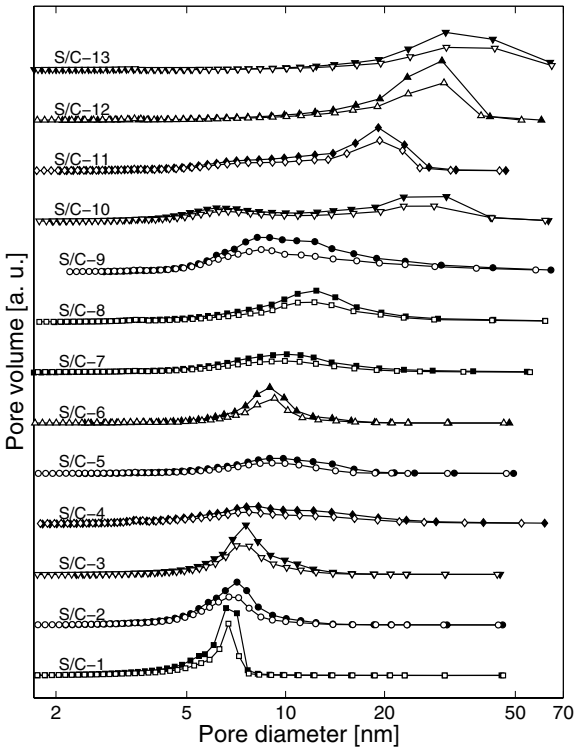

Figure 4.14: Support and catalyst pore size distributions (filled symbol = support, open symbol = catalyst).

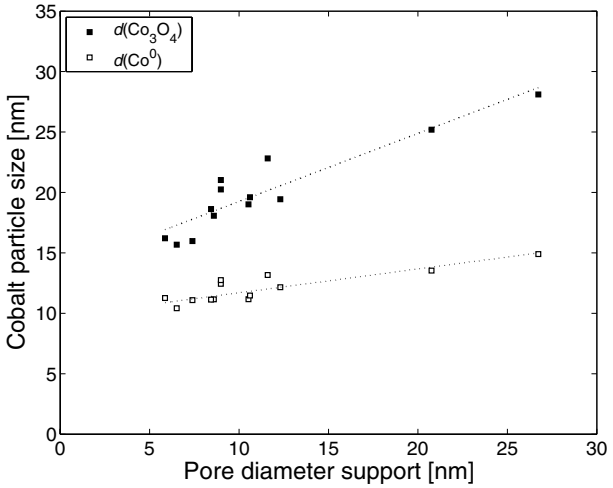

Figure 4.15: Effect of the support pore diameter on the cobalt particle size.

Table 4.5: Surface area and pore characteristics.

Sample	N_2 sorption			Hg porosimetry
	Surface area (m^2/g)	Pore diameter (nm)	Pore volume (cm^3/g)	Pore volume (cm^3/g)
S-1	232	5.9	0.46	
C-1	168	5.7	0.28	
S-2	204	6.5	0.46	
C-2	175	6.1	0.31	
S-3	184	7.4	0.48	
C-3	143	7.1	0.30	
S-4	190	8.6	0.51	
C-4	165	7.9	0.34	
S-5	103	9.0	0.31	
C-5	86	7.9	0.19	
S-6	129	8.4	0.37	
C-6	112	8.1	0.24	
S-7	161	9.0	0.44	
C-7	136	8.2	0.30	
S-8	205	10.5	0.67	
C-8	169	10.2	0.47	
S-9	262	10.6	0.93	
C-9	193	10.4	0.61	
S-10	191	11.6	0.78	0.76
C-10	149	11.6	0.51	0.51
S-11	186	12.3	0.73	
C-11	148	11.6	0.50	0.45
S-12	155	20.8	0.98	
C-12	123	18.3	0.62	0.65
S-13	114	26.7	0.86	
C-13	92	23.7	0.57	0.76

According to Figure 4.15, the average Co_3O_4 particle size was larger than the average support pore diameter. Thus, seemingly, the particles were mainly located on the exterior of the support. However, as argued in Section 4.2, the particles were probably located inside the porous system.

Chemisorption of hydrogen on reduced catalysts was used to measure cobalt dispersion and to calculate cobalt metal particle sizes. The supports did not adsorb any hydrogen. Figure 4.15 (open squares) indicates a positive, albeit weak correlation between the support pore diameter and the cobalt particle size. It should also be mentioned that mild variations in drying conditions had negligible effect on the Co^0 particle size. One catalyst precursor was split into three parts. One was dried in the normal way (labelled C-11 after calcination). For the two other parts, the temperature was ramped from ambient to 383 K at a rate of 1 and 10 K/min, respectively. After 3 h of drying, the three samples were calcined in the normal way. Hydrogen chemisorption showed identical cobalt dispersions and, therefore, Co^0 particle sizes.

As shown in Figure 4.15, the individual Co_3O_4 particle sizes almost systematically followed the individual Co^0 particle sizes. However, the difference between the Co_3O_4 and Co^0 particle sizes increases with increasing support pore diameter.

The reducibility of the calcined catalysts was also studied by temperature programmed reduction. Reduction profiles are presented in Figure 4.16. The curves recorded after calcination showed three main reduction areas, centred approximately at 530, 640, and 800 K.

The first reduction process can be attributed to the reduction of supported cobalt nitrate remaining after calcination [102]. To confirm the nature of the peak, the temperature programmed reduction products were analysed on a mass spectrometer. The results of catalyst C-11 are shown in Figure 4.17. A clear peak of $m/e = 30$ was observed at exactly the same time as the low temperature reduction peak appeared. This mass number corresponds to the NO^+ ion which is the most intense fragment ion of both NO and NO_2. Conclusively, the low-temperature peak can be ascribed to the reduction of residual nitrate present after calcination.

The last two peaks most likely represent a two-step reduction of Co_3O_4 to cobalt metal with CoO as intermediate. A two-step reduction fits well with the hydrogen consumption ratio during the last two separate peaks for all the catalysts in this study. All values (0.35-0.39) were close, but slightly higher

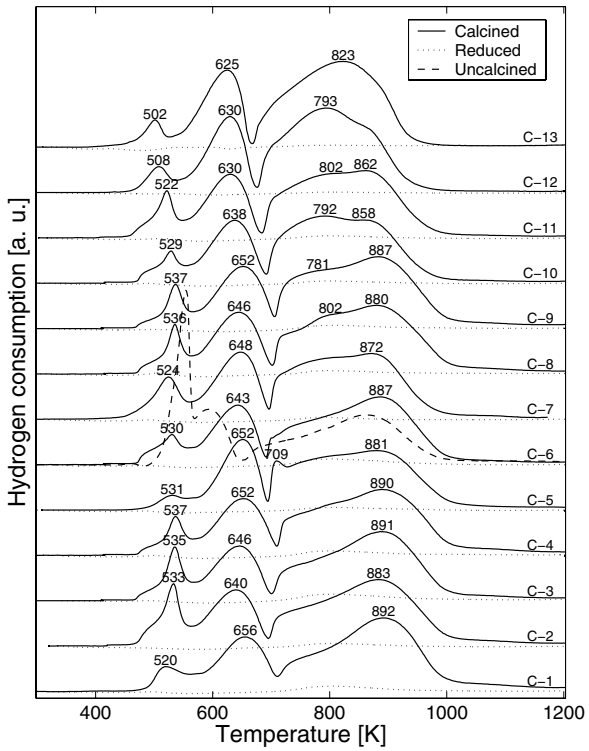

Figure 4.16: Temperature programmed reduction profiles.

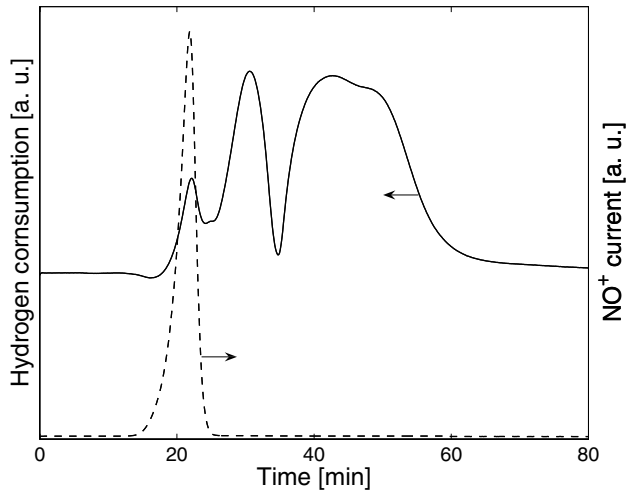

Figure 4.17: Temperature programmed reduction profile and current of the NO^+ ion for catalyst C-11.

than the theoretical value of 1/3, probably due to the poor separation of peaks or incomplete reduction of CoO.

The reduction profiles in Figure 4.16 indicate that the reduction of Co_3O_4 to CoO did not depend on the Co_3O_4 particle size, but took place in the same temperature interval for all the catalysts. However, further conversion of CoO to cobalt metal appeared to be sensitive to the catalyst properties. The high-temperature reduction area moved to slightly lower temperatures with increasing catalyst number (and pore and particle size). A lower temperature implies an easier reduction. In fact, the reduction curves of catalyst C-12 and C-13 resembled the reduction patterns of bulk Co_3O_4 [106].

Oxygen titration data confirmed the indications drawn from the reduction profiles. A positive correlation was found between the Co_3O_4 particle size (and pore diameter) and the degree of reduction. The reason is probably weaker metal-support interactions for large particles located in wide pores than for small particles present in narrow pores.

The Fischer-Tropsch synthesis measurements were recorded at T = 483 K, P = 20 bar, and H_2/CO = 2.1. The reaction was for one catalyst (C-3) run with different particle sizes as shown in Figure 4.18. Both the activity and the selectivity were, within experimental error, unaffected by the catalyst particle

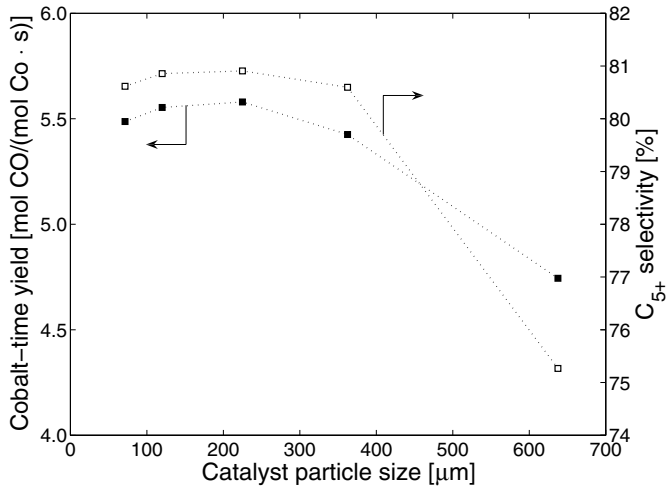

Figure 4.18: Effect of the catalyst particle size on the catalytic performance of catalyst C-3 at 483 K, 20 bar, H_2/CO = 2.1. The C_{5+} selectivity was recorded at 50% CO conversion.

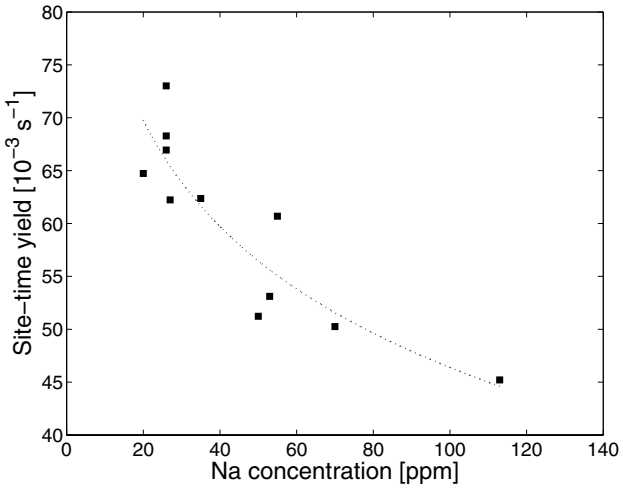

Figure 4.19: Site-time yield after 8 h on stream at 483 K, 20 bar, and H_2/CO = 2.1.

size in the range 53-225 μm. However, for larger catalyst particles, the catalytic performance was poorer, most likely because of mass transfer limitations. To avoid limitations, all results were obtained on catalyst particles of 53-90 μm in size.

As shown in Figure 4.19, the small variations in site-time yield (45-73 $\cdot$ 10^{-3} s^{-1}) could be related to the chemical purity of the catalyst samples. Sodium clearly had a negative impact on the site-time yield. Although Figure 4.19 demonstrates variations in site-time yield, no significant difference in intrinsic activity was measured by SSITKA at methanation conditions. The reason is not clear. Finally, it should be mentioned that there was no correlation between the cobalt-time yield or site-time yield and the physical parameters of the catalysts (*i.e.* surface area, pore diameter, and pore volume).

Since the product distribution is extremely sensitive to the CO conversion, all hydrocarbon selectivities were recorded at exactly the same conversion level, in this case 50%.

Figure 4.20 shows that the C_{5+} can be increased by choosing a starting support that contains wide pores. The increased C_{5+} selectivity is a result of both decreased methane and C_2-C_4 selectivity. Thus, wide-pore catalysts have a higher chain growth probability than narrow-pore catalysts. This conclusion is not a result of variations in the sodium content. In fact, five catalysts that

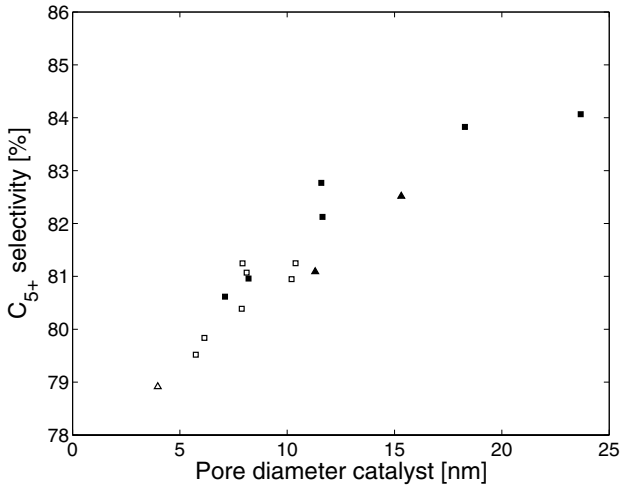

Figure 4.20: Effect of catalyst pore diameter on C_{5+} selectivity. The catalysts are supported on: ■ = γ-Al_2O_3 from Sasol, □ = γ-Al_2O_3 from other vendors, ▲ = $\gamma/\theta/\delta$-Al_2O_3 from Sasol, △ = boehmite.

contained practically the same amount of sodium showed significant variations in C_{5+} selectivity.

According to Iglesia *et al.* [39, 44, 45], the C_{5+} selectivity can be explained solely from the extent of α-olefin re-adsorption. This principle cannot explain the variations in selectivity for the catalysts in this work. As shown in Figure 4.21, there was no relationship between the olefin/paraffin ratios and the product selectivity.

Since the cobalt particle size increases with increasing pore diameter, the C_{5+} selectivity also increases with increasing cobalt particle size as illustrated in Figure 4.22. Bezemer *et al.* [42] also recently found the cobalt particle size to affect the C_{5+} selectivity for particles smaller than 8 nm in diameter. However, Figure 4.22 shows a relationship also for particles larger than 8 nm. In addition, Storsæter *et al.* [24] observed very high selectivity for cobalt supported on TiO_2. The average size of the cobalt particles was 40 nm.

Figure 4.23 further illustrates that the particle size is important for the product selectivity. Even though the CO conversion decreased with time on stream, the catalyst gave similar C_{5+} selectivity which is surprising from the relationship between conversion and selectivity. Indeed, Figure 4.23 shows that the ratio between selectivity and conversion increased with time on stream for catalyst

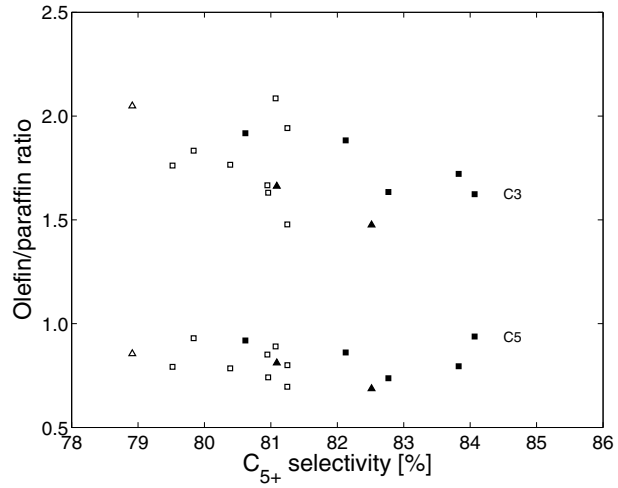

Figure 4.21: Olefin/paraffin ratios. The catalysts are supported on: ■ = γ-Al_2O_3 from Sasol, □ = γ-Al_2O_3 from other vendors, ▲ = $\gamma/\theta/\delta$-Al_2O_3 from Sasol, △ = boehmite.

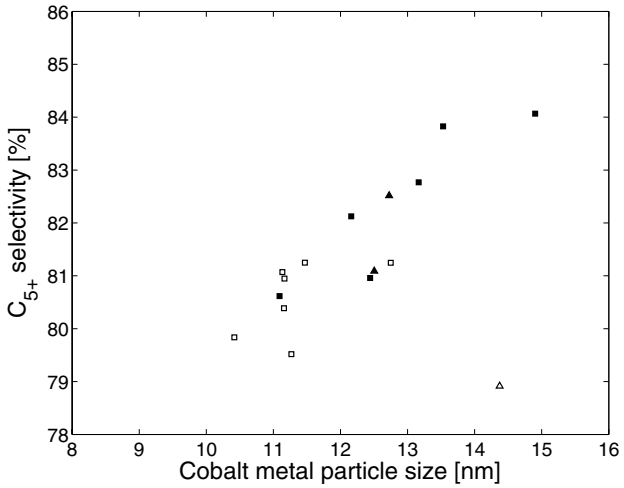

Figure 4.22: Effect of cobalt particle size on C_{5+} selectivity. The catalysts are supported on: ■ = γ-Al_2O_3 from Sasol, □ = γ-Al_2O_3 from other vendors, ▲ = $\gamma/\theta/\delta$-Al_2O_3 from Sasol, △ = boehmite.

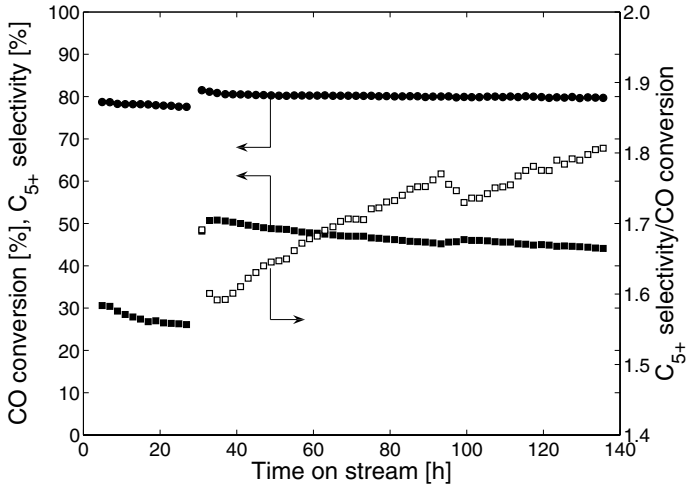

Figure 4.23: CO conversion and C_{5+} selectivity of catalyst C-11 at 483 K, 20 bar, and $H_2/CO = 2.1$.

C-11. This phenomenon can possibly be explained by an increase in the average particle size because of deactivation. Both sintering and oxidation of small cobalt particles increase the average cobalt particle size. Probably, the increased average cobalt particle size of catalyst C-11 gave higher C_{5+} selectivity which could counteract the decrease in selectivity because of lower CO conversion.

To summarise, it seems difficult to explain the variations in C_{5+} selectivity with diffusion effects. Instead, the cobalt particle size or possibly the particle shape and appearance seem to control the product distribution. A particle size dependent C_{5+} selectivity is in agreement with the recent investigation by Bezemer *et al.* [42]. However, this study showed that the C_{5+} selectivity depends on the particle size also for particles larger than the size limit set by Bezemer *et al.* [42].

4.5 *Paper E: Fischer-Tropsch synthesis over different alumina supported cobalt catalysts*

Four catalysts containing 20 wt% cobalt and 0.5 wt% Re were prepared by one step-incipient wetness impregnation of different supports (S-1 to S-4) with aqueous solutions of cobalt nitrate hexahydrate and perrhenic acid. While support S-1 was used as received, the other supports were calcined before

Table 4.6: Calcination parameters.

Support	Calcination temperature (K)	Calcination time (h)	Support nature
S-1	-	-	Boehmite
S-2	773	10	γ-Al_2O_3
S-3	773	10	$\gamma/\theta/\delta$-Al_2O_3
S-4	1413	10	α-Al_2O_3

impregnation. Samples S-2 and S-3 were calcined at 773 K and support S-4 at 1413 K. Complete calcination parameters as well as the final support phase are given in Table 4.6.

X-ray diffraction patterns of S-1 and S-2 showed reflections of boehmite and γ-Al_2O_3, respectively. For support S-3, a mixture of γ-, δ-, and θ-Al_2O_3 was present. The high temperature calcined sample S-4 showed peaks representative for α-Al_2O_3. Thus, a wide variety of alumina phases was represented in the four samples. A calcination temperature of 773 K is usually not sufficient to transform γ-Al_2O_3 into transition aluminas. However, support S-3 was calcined at higher temperatures by the vendor prior to receipt.

Diffraction patterns were also recorded for the impregnated samples after calcination. Apart from peaks originating from the supports, the diffractograms only contained peaks typical of Co_3O_4. The Co_3O_4 particle size was calculated from the reflection located at $2\theta = 36.9°$. The results are shown in Table 4.7.

Chemisorption of hydrogen after reduction was used to measure cobalt dispersion and to calculate cobalt metal particle sizes. The results are given in the last column of Table 4.7. The largest average particle size was found in the α-Al_2O_3 based sample C-4.

Table 4.7: X-ray diffraction and hydrogen chemisorption data.

Catalyst	X-ray diffraction		Hydrogen chemisorption	
	$d(Co_3O_4)$ (nm)	$d(Co^0)$ (nm)	D (%)	$d(Co^0)$ (nm)
C-1	19	14	6.7	14
C-2	19	15	7.9	12
C-3	22	16	7.6	13
C-4	53	40	2.7	36

Table 4.8: Surface area and pore characteristics.

Catalyst	Surface area (m^2/g)	Pore volume (cm^3/g)	Pore diameter (nm)
C-1	160	0.17	4.0
C-2	148	0.50	11.6
C-3	129	0.29	15.3
C-4	15	0.23	150

Strong correlations between the temperature of calcination and the physical parameters in Table 4.8 were found. More specifically, the pore diameter increased in the order C-1, C-2, C-3, C-4. The opposite trend was found for the surface area and pore volume.

Reduction profiles are given in Figure 4.24. The catalysts showed several different reduction areas. For catalysts C-1, C-2, and C-3, the first peak represented reduction of supported cobalt nitrate remaining after calcination [102]. The α-Al_2O_3 based catalyst showed only traces of left-over nitrate. Possibly, there was a relation between the pore diameter and the amount of residual nitrate. The peaks at 643, 646, 630, and 688 K represent reduction of Co_3O_4 to CoO. The further reduction in Figure 4.24 can be attributed to the transformation of CoO to metallic cobalt. The ease of reduction increased with increasing pore diameter and particle size.

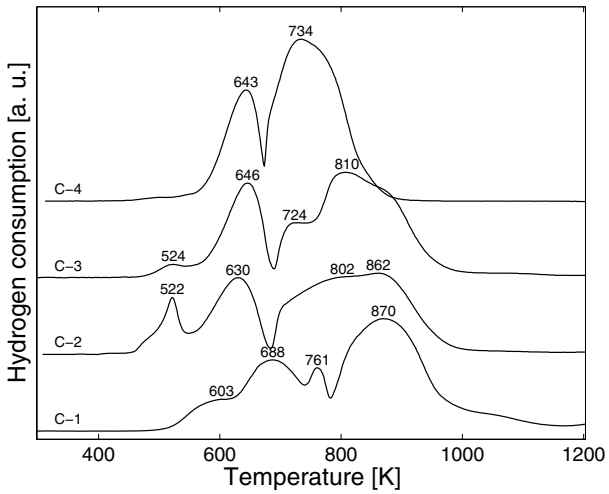

Figure 4.24: Temperature programmed reduction profiles.

Table 4.9: Fischer-Tropsch synthesis data.

Catalyst	$CTY \cdot 10^3$ (mol CO/(mol Co · s))	$STY \cdot 10^3$ (s^{-1})	$S_{C_{5+}}$ (%)	S_{CH_4} (%)
C-1	3.6	54	78.9	10.0
C-2	5.3	67	82.1	9.0
C-3	4.5	59	82.5	8.9
C-4	1.8	65	86.6	7.7

The Fischer-Tropsch synthesis performance is summarised in Table 4.9. The cobalt-time yield (CTY) was recorded after 8 h on stream. The site-time yield (STY) is based on this cobalt-time yield and the cobalt dispersion as determined by chemisorption. The C_{5+} and CH_4 selectivities ($S_{C_{5+}}$ and S_{CH_4}) were recorded at 483 K, 20 bar, $H_2/CO = 2.1$, and exactly 50% CO conversion. Although differences in the cobalt-time yields were observed (1.8-3.6 $\cdot 10^{-3}$ mol CO/(mol Co · s)), Table 4.9 shows that the site-time yield was constant for all the samples (54-67 $\cdot 10^{-3}$ s^{-1}). Constant site-time yield is in accordance with previous studies [39–41].

As shown in Table 4.9, the catalysts fell in three groups with respect to C_{5+} selectivity. First, the selectivity of C-1 was significantly lower than the selectivity of the three other samples. Second, the selectivity of catalysts C-2 and C-3 was similar. Third, cobalt supported on α-Al_2O_3 gave very high C_{5+} selectivity. The results showed that the product distribution in fact was very dependent on the support.

To summarise, the Fischer-Tropsch activity could be estimated from the cobalt dispersion as measured by hydrogen chemisorption. The selectivity was dependent on the support. However, whether the pore diameter, the particle size, or possibly both factors are decisive cannot be concluded from this study only.

4.6 *Paper F: Fischer-Tropsch synthesis over un-promoted and Re-promoted γ-Al_2O_3 supported cobalt catalysts with different pore sizes*

The effect of rhenium on the Fischer-Tropsch synthesis activity and selectivity of γ-Al_2O_3 supported cobalt catalysts was investigated a fixed-bed reactor at $T = 483$ K, $P = 20$ bar, and $H_2/CO = 2.0$. Three sets of un-promoted and Re-promoted catalysts were prepared by incipient wetness impregnation and consisted of 20 wt% cobalt and 0 or 0.5 wt% rhenium deposited on γ-Al_2O_3 supports with different pore characteristics.

Table 4.10: Surface area and pore characteristics.

Catalyst	Surface area (m^2/g)	Pore volume (cm^3/g)	Pore diameter (nm)
NPA	184	0.48	7.4
Co/NPA	141	0.31	6.8
CoRe/NPA	143	0.30	7.1
MPA	186	0.73	12.3
Co/MPA	138	0.49	11.5
CoRe/MPA	148	0.50	11.6
WPA	114	0.86	26.7
Co/WPA	77	0.58	26.6
CoRe/WPA	92	0.57	23.7

Pore size data were calculated from the Barrrett-Joyner-Halenda model. Figure 4.25 shows significant differences in pore size distributions for the three supports. Deposition of metal precursors on the supports did not influence the shape of the support pore size distribution, but merely reduced the nitrogen uptake. Also, there was no significant difference for the un-promoted and promoted samples. Table 4.10 gives the physical properties of all samples.

X-ray diffraction patterns confirmed that the chemical identity of all supports was γ-Al_2O_3 [89]. In addition to the γ-Al_2O_3 peaks, the catalysts exhibited

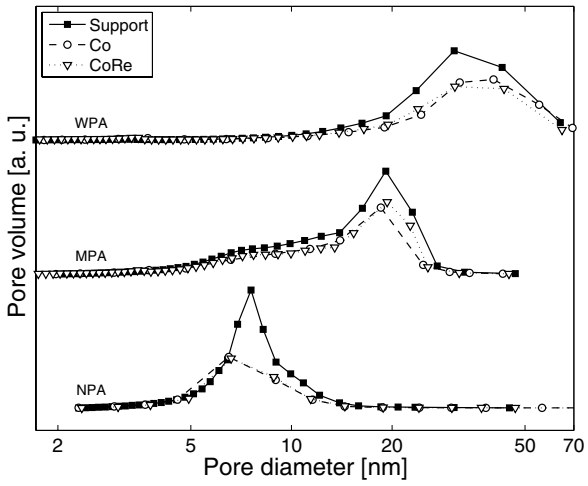

Figure 4.25: Pore size distributions.

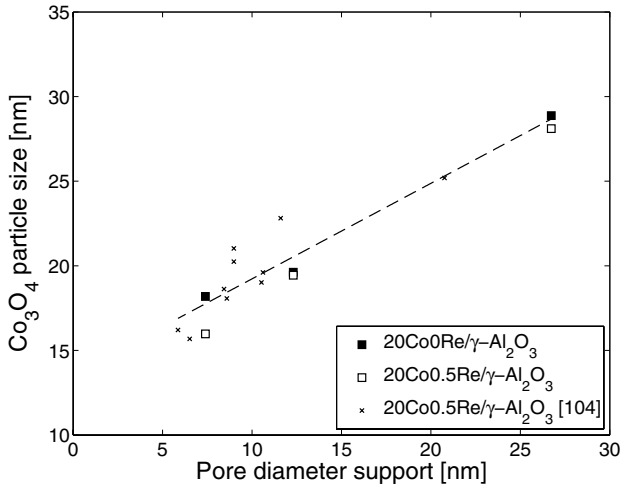

Figure 4.26: Co_3O_4 particle size data.

peaks of Co_3O_4 [89]. There was no significant difference in the diffractogram for the un-promoted and the promoted samples. The concentration of rhenium was probably too low to give detectable peaks.

For all catalysts, the Co_3O_4 particle size was calculated from the diffraction peak located at $2\theta = 36.9°$. The results are presented in Figure 4.26. Two conclusions can be drawn. First, and clearly most important, the Co_3O_4 particle size was controlled by the support pore size. Second, the particle sizes were slightly smaller for the promoted samples than for the un-promoted samples. Mauldin and Varnado [56] also observed that the presence of rhenium gives better cobalt oxide dispersion.

Temperature programmed profiles are presented in Figure 4.27. The reduction peaks located close to 515 K can be attributed to the reduction of residual nitrate remaining after calcination. The second and third peak correspond to a two-step reduction of Co_3O_4 to Co^0 with CoO as an intermediate species.

For all six catalysts, the peak attributed to the reduction of Co_3O_4 was located in a narrow temperature region. Thus, the reducibility of Co_3O_4 did not depend on catalyst properties such as particle size, morphology, pore size, and surface area. In contrast, the second reduction step was largely dependent on catalyst properties. For both the un-promoted and promoted series of catalysts, the reduction area moved to slightly lower temperatures with increasing pore and particle size. Figure 4.27 also shows that Re significantly facilitated

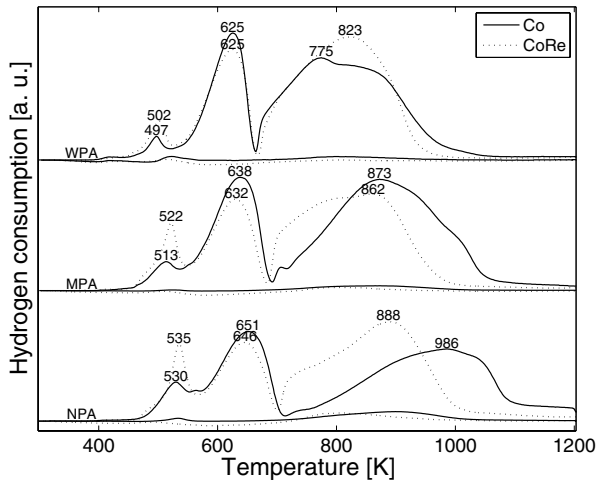

Figure 4.27: Temperature programmed reduction profiles.

the reduction of CoO. However, the role of Re as a reduction promoter was less pronounced at increasing pore and particle size.

The oxygen uptake data in Figure 4.28 are in perfect agreement with the temperature programmed reduction data. For the un-promoted series, the oxygen consumption increased strongly with increasing pore and particle size. The reduction profiles in Figure 4.27 also showed that the CoO to Co^0 peak was shifted significantly to lower temperatures as the pore and particle size increased for the same catalysts. For the series of promoted catalysts, the increase in oxygen uptake with increasing pore and particle size was more moderate. The reduction profiles of the promoted catalysts were also very similar. Finally, it should also be noted that the two catalysts supported on wide-pore alumina showed very similar reduction profiles and practically identical oxygen uptake.

Chemisorption of hydrogen on the reduced samples was used to measure cobalt dispersion and estimate particle sizes. Table 4.11 shows that the cobalt dispersion decreased with increasing pore size for both the un-promoted and the promoted catalysts. Presence of rhenium, however, had the strongest impact on cobalt dispersion. The cobalt dispersion of the promoted samples was almost twice as high as the dispersion of the un-promoted samples. The Co^0 particle size was estimated from the cobalt dispersion value and the degree of reducibility. For both the un-promoted and the promoted samples, the Co^0

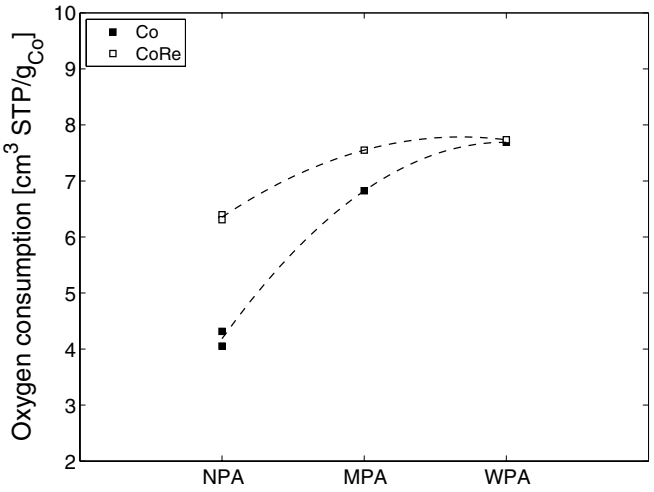

Figure 4.28: Oxygen uptake at 673 K.

particle increased with increasing pore diameter. This is consistent with Figure 4.15.

XANES spectra were recorded for two catalysts (Co/NPA and CoRe/NPA) during *in situ* reduction. These were compared with reference spectra of Co_3O_4, CoO, and a Co^0 foil. Co_3O_4 was reduced in two steps to Co^0 with CoO as intermediate. The first reduction step took place at 623 K for both catalysts. This temperature correlates well with the temperatures observed for the same samples in standard temperature programmed reduction (646 and 651 K). The further reduction was very different for the two samples. In

Table 4.11: Hydrogen chemisorption and oxygen titration data.

Catalyst	D (%)	$d(Co^0)_{uncorr}$ [a] (nm)	Amount of O_2 adsorbed (μmol/g)	Degree of reduction (%)	$d(Co^0)_{corr}$ [b] (nm)
Co/NPA	4.5	21.5	187	41	8.9
CoRe/NPA	8.7	11.1	283	67	6.9
Co/MPA	4.0	23.8	304	76	16.0
CoRe/MPA	7.9	12.2	337	63	9.1
Co/WPA	3.7	25.8	362	74	19.6
CoRe/WPA	6.5	14.9	345	76	11.4

agreement with TPR and O_2 titration data, the degree of reduction was significantly higher for catalyst CoRe/NPA than for catalyst Co/NPA. After 3.5 h of reduction, the degree of reduction of these samples was 70 and 22%, respectively. It should also be mentioned that the degree of reduction did not change when the catalyst was exposed to synthesis gas. Thus, no oxidation occurred at the applied experimental conditions. However, note that the CO conversion and, accordingly, the water level were not measured during the course of the reaction.

Fischer-Tropsch synthesis results are presented in Figure 4.29. The site-time yields were calculated after 8-12 h on stream. Although the cobalt-time yields varied significantly (3.1-6.7 $\cdot$ 10^{-3} mol CO/(mol Co $\cdot$ s)), the site-time yields were, within experimental error, constant (51-64 $\cdot$ 10^{-3} s^{-1}). Accordingly, Re does not modify the site-time yield.

Figure 4.29 shows that the initial difference in cobalt-time yield between the un-promoted and Re-promoted catalysts was dependent on the γ-Al_2O_3 support. The difference increased in the support order WPA $<$ MPA $\leq$ NPA. These results correlate well with the temperature programmed reduction profiles and oxygen uptake data. Figure 4.29 also shows that the deactivation rates from 0 to 24 h were higher for the most active catalysts. Thus, higher CO conversion leads to more rapid deactivation [59]. The deactivation rates

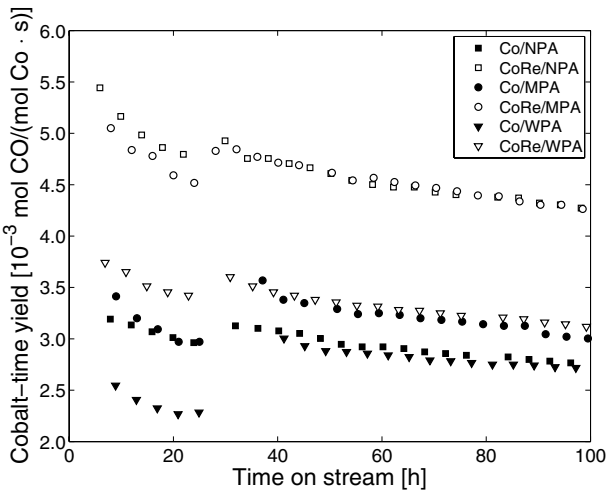

Figure 4.29: Cobalt-time yield measured at T = 483 K, P = 20 bar, and H_2/CO = 2.0.

were similar for all samples from 24 to 100 h. This is surprising since some of the catalysts contained Re and others not. Also, there were large variations in cobalt particle size. These results add further speculations as to what the causes of deactivation of cobalt Fischer-Tropsch catalysts could be. While oxidation of cobalt has been postulated as a deactivation mechanism for a long time [65], Saib *et al.* [88] recently ruled this possibility out for cobalt particles larger or equal to 6 nm in diameter.

Figure 4.30 shows that the conversion level was similar for all catalysts. This ensured a reliable comparison of C_{5+} selectivity between the catalysts.

As shown in Figure 4.31, the C_{5+} selectivity strongly increased with increasing pore diameter for both series of catalysts. Table 4.12 shows that both a lower CH_4 and C_2-C_4 selectivity contributed to the improved C_{5+} selectivity. Thus, the chain growth probability increased with increasing pore diameter. Since the olefin/paraffin ratios of all catalysts were very similar (Table 4.12), the differences in selectivity can probably not be explained by different degrees of olefin re-adsorption.

The C_{5+} selectivity of the Re-promoted samples was higher than the selectivity of the un-promoted catalysts. The results are in agreement with Schanke *et al.* [50] who found a slightly higher selectivity for cobalt supported on γ-Al_2O_3 in the presence of Re than in the absence of Re.

Figure 4.32 shows that the C_{5+} selectivity can be correlated to the cobalt particle size. Since it seems difficult to explain the variations in selectivity with diffusion effects, the C_{5+} selectivity is probably related to the cobalt particle sizes. As shown in Figure 4.32, the Re samples exhibited higher selectivity at a similar particle size. Thus, it can be speculated that Re changes the termination probability of the growing hydrocarbon chain through a chemical effect.

Interestingly, the decrease in C_{5+} selectivity with CO conversion is different for the different samples (Figure 4.31). The selectivity decreased most rapidly for the two catalysts supported on the narrow-pore γ-Al_2O_3. The C_{5+} selectivity/CO conversion slopes of the wide-pore based catalysts were smallest. The reason is not clear.

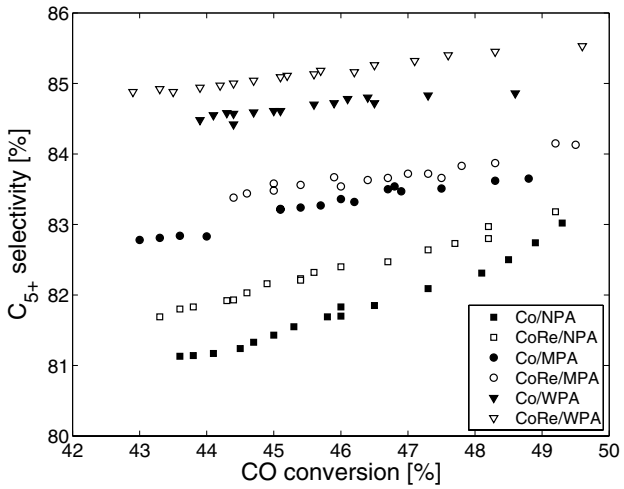

Figure 4.30: C_{5+} selectivity measured at T = 483 K, P = 20 bar, and H_2/CO = 2.0.

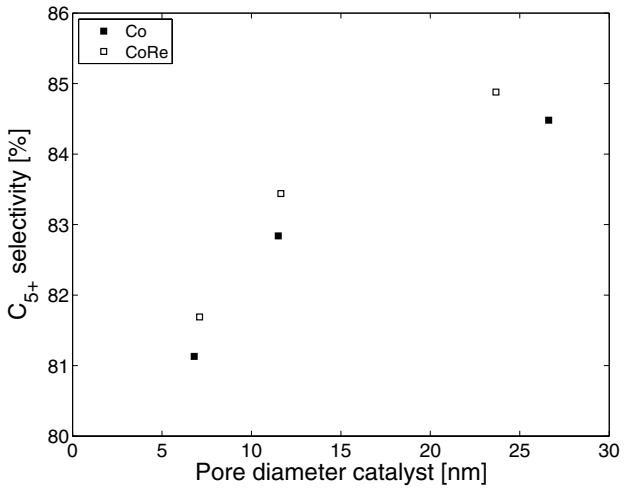

Figure 4.31: Effect of pore diameter on the C_{5+} selectivity at T = 483 K, P = 20 bar, and H_2/CO = 2.0, and 43-44% CO conversion.

Table 4.12: Selectivity data at $T = 483$ K, $P = 20$ bar, $H_2/CO = 2.0$, and 43-44% CO conversion.

Catalyst	Selectivity (%)			Olefin/paraffin ratios				
	C_1	C_2-C_4	C_{5+}	$C_{2=}/C_{2-}$	$C_{3=}/C_{3-}$	$C_{4=}/C_{4-}$	$C_{5=}/C_{5-}$	$C_{6=}/C_{6-}$
Co/NPA	8.96	9.91	81.13	0.12	2.44	1.47	1.22	0.85
CoRe/NPA	8.79	9.52	81.69	0.12	2.42	1.45	1.19	0.83
Co/MPA	8.56	8.65	82.78	0.10	2.10	1.22	0.95	0.63
CoRe/MPA	8.35	8.27	83.38	0.10	2.34	1.38	1.10	0.74
Co/WPA	8.02	7.50	84.48	0.08	2.09	1.20	0.92	0.59
CoRe/WPA	7.96	7.15	84.88	0.08	2.34	1.38	1.11	0.74

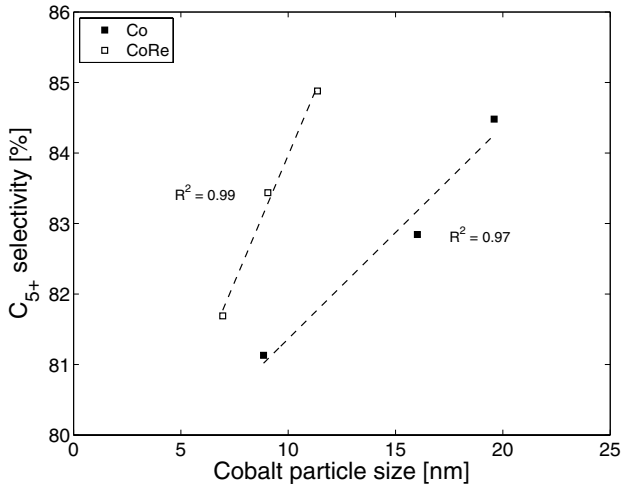

Figure 4.32: Effect of cobalt particle size on the C_{5+} selectivity at $T = 483$ K, $P = 20$ bar, and $H_2/CO = 2.0$, and 43-44% CO conversion.

4.7 *Paper G: The effect of water on the activity and selectivity for γ-alumina supported cobalt Fischer-Tropsch catalysts with different pore sizes*

By the addition of water to the synthesis gas feed in a conventional fixed-bed reactor during Fischer-Tropsch synthesis, high conversions can be simulated without using long residence times. The effect of water on the activity and selectivity for a series of γ-Al_2O_3 supported cobalt Fischer-Tropsch catalysts was studied at $T = 483$ K, $P = 20$ bar, and $H_2/CO = 2.1$. The catalysts were produced applying incipient wetness impregnation and consisted of 20 wt% cobalt and 0.5 wt% rhenium deposited on γ-Al_2O_3 supports with different pore characteristics.

X-ray diffraction patterns of all supports confirmed the presence of only γ-Al_2O_3 [89]. The diffractograms of the respective impregnated and calcined samples exhibited peaks identical to γ-Al_2O_3 and Co_3O_4 [89]. Cobalt particle sizes calculated from X-ray diffraction and hydrogen chemisorption data are given in Table 4.13.

Although the chemical identity of the supports always was γ-Al_2O_3, there were large variations in physical properties as shown in Table 4.14. For instance, the average pore diameter of the supports ranged from 7.4 to 20.8 nm. In the remainder of this study, supports S-1 to S-4 will be referred to as "narrow-pore"

Table 4.13: Cobalt particle sizes of the calcined catalysts.

Catalyst	Co_3O_4 particle size (nm)	Co^0 particle size (nm)
C-1	16	11
C-2	20	12
C-3	23	13
C-4	19	12
C-5	25	14

supports, while S-5 will be denoted a "wide-pore" support. In the same way, catalysts C-1 to C-4 are "narrow-pore" catalysts while C-5 is a "wide-pore" catalyst.

The effect of water on the activity was studied by increasing the CO conversion, from 20-35 to 50%. In addition, the influence of water was investigated by co-feeding different amounts of water. The water concentration at reactor inlet was 20 and 33 mol%. In order to discover the extent of catalyst deactivation due to water exposure, the external water supply was stopped while the synthesis gas was kept flowing at the same rate. Finally, it should be kept in mind that the effect of indigenous water may be different from externally added water.

Table 4.14: Surface area and pore characteristics.

Sample	Surface area (m^2/g)	Pore diameter (nm)	Pore volume (cm^3/g)
S-1	184	7.4	0.48
C-1	143	7.1	0.30
S-2	161	9.0	0.44
C-2	136	8.2	0.30
S-3	191	12.5	0.78
C-3	149	11.6	0.51
S-4	186	12.3	0.73
C-4	148	11.6	0.50
S-5	155	20.8	0.98
C-5	123	18.3	0.62

Since the catalysts deactivate with time on stream irrespective of whether water is introduced to the synthesis gas or not, experiments were also done without adding any water to the feed. Comparison of the "wet" and "dry" experiments makes it possible to separate the contribution of added water on total deactivation.

Reaction rates of catalysts C-4 and C-5 are shown in Figure 4.33 and 4.34, respectively. The space velocity of synthesis gas was decreased after 26 h in order to reach 50% CO conversion. For both catalysts, the increase in conversion and, accordingly, reactor water concentration led to an increase in catalytic productivity. Thus, at relatively low reactor water concentrations, there was a positive correlation between water amount and the hydrocarbon formation rate. Similar results have been shown for cobalt supported on narrow-pore γ-Al_2O_3, SiO_2, and TiO_2 [24, 34].

Although the two catalysts reacted similarly activity-wise at low water pressures, the response was different when the catalysts after 54 h were exposed to larger amounts of water (20 mol%). As shown in Figure 4.33, the addition of water decreased the activity for catalyst C-4. The same scenario was experienced for catalysts C-1 to C-3. In contrast, an introduction of 20 mol% water was in fact beneficial for the reaction rates for the wide-pore catalyst. To our best knowledge, this is the first time that addition of moderate amounts of

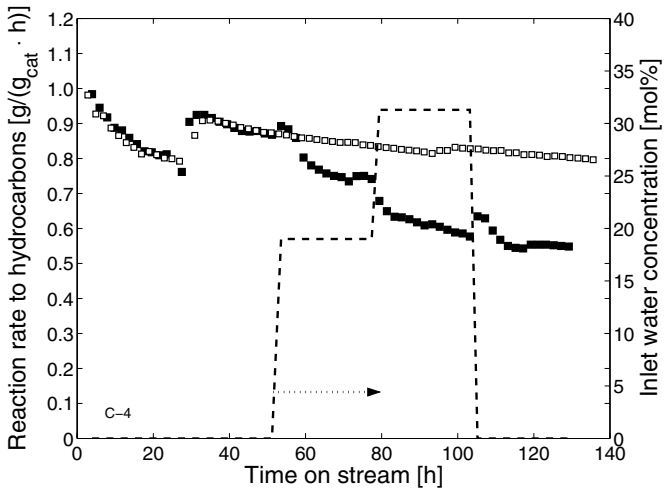

Figure 4.33: Reaction rate for formation of hydrocarbons vs. time on stream for catalyst C-4 (■ = water run, □ = dry run, - - = water concentration).

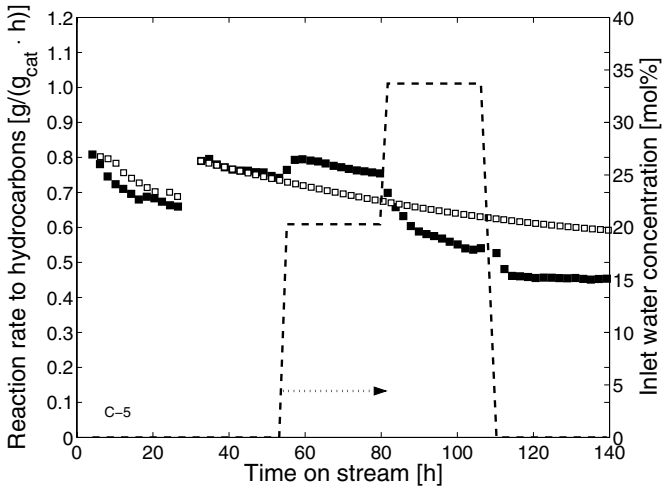

Figure 4.34: Reaction rate for formation of hydrocarbons vs. time on stream for catalyst C-5 (■ = water run, □ = dry run, - - = water concentration).

water has increased the reaction rates for cobalt supported on γ-Al_2O_3.

Figure 4.35 shows that the effect of an addition 20 mol% water was reversible. Similarly, Jacobs *et al.* [68, 71] observed for various promoted and unpromoted γ-Al_2O_3 supported cobalt catalysts that below 25 vol%, no permanent deactivation of cobalt occurred.

As the water concentration at the reactor was increased from 20 to 33 mol%, all catalysts reacted negatively with respect to activity. Apparently, for the wide-pore γ-Al_2O_3 support, there exists an optimum value for the water concentration between 0 and 33 mol.%.

Comparing reaction rates before and after external water addition gives a reliable estimate of the extent of deactivation. After exposure to 33 mol% water, the reaction rates did not return to the same level as expected from the dry experiments as shown in Figures 4.33 and 4.34. Accordingly, permanent deactivation of the catalysts occurred. This is in agreement with the results of Jacobs *et al.* [71] showing that irreversible deactivation occurs at sufficiently high concentrations of water ($>$ 25 vol%). XANES scans of catalysts exposed to water indicated the formation of a species chemically resembling cobalt aluminate [68].

Figure 4.36 and 4.37 show a clear positive correlation between the amount of

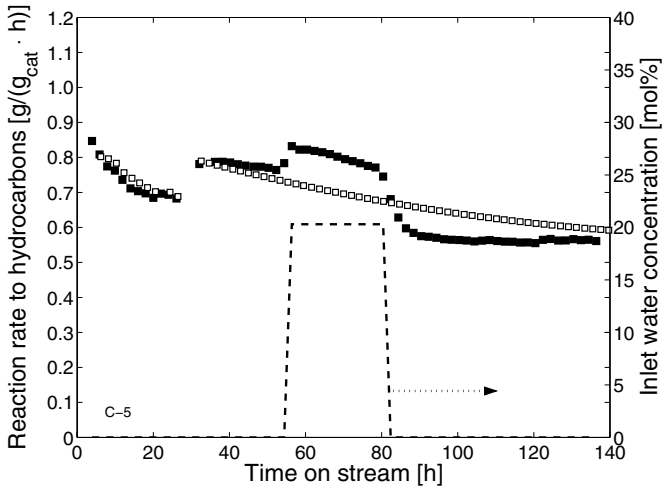

Figure 4.35: Reaction rate for formation of hydrocarbons vs. time on stream for catalyst C-5 (■ = water run, □ = dry run, - - = water concentration).

water in the reactor and the selectivity to long-chain hydrocarbons. The plots are based on experiments at dry conditions, at two different water addition levels, and after removal of water. These results are consistent with previous results [24, 34, 40, 66, 77–79, 81–85].

4.8 *Paper H: Fischer-Tropsch synthesis. Recent studies on the relation between the properties of supported cobalt catalysts and the activity and the selectivity*

The activity and selectivity of a large number of catalysts were studied at 483 K, 20 bar, and $H_2/CO = 2.1$. Cobalt was supported on carbon nanofibers, γ-Al_2O_3, α-Al_2O_3, SiO_2, and TiO_2.

SSITKA studies have shown that the intrinsic site-time yield seems to be independent of the support and the promoter at least at methanation conditions. One exception exists. Promoted cobalt supported on TiO_2 showed higher apparent site-time yield. The deviation for TiO_2 supported catalysts is a well-known phenomenon [24, 58]. To a large extent, the same conclusions can be drawn at Fischer-Tropsch conditions. However, sodium has been identified as a catalyst poison. Sodium decreases the cobalt-time yield, but does not lower the amount of chemisorbed hydrogen measured *ex situ*.

The support is important for the C_{5+} selectivity. Catalysts that contain large

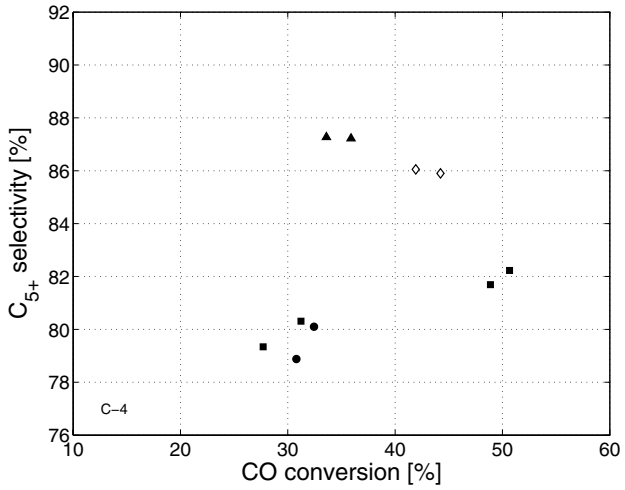

Figure 4.36: C_{5+} selectivity vs. the CO conversion for catalyst C-4 before, during, and after water addition (■ = before water addition, ◇ = 20% water, ▲ = 33% water, ● = after water addition).

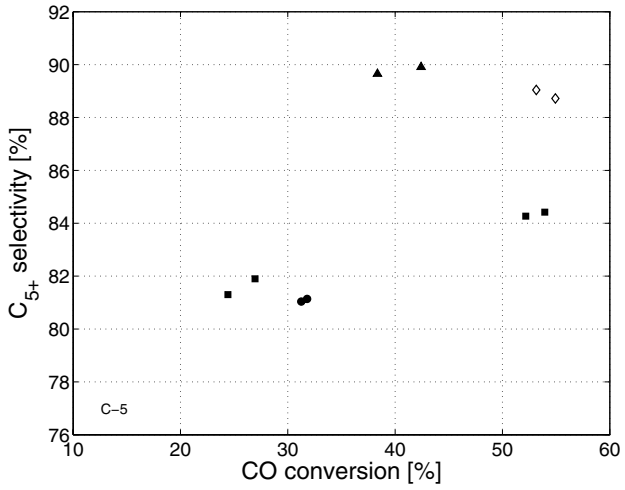

Figure 4.37: C_{5+} selectivity vs. the CO conversion for catalyst C-5 before, during, and after water addition (■ = before water addition, ◇ = 20% water, ▲ = 33% water, ● = after water addition).

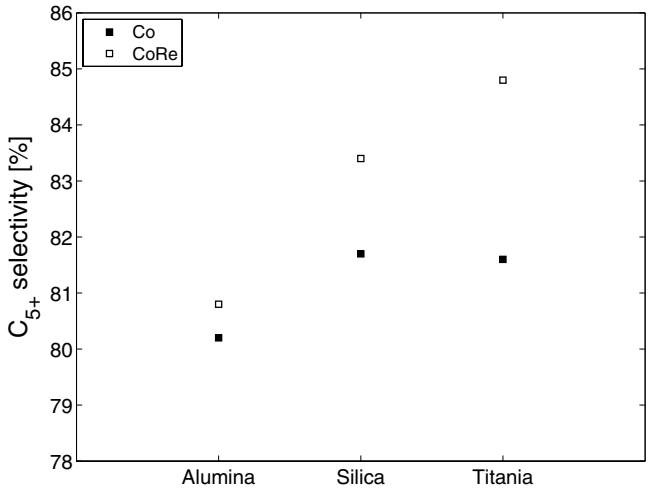

Figure 4.38: C_{5+} selectivity for un-promoted and promoted cobalt supported on γ-Al_2O_3, SiO_2, TiO_2 at 483 K, 20 bar, H_2/CO = 2.1, and 40-45% CO conversion [24]. The catalysts contained 12 wt% Co and 0 or 0.5 wt% Re.

particles located in wide pores show significantly higher selectivity than catalysts that have small particles in narrow pores. As shown in Figure 4.38, the selectivity increased in the order γ-Al_2O_3 < SiO_2 < TiO_2 [24]. Introduction of Re increased the C_{5+} selectivity, but more weakly for cobalt supported on γ-Al_2O_3 than for the SiO_2 and TiO_2 based catalysts.

Interestingly, equally large variations in C_{5+} selectivity as observed in Figure 4.38 was found for a large series of γ-Al_2O_3 based catalysts (Section 4.4). The only difference between the alumina supports was the pore characteristics. Thus, we believe that the effect of chemical identity is much weaker than the effect of pore and particle size. This is supported by catalytic measurements at moderate water concentrations. For wide-pore catalysts (wide-pore γ-Al_2O_3, SiO_2, TiO_2), the activity increases when moderate amounts of water are introduced. In contrast, for narrow-pore catalysts (narrow-pore γ-Al_2O_3), the activity decreases.

Chapter 5

Conclusions

The main scientific objective of this work was to investigate the role of support on the Fischer-Tropsch synthesis performance. This is not a trivial task, not only from a scientific point of view, but also from an experimental point of view. Preparation of metal oxide supported cobalt catalysts involves several steps and the conditions in each step have a significant impact on the properties of the final catalyst. Thus, in order to obtain reliable data, strict control of preparation variables and reaction conditions are necessary. A great effort was done to overcome all possible pitfalls.

For a large series of promoted γ-Al_2O_3 based cobalt catalysts, the pore characteristics of the starting alumina were the only variables. Large variations in catalytic behaviour were observed for these catalysts. The starting γ-Al_2O_3 was important both for the activity and selectivity. The pore characteristics controlled the cobalt particle size distribution, which in turn had a great impact both on the activity and product distribution. Furthermore, the catalysts also behaved differently in water-rich environments. In fact, variations normally attributed to the chemical identity of the support were also found for the series of γ-Al_2O_3 based catalysts. To conclude, the pore characteristics of the starting support, and not the chemical identity, has the most dominant impact on the properties of the final Fisher-Tropsch catalyst. However, the level of impurities is also important for the catalytic performance.

Although this thesis provides a great deal of information, it leaves several open questions. For instance, it is difficult to conclude whether the pore size or cobalt particle size controls the product distribution. The problem originates

from the choice of preparation variables. By using incipient wetness impregnation and an aqueous solution of cobalt nitrate hexahydrate, it is difficult or impossible to prepare catalysts with different cobalt particle sizes on supports with constant properties and loadings. Thus, a key goal of further work is to synthesise cobalt catalysts with controlled particle size on γ-Al_2O_3. However, it is vital to produce these catalysts from the same cobalt and rhenium precursors and keep the cobalt loading constant.

An improved description of the pore system in γ-Al_2O_3 is necessary. The pores in γ-Al_2O_3 are far from ideal. The Barrett-Joyner-Halenda model is based on the modified Kelvin equation and the accuracy of the calculated pore size distribution depends on the applicability and the deficiencies of the Kelvin equation. More modern approaches such as Non-Local Density Functional Theory (NLDFT) should be investigated.

It would be very useful to develop a kinetic model for the Fischer-Tropsch synthesis. A model has recently been developed [16] for formation of C_1 and C_2 hydrocarbons, but this should be extended. A kinetic model could in favourable cases give information about the Fischer-Tropsch synthesis mechanism and the effect of parameters such as promoters, particle sizes, and pore diameters on the catalytic performance.

Bibliography

[1] British Petroleum. Statistical Review of World Energy 2006. *BP.com*, 18 March 2007.

[2] Hydrocarbon Publishing Company. Worldwide Refinery Processing Review Third Quarter 2005, 2005.

[3] InflationData.com. Historical Crude Oil Prices. *InflationData.com*, 18 March 2007.

[4] P. Sabatier and J. B. Senderens. New synthesis of methane. *Compt. Rend. Acad. Sci.*, 134:514–516, 1902.

[5] F. Fischer and H. Tropsch. The preparation of synthetic oil mixtures (synthol) from carbon monoxide and hydrogen. *Brennstoff-Chem.*, 4:276–285, 1923.

[6] F. Fischer and H. Tropsch. The synthesis of petroleum at atmospheric pressure from gasification products of coal. *Brennstoff-Chem.*, 7:97–104, 1926.

[7] R. B. Anderson. *The Fischer-Tropsch synthesis.* Academic Press, Inc., Orlando, 1984.

[8] P. K. Bakkerud. Update on synthesis gas production for GTL. *Catal. Today*, 106:30–33, 2005.

[9] G. P. van der Laan and A. A. C. M. Beenackers. Kinetics and Selectivity of the Fischer-Tropsch Synthesis: A Literature Review. *Catal. Rev. - Sci. Eng.*, 41:255–318, 1999.

[10] J. A. Moulijn, M. Makkee, and A. van Diepen. *Chemical Process Technology.* John Wiley & Sons, Ltd., Chichester, 2001.

[11] A. A. Adesina. Hydrocarbon synthesis via Fischer-Tropsch reaction: travails and triumphs. *Appl. Catal. A*, 138:345–367, 1996.

[12] H. H. Storch, N. Golumbic, and R. B. Anderson. *The Fischer-Tropsch and Related Syntheses.* John Wiley & Sons, Inc., New York, 1951.

[13] H. Pichler and H. Schulz. Recent results in the synthesis of hydrocarbons from carbon monoxide and hydrogen. *Chem. Ing. Tech.*, 42:1162–1174, 1970.

[14] J. T. Kummer, H. H. Podgurski, W. B. Spencer, and P. H. Emmett. Mechanism Studies of the Fischer-Tropsch Synthesis. The Addition of Radioactive Alcohol. *J. Am. Chem. Soc.*, 73:564–569, 1951.

[15] J. T. Kummer and P. H. Emmett. Fischer-Tropsch Synthesis Mechanism Studies. The Addition of Radioactive Alcohols to the Synthesis Gas. *J. Am. Chem. Soc.*, 75:5177–5183, 1953.

[16] S. Storsæter, D. Chen, and A. Holmen. Microkinetic modelling of the formation of C_1 and C_2 products in the Fischer-Tropsch synthesis over cobalt catalysts. *Surf. Sci.*, 600:2051–2063, 2006.

[17] M. E. Dry. High quality diesel via the Fischer-Tropsch process - a review. *J. Chem. Technol. Biotechnol.*, 77:43–50, 2001.

[18] D. G. Castner, P. R. Watson, and I. Y. Chan. X-ray Absorption Spectroscopy, X-ray Photoelectron Spectroscopy, and Analytical Electron Microscopy Studies of Cobalt Catalysts. 1. Characterization of Calcined Catalysts. *J. Phys. Chem.*, 93:3188–3194, 1989.

[19] A. M. Saib, M. Claeys, and E. van Steen. Silica supported cobalt Fischer-Tropsch catalysts: effect of pore diameter of support. *Catal. Today*, 71:395–402, 2002.

[20] A. Y. Khodakov, R. Bechara, and A. Griboval-Constant. Structure and catalytic performance of cobalt Fischer Tropsch catalysts supported by periodic mesoporous silicas. *Stud. Surf. Sci. Catal.*, 142:1133–1140, 2002.

[21] A. Y. Khodakov, A. Griboval-Constant, R. Bechara, and F. Villain. Pore-Size Control of Cobalt Dispersion and Reducibility in Mesoporous Silicas. *J. Phys. Chem. B*, 105:9805–9811, 2001.

[22] A. Y. Khodakov, A. Griboval-Constant, R. Bechara, and V. L. Zholobenko. Pore Size Effects in Fischer Tropsch Synthesis over Cobalt-Supported Mesoporous Silicas. *J. Catal.*, 206:230–241, 2002.

[23] A. Y. Khodakov, R. Bechara, and A. Griboval-Constant. Fischer-Tropsch synthesis over silica supported cobalt catalysts: mesoporous structure versus cobalt surface density. *Appl. Catal. A*, 254:273–288, 2003.

[24] S. Storsæter, Ø. Borg, E. A. Blekkan, and A. Holmen. Study of the effect of water on Fischer-Tropsch synthesis over supported cobalt catalysts. *J. Catal.*, 231:405–419, 2005.

[25] H. Xiong, Y. Zhang, S. Wang, and J. Li. Fischer-Tropsch synthesis: the effect of Al_2O_3 porosity on the performance of Co/Al_2O_3 catalyst. *Catal. Commun.*, 6:512–516, 2005.

[26] D. Song and J. Li. Effect of catalyst pore size on the catalytic performance of silica supported cobalt Fischer-Tropsch catalysts. *J. Mol. Catal. A*, 247:206–212, 2006.

[27] H. Li, J. Li, H. Ni, and D. Song. Studies on cobalt catalyst supported on silica with different pore size for Fischer-Tropsch synthesis. *Catal. Lett.*, 110:71–76, 2006.

[28] A. K. Dalai, T. K. Das, K. V. Chaudhari, and G. Jacobs amd B. H. Davis. Fischer-Tropsch synthesis: Water effects on Co supported on narrow and wide-pore silica. *Appl. Catal. A*, 289:135–142, 2005.

[29] C. M. Lok. Novel highly dispersed cobalt catalysts for improved Fischer-Tropsch productivity. *Stud. Surf. Sci. Catal.*, 147:283–288, 2004.

[30] D. Reinalda and J. Kars. Process for the preparation of a catalyst or catalyst precursor suitable for the preparation of hydrocarbons from carbon monoxide and hydrogen, and said catalyst. European Patent Application 0 421 502 A2, 1991.

[31] J. van de Loosdrecht, S. Barradas, E. A. Caricato, N. G. Ngwenya, P. S. Nkwanyana, M. A. S. Rawat, B. H. Sigwebela, P. J. van Berge, and J. L. Visagie. Calcination of Co-based Fischer-Tropsch synthesis catalysts. *Top. Catal.*, 26:121–127, 2003.

[32] A. Feller, M. Claeys, and E. van Steen. Cobalt Cluster Effects in Zirconium Promoted Co/SiO_2 Fischer-Tropsch Catalysts. *J. Catal.*, 185:120–130, 1999.

[33] S. Storsæter, B. Tøtdal, J. C. Walmsley, B. S. Tanem, and A. Holmen. Characterization of alumina-, silica-, and titania-supported cobalt Fischer-Tropsch catalysts. *J. Catal.*, 236:139–152, 2005.

[34] S. Storsæter, Ø. Borg, E. A. Blekkan, B. Tøtdal, and A. Holmen. Fischer-Tropsch synthesis over Re-promoted Co supported on Al_2O_3, SiO_2 and TiO_2: Effect of water. *Catal. Today*, 100:343–347, 2005.

[35] G. Jacobs, T. K. Das, Y. Zhang, J. Li, G. Racoillet, and B. H. Davis. Fischer-Tropsch synthesis: support, loading, and promoter effects on the reducibility of cobalt catalysts. *Appl. Catal. A*, 233:263–281, 2002.

[36] A. Y. Khodakov, J. Lynch, D. Bazin, B. Rebours, N. Zanier, B. Moisson, and P. Chaumette. Reducibility of Cobalt Species in Silica-Supported Fischer-Tropsch Catalysts. *J. Catal.*, 168:16–25, 1997.

[37] D. G. Castner, P. R. Watson, and I. Y. Chan. X-ray Absorption Spectroscopy, X-ray Photoelectron Spectroscopy, and Analytical Electron Microscopy Studies of Cobalt Catalysts. 2. Hydrogen Reduction Properties. *J. Phys. Chem.*, 94:819–828, 1990.

[38] J. Zhang, J. Chen, J. Ren, and Y. Sun. Chemical treatment of γ-Al_2O_3 and its influence on the properties of Co-based catalysts for Fischer-Tropsch synthesis. *Appl. Catal. A*, 243:121–133, 2003.

[39] E. Iglesia, S. L. Soled, and R. A. Fiato. Fischer-Tropsch Synthesis on Cobalt and Ruthenium. Metal Dispersion and Support Effects on Reaction Rate and Selectivity. *J. Catal.*, 137:212–224, 1992.

[40] E. Iglesia. Design, synthesis, and use of cobalt-based Fischer-Tropsch synthesis catalysts. *Appl. Catal. A*, 161:59–78, 1997.

[41] E. Iglesia. Fischer-Tropsch Synthesis on Cobalt Catalysts: Structural Requirements and Reaction Pathways. *Stud. Surf. Sci. Catal.*, 107:153–162, 1997.

[42] G. L. Bezemer, J. H. Bitter, H. P. C. E. Kuipers, H. Oosterbeek, J. E. Holewijn, X. Xu, F. Kapteijn, A. J. van Dillen, and K. P. de Jong. Cobalt Particle Size Effects in the Fischer-Tropsch Reaction Studied with Carbon Nanofiber Supported Catalysts. *J. Am. Chem. Soc.*, 128:3956–3964, 2006.

[43] R. B. Anderson. *Catalysis*, volume IV, chapter Catalysts for the Fischer-Tropsch Synthesis, pages 29–255. Van Nostrand-Reinhold, New York, 1956.

[44] E. Iglesia, S. C. Reyes, R. J. Madon, and S. L. Soled. Selectivity Control and Catalyst Design in the Fischer-Tropsch Synthesis: Sites, Pellets, and Reactors. *Adv. Catal.*, 39:221–302, 1993.

[45] E. Iglesia, S. L. Soled, R. A. Fiato, and G. H. Via. Dispersion, support, and bimetallic effects in Fischer-Tropsch synthesis on cobalt catalysts. *Stud. Surf. Sci. Catal.*, 81:433–442, 1994.

[46] B. Shi and B. H. Davis. Fischer-Tropsch synthesis: The paraffin to olefin ratio as a function of carbon number. *Catal. Today*, 106:129–131, 2005.

[47] E. van Steen, G. S. Sewell, R. A. Makhothe, C. Micklethwaite, H. Manstein, M. de Lange, and C. T. O'Connor. TPR Study on the Preparation of Impregnated Co/SiO_2 Catalysts. *J. Catal.*, 162:220–229, 1996.

[48] W.-J. Wang and Y.-W. Chen. Influence of metal loading on the reducibility and hydrogenation activity of cobalt/alumina catalysts. *Appl. Catal.*, 77:223–233, 1991.

[49] M. E. Dry. The Fischer-Tropsch process: 1950-2000. *Catal. Today*, 71:227–241, 2002.

[50] D. Schanke, S. Eri, E. Rytter, C. Aaserud, A.-M. Hilmen, O. A. Lindvåg, E. Bergene, and A. Holmen. Fischer-Tropsch synthesis on cobalt catalysts supported on different aluminas. *Stud. Surf. Sci. Catal.*, 147:301–306, 2004.

[51] C. J. Bertole, C. A. Mims, and G. Kiss. Support and rhenium effects on the intrinsic site activity and methane selectivity of cobalt Fischer-Tropsch catalysts. *J. Catal.*, 221:191–203, 2004.

[52] J. Zhang, J. Chen, J. Ren, Y. Li, and Y. Sun. Support effect of Co/Al_2O_3 catalysts for Fischer-Tropsch synthesis. *Fuel*, 82:581–586, 2003.

[53] C. J. Bertole, G. Kiss, and C. A. Mims. The effect of surface-active carbon on hydrocarbon selectivity in the cobalt-catalyzed Fischer-Tropsch synthesis. *J. Catal.*, 223:309–318, 2004.

[54] F. Morales and B. M. Weckhuysen. Promotion effects in Co-based Fischer-Tropsch Catalysis. *Catal.*, 19:1–40, 2006.

[55] C. H. Mauldin. Cobalt catalysts for the conversion of methanol to hydrocarbons and for Fischer-Tropsch synthesis. United States Patent 4,568,663, 1986.

[56] C. H. Mauldin and D. E. Varnado. Rhenium as a promoter of titania-supported cobalt Fischer-Tropsch catalysts. *Stud. Surf. Sci. Catal.*, 136:417–422, 2001.

[57] G. Jacobs, J. A. Chaney, P. M. Patterson, T. K. Das, and B. H. Davis. Fischer-Tropsch synthesis: study of the promotion of Re on the reduction property of Co/Al_2O_3 catalysts by in situ EXAFS/XANES of Co K and Re L_{III} edges and XPS. *Appl. Catal. A*, 264:203–212, 2004.

[58] G. L. Haller and D. E. Resasco. Metal-Support Interaction: Group VIII Metals and Reducible Oxides. *Adv. Catal.*, 36:173–235, 1989.

[59] T. K. Das, G. Jacobs, P. M. Patterson, W. A. Conner, J. Li, and B. H. Davis. Fischer-Tropsch synthesis: characterization and catalytic properties of rhenium promoted cobalt alumina catalysts. *Fuel*, 82:805–815, 2003.

[60] J. K. Minderhoud, M. F. M. Post, S. T. Sie, and E. J. R. Sudholter. Process for the preparation of hydrocarbons from a mixture of CO and H_2. United States Patent 4,628,133, 1986.

[61] J. K. Minderhoud, M. F. M. Post, S. T. Sie, and E. J. R. Sudhölter. Process for the preparation of hydrocarbons. European Patent Application 0 142 888 A2, 1985.

[62] D. Schanke, A. M. Hilmen, E. Bergene, K. Kinnari, E. Rytter, E. Ådnanes, and A. Holmen. Study of the deactivation mechanism of Al_2O_3-supported cobalt Fischer-Tropsch catalysts. *Catal. Lett.*, 34:269–284, 1995.

[63] D. Schanke, A. M. Hilmen, E. Bergene, K. Kinnari, E. Rytter, E. Ådnanes, and A. Holmen. Reoxidation and Deactivation of Supported Cobalt Fischer-Tropsch Catalysts. *Energy Fuels*, 10:867–872, 1996.

[64] A. M. Hilmen, D. Schanke, and A. Holmen. Reoxidation of supported cobalt Fischer-Tropsch catalysts. *Stud. Surf. Sci. Catal.*, 107:237–242, 1997.

[65] A. M. Hilmen, D. Schanke, K. F. Hanssen, and A. Holmen. Study of the effect of water on alumina supported cobalt Fischer-Tropsch catalysts. *Appl. Catal. A*, 186:169–188, 1999.

[66] A.-M. Hilmen, O. A. Lindvåg, E. Bergene, D. Schanke, S. Eri, and A. Holmen. Selectivity and activity changes upon water addition during Fischer-Tropsch synthesis. *Stud. Surf. Sci. Catal.*, 136:295–300, 2001.

[67] G. Jacobs, P. M. Patterson, Y. Zhang, T. Das, J. Li, and B. H. Davis. Fischer-Tropsch synthesis: deactivation of noble metal-promoted Co/Al_2O_3 catalysts. *Appl. Catal. A*, 233:215–226, 2002.

[68] G. Jacobs, P. M. Patterson, T. K. Das, M. Luo, and B. H. Davis. Fischer-Tropsch synthesis: effect of water on Co/Al_2O_3 catalysts and XAFS characterization of reoxidation phenomena. *Appl. Catal. A*, 270:65–76, 2004.

[69] P. J. van Berge, J. van de Loosdrecht, S. Barradas, and A. M. van der Kraan. Oxidation of cobalt based Fischer-Tropsch catalysts as a deactivation mechanism. *Catal. Today*, 58:321–334, 2000.

[70] J. Li, X. Zhan, Y. Zhang, G. Jacobs, T. Das, and B. H. Davis. Fischer-Tropsch synthesis: effect of water on the deactivation of Pt promoted Co/Al_2O_3 catalysts. *Appl. Catal. A*, 228:203–212, 2002.

[71] G. Jacobs, T. K. Das, P. M. Patterson, J. Li, L. Sanchez, and B. H. Davis. Fischer-Tropsch synthesis XAFS XAFS studies of the effect of water on a Pt-promoted Co/Al_2O_3 catalyst. *Appl. Catal. A*, 247:335–343, 2003.

[72] G. W. Huber, C. G. Guymon, T. L. Conrad, B. C. Stephenson, and C. H. Bartholomew. Hydrothermal Stability of Co/SiO_2 Fischer-Tropsch Synthesis Catalysts. *Stud. Surf. Sci. Catal.*, 139:423–430, 2001.

[73] J.-G. Chen, X.-Z. Wang, H.-W. Xiang, and Y.-H. Sun. Study on stability of $Co/ZrO_2/SiO_2$ catalyst for F-T synthesis. *Stud. Surf. Sci. Catal.*, 136:525–529, 2001.

[74] J. Li, G. Jacobs, T. Das, and B. H. Davis. Fischer-Tropsch synthesis: effect of water on the catalytic properties of a ruthenium promoted Co/TiO_2 catalyst. *Appl. Catal. A*, 233:255–262, 2002.

[75] G. Kiss, C. E. Kliewer, G. J. DeMartin, C. C. Culross, and J. E. Baumgartner. Hydrothermal deactivation of silica-supported cobalt catalysts in Fischer-Tropsch synthesis. *J. Catal.*, 217:127–140, 2003.

[76] T. K. Das, W. A. Conner, J. Li, G. Jacobs, M. E. Dry, and B. H. Davis. Fischer-Tropsch Synthesis: Kinetics and Effect of Water for a Co/SiO_2 Catalyst. *Energy Fuels*, 19:1430–1439, 2005.

[77] H. Schulz, E. van Steen, and M. Claeys. Selectivity and mechanism of Fischer-Tropsch synthesis with iron and cobalt catalysts. *Stud. Surf. Sci. Catal.*, 81:455–460, 1994.

[78] S. Krishnamoorthy, M. Tu, M. P. Ojeda, D. Pinna, and E. Iglesia. An Investigation of the Effects of Water on Rate and Selectivity for the Fischer-Tropsch Synthesis on Cobalt-Based Catalysts. *J. Catal.*, 211:422–433, 2002.

[79] C. J. Bertole, C. A. Mims, and G. Kiss. The Effect of Water on the Cobalt-Catalyzed Fischer-Tropsch Synthesis. *J. Catal.*, 210:84–96, 2002.

[80] J. Li, G. Jacobs, T. Das, Y. Zhang, and B. Davis. Fischer-Tropsch synthesis: effect of water on the catalytic properties of a Co/SiO_2 catalyst. *Appl. Catal. A*, 236:67–76, 2002.

[81] S. Eri, K. J. Kinnari, D. Schanke, and A.-M. Hilmen. Fischer-Tropsch catalyst with low surface area alumina, its preparation and use thereof. International Publication Number WO 02/47816 A1, 2002.

[82] C. J. Kim. Process for hydrocarbon synthesis catalyzed by cobalt on titania, enhanced by water addition. European Patent Specification 0 339 923 B1, 1994.

[83] C. J. Kim. Process for catalytic hydrocarbon synthesis from CO and H_2 over metallic cobalt. European Patent Application 0 355 218 A1, 1990.

[84] C. J. Kim. Water addition for increased CO/H_2 hydrocarbon synthesis activity over catalysts comprising cobalt, ruthenium and mixtures thereof which may include a promoter metal. United States Patent 5,227,407, 1993.

[85] H. Schulz, M. Claeys, and S. Harms. Effect of water partial pressure on steady state Fischer-Tropsch activity and selectivity of a promoted cobalt catalyst. *Stud. Surf. Sci. Catal.*, 107:193–200, 1997.

[86] E. van Steen and H. Schulz. Polymerisation kinetics of the Fischer-Tropsch CO hydrogenation using iron and cobalt based catalysts. *Appl. Catal. A*, 186:309–320, 1999.

[87] E. van Steen, M. Claeys, M. E. Dry, J. van de Loosdrecht, E. L. Viljoen, and J. L. Visagie. Stability of Nanocrystals: Thermodynamic Analysis of Oxidation and Re-reduction of Cobalt in Water/Hydrogen Mixtures. *J. Phys. Chem. B*, 109:3575–3577, 2005.

[88] A. M. Saib, A. Borgna, J. van de Loosdrecht, P. J. van Berge, and J. W. Niemantsverdriet. XANES study of the susceptibility of nano-sized cobalt crystallites to oxidation during realistic Fischer-Tropsch synthesis. *Appl. Catal. A*, 312:12–19, 2006.

[89] Bruker AXS Inc. DIFFRAC^{plus} EVA Release 2001 Version 7.0 rev.0, 2001.

[90] J. L. Lemaitre, P. Govind Menon, and F. Delannay. *Characterization of Heterogeneous Catalysts*, chapter The Measurement of Catalyst Dispersion, pages 299–365. Marcel Dekker, Inc., New York, 1984.

[91] E. A. Blekkan, A. Holmen, and S. Vada. Alkali Promotion of Alumina-Supported Cobalt Fischer-Tropsch Catalysts Studied by TPR, TPD and Pulse Chemisorption. *Acta Chem. Scand.*, 47:275–280, 1993.

[92] C. H. Bartholomew and R. J. Farrauto. Chemistry of Nickel-Alumina Catalysts. *J. Catal.*, 45:41–53, 1976.

[93] R. D. Jones and C. H. Bartholomew. Improved Flow Technique for Measurement of Hydrogen Chemisorption on Metal Catalysts. *Appl. Catal.*, 39:77–88, 1988.

[94] E. P. Barrett, L. G. Joyner, and P. P. Halenda. The Determination of Pore Volume and Area Distributions in Porous Substances. I. Computations from Nitrogen Isotherms. *J. Am. Chem. Soc.*, 73:373–380, 1951.

[95] S. Lowell, J. E. Shields, M. A. Thomas, and M. Thommes. *Characterization of Porous Solids and Powders: Surface Area, Pore Size and Density.* Kluwer Academic Publishers, Dordrecht, 2004.

[96] F. W. Lytle, R. B. Greegor, E. C. Marques, D. R. Sandstrom, G. H. Via, and J. H. Sinfelt. Structural Genesis of Pt on SiO_2: Determination by X-ray Absorption Spectroscopy. *J. Catal.*, 95:546–557, 1985.

[97] T. Ressler. WinXAS: a Program for X-ray Absorption Spectroscopy Data Analysis under MS-Windows. *J. Synchrotron Rad.*, 5:118–122, 1998.

[98] T. Ressler, J. Wong, J. Roos, and I. L. Smith. Quantitative Speciation of Mn-Bearing Particulates Emitted from Autos Burning (Methylcyclopentadienyl)manganese Tricarbonyl-Added Gasolines Using XANES Spectroscopy. *Environ. Sci. Technol.*, 34:950–958, 2000.

[99] N. Binsted. EXCURV98: CCLRC Daresbury Laboratory computer program, 1998.

[100] S. J. Gurman, N. Binsted, and I. Ross. A rapid, exact curved-wave theory for EXAFS calculations. *J. Phys. C.*, 17:143–151, 1984.

[101] P. Scherrer. Bestimmung der Grösse und der inneren Struktur von Kolloidteilchen mittels Röntgenstrahlen. *Göttingen Nachrichten*, 2:98–100, 1918.

[102] A. Lapidus, A. Krylova, V. Kazanskii, V. Borovkov, A. Zaitsev, J. Rathousky, A. Zukal, and M. Jančálková. Hydrocarbon synthesis from carbon monoxide and hydrogen on impregnated cobalt catalysts. Part I. Physico-chemical properties of 10% cobalt/alumina and 10% cobalt/silica. *Appl. Catal.*, 73:65–82, 1991.

[103] E. Rytter, D. Schanke, S. Eri, H. Wigum, T. H. Skagseth, and N. Sincadu. Some QA and Optimization Issues During Development of Statoil FT Catalyst. *Prepr. - Am. Chem. Soc., Div. Pet. Chem.*, 50:198–199.

[104] Ø. Borg, S. Eri, E. A. Blekkan, S. Storsæter, H. Wigum, E. Rytter, and A. Holmen. Fischer-Tropsch synthesis over γ-alumina supported cobalt catalysts: Effect of support variables. *J. Catal., doi:10.1016/j.jcat.2007.03.008*, 2007.

[105] E. Rytter and S. Eri. Cobalt and rhenium containing Fischer-Tropsch catalyst. International Publication Number WO 2006/010936 A1, 2006.

[106] A. M. Hilmen, D. Schanke, and A. Holmen. TPR study of the mechanism of rhenium promotion of alumina-supported cobalt Fischer-Tropsch catalysts. *Catal. Lett.*, 38:143–147, 1996.

Appendix A

Additional papers and presentations

Further publications in which the author has played a significant role are given below. The work was done during the work with this thesis.

Papers

- ***Ø. Borg***, Z. Yu, D. Chen, E. Rytter, V. Frøseth, H. Wigum, and A. Holmen. Fischer-Tropsch synthesis over carbon nanofiber supported cobalt catalysts. In preparation.
- ***Ø. Borg***, Z. Yu, D. Chen, E. A. Blekkan, E. Rytter, and A. Holmen. The effect of water on the activity and selectivity for carbon nanofiber supported cobalt Fischer-Tropsch catalysts. In preparation.
- V. Frøseth, S. Storsæter, ***Ø. Borg***, E. A. Blekkan, M. Rønning, and A. Holmen. Steady-State Isotopic Transient Kinetic Analysis (SSITKA) of CO Hydrogenation on different Co catalysts. *Appl. Catal. A*, 289:10-15, 2005.
- S. Storsæter, ***Ø. Borg***, E. A. Blekkan, and A. Holmen. Study of the effect of water on Fischer-Tropsch synthesis over supported cobalt catalysts. *J. Catal.*, 231:405-419, 2005.
- S. Storsæter, ***Ø. Borg***, E. A. Blekkan, B. Tøtdal, and A. Holmen. Fischer-Tropsch synthesis over Re-promoted Co supported on Al_2O_3, SiO_2 and TiO_2: Effect of water. *Catal. Today*, 100:343-347, 2005.

- D. Tristantini, S. Lögdberg, B. Gevert, ***Ø. Borg***, and A. Holmen. Direct use of H_2-poor bio-syngas model in Fischer-Tropsch synthesis over unpromoted and rhenium promoted alumina-supported cobalt catalysts. *Prepr. Symp. - Am. Chem. Soc., Div. Fuel Chem.*, 51:68-72, 2006.

- Z. Yu, ***Ø. Borg***, D. Chen, B. C. Enger, V. Frøseth, E. Rytter, H. Wigum, and A. Holmen. Carbon nanofiber supported cobalt catalysts for Fischer-Tropsch synthesis with high activity and selectivity. *Catal. Lett.*, 109:43-47, 2006.

- Z. Yu, ***Ø. Borg***, D. Chen, E. Rytter, and A. Holmen. Role of surface oxygen in the preparation and deactivation of carbon nanofiber supported cobalt Fischer-Tropsch catalysts. *Top. Catal.*, DOI: 10.1007/s11244-007-0242-7, 2007.

- D. Tristantini, S. Lögdberg, B. Gevert, ***Ø. Borg***, and A. Holmen. The effect of synthesis gas composition on the Fischer-Tropsch synthesis over Co/γ-Al_2O_3 and CoRe/γ-Al_2O_3 catalysts. Accepted *Fuel. Process. Technol.*

- D. Tristantini, S. Lögdberg, ***Ø. Borg***, B. Gevert, E. A. Blekkan, and A. Holmen. Hydrocarbon production via Fischer-Tropsch synthesis from H_2-poor syngas over different Fe-Co/γ-Al_2O_3 bimetallic catalysts. Submitted.

- B. C. Enger, V. Frøseth, ***Ø. Borg***, and A. Holmen. Cobalt catalysts on modified low surface area alumina in the Fischer-Tropsch synthesis. In preparation.

- J. Xiong, ***Ø. Borg***, E. A. Blekkan, D. Chen, and A. Holmen. Hydrogen chemisorption of rhenium-promoted γ-alumina supported cobalt catalysts. In preparation.

Presentations

- ***Ø. Borg***, Z. Yu, D. Chen, E. Rytter, and A. Holmen. The effect of water on the activity and selectivity for carbon nanofiber supported cobalt catalysts. Poster presentation, 8th Natural Gas Conversion Symposium, Natal, Brazil, 27 - 31 May 2007.

- ***V. Frøseth***, S. Storsæter, Ø. Borg, M. Rønning, E. A. Blekkan, and A. Holmen. Steady State Isotopic Transient Kinetic Analysis (SSITKA)

of CO Hydrogenation on different Co catalysts. Poster presentation, ISOTOPCAT, Poitiers, France, 7 - 9 July 2004.

- ***S. Lögdberg***, Ø. Borg, M. Boutonnet, S. Järås, and A. Holmen. Preparation of cobalt-based Fischer-Tropsch catalysts by the microemulsion technique. Poster presentation, 2nd World Conference and Technological Exhibition on Biomass for Energy, Industry and Climate Protection, Rome, Italy, 10 - 14 May 2004.

- ***S. Lögdberg***, Ø. Borg, M. Boutonnet, S. Järås, and A. Holmen. Preparation of cobalt-based Fischer-Tropsch catalysts by the microemulsion technique. Poster presentation, 11th Nordic Symposium on Catalysis, Oulu, Finland, 23 - 25 May 2004.

- ***S. Lögdberg***, Ø. Borg, V. Frøseth, E. A. Blekkan, M. Boutonnet, S. Järås, and A. Holmen. Cobalt particle size effects in α- and γ-Al_2O_3 supported catalysts for Fischer-Tropsch synthesis. Oral presentation, Gas-Fuel 05, Brugge, Belgium, 14 - 16 November 2005.

- ***S. Lögdberg***, Ø. Borg, M. Boutonnet, A. Holmen, and S. Järås. Study of cobalt particle size effects on selectivity in the Fischer-Tropsch synthesis. Oral presentation, 12th Nordic Symposium on Catalysis, Trondheim, Norway, 28 - 30 May 2006.

- ***M. Rønning***, Ø. Borg, S. Storsæter, W. van Beek, E. A. Blekkan, and A. Holmen. Identification of cobalt species in the temperature programmed reduction of Fischer-Tropsch catalysts using *in situ* X-ray absorption spectroscopy. Oral presentation, 3rd Norwegian User Meeting - Application of Synchrotron Radiation, Orkanger, Norway, 10 - 11 March 2005.

- ***S. Storsæter***, Ø. Borg, E. A. Blekkan, and A. Holmen. Effect of water on Co-Supported Fischer-Tropsch Catalysts. Oral presentation, Norwegian Catalysis Symposium, Bergen, Norway, 20 - 21 November 2003.

- ***S. Storsæter***, Ø. Borg, and A. Holmen. The effect of water on the Fischer-Tropsch synthesis on supported cobalt catalysts. Poster presentation, EuropaCat-VI, Innsbruck, Austria, 31 August - 4 September 2003.

- ***S. Storsæter***, Ø. Borg, E. A. Blekkan, and A. Holmen. Effect of water on cobalt supported Fischer-Tropsch catalysts. Poster presentation, 11th Nordic Symposium on Catalysis, Oulu, Finland, 23 - 25 May 2004.

- ***S. Storsæter***, Ø. Borg, E. A. Blekkan, and A. Holmen. Effect of water on Co-supported Fischer-Tropsch catalysts. Poster presentation, 13th International Congress on Catalysis, Paris, France, 11 - 16 July 2004.
- S. Storsæter, ***Ø. Borg***, E. A. Blekkan, and A. Holmen. Effect of water on cobalt supported Fischer-Tropsch catalysts. Poster presentation, 3rd School on Catalysis, Ustroń, Poland, 21 - 26 September 2004.
- ***D. Tristantini***, S. Lögdberg, B. Gevert, Ø. Borg, and A. Holmen. A study of hydrocarbon production via Fischer-Tropsch (FT) synthesis from different model bio-syngases over un-promoted and rhenium-promoted alumina supported cobalt catalyst. Poster presentation, SYNBIOS: Second-Generation Automotive Biofuels, Stockholm, Sweden, 18 - 20 May 2005.
- ***D. Tristantini***, S. Lögdberg, B. Gevert, Ø. Borg, and A. Holmen. Effect of water addition on hydrocarbon production via Fischer-Tropsch synthesis from different model bio-syngases over unpromoted and rhenium-promoted alumina-supported cobalt catalysts. Poster presentation, Europacat-VII, Sofia, Bulgaria, 28 August - 1 September 2005.
- ***D. Tristantini***, S. Lögdberg, B. Gevert, Ø. Borg, and A. Holmen. Direct use of H_2-poor bio-syngas model in Fischer-Tropsch synthesis over unpromoted and rhenium promoted alumina-supported cobalt catalysts. Oral presentation, 231st ACS National Meeting, Atlanta, USA, 26 - 30 March 2006.
- ***D. Tristantini***, S. Lögdberg, Ø. Borg, B. Gevert, and A. Holmen. Hydrocarbon production via Fischer-Tropsch synthesis from CO-rich syngas over different Fe-Co/Al_2O_3 bimetallic catalysts: the effect of water. Poster presentation, 12th Nordic Symposium on Catalysis, Trondheim, Norway, 28 - 30 May 2006.
- ***Z. Yu***, Ø. Borg, V. Frøseth, B. C. Enger, D. Chen, A. Holmen, E. Rytter, K. Moljord, and H. Wigum. Carbon nanofiber supported cobalt catalysts for Fischer-Tropsch synthesis with high activity and selectivity. Oral presentation, 2nd NTNU SEMINAR Synthesis and Applications of Carbon Nanofibers/Nanotubes, Trondheim, Norway, 21 September 2005.
- ***Z. Yu***, Ø. Borg, D. Chen, E. Rytter, and A. Holmen. Role of surface oxygen in the preparation and deactivation of carbon nanofiber supported Fischer-Tropsch cobalt catalysts. Oral presentation, 12th Nordic Symposium on Catalysis, Trondheim, Norway, 28 - 30 May 2006.

- ***Z. Yu***, Ø. Borg, D. Chen, E. Rytter, and A. Holmen. Co/CNF as Fischer-Trospch synthesis catalysts. Oral presentation, 3rd NTNU SEMINAR Synthesis and Applications of Carbon Nanofibers/Nanotubes, Trondheim, Norway, 14 February 2007.

Paper A

Effect of calcination atmosphere and temperature on γ-Al_2O_3 supported cobalt Fischer-Tropsch catalysts

Øyvind Borg[a], Edd Anders Blekkan[a], Sigrid Eri[b], Duncan Akporiaye[c], Bente Vigerust[c], Erling Rytter[a,b], Anders Holmen[a]

[a]: Department of Chemical Engineering,
Norwegian University of Science and Technology,
NO-7491 Trondheim, Norway

[b]: Statoil R&D, Research Centre, Postuttak,
NO-7005 Trondheim, Norway

[c]: SINTEF Materials and Chemistry, Postboks 124, Blindern,
NO-0314 Oslo, Norway

This paper has been accepted for publication in *Top. Catal.*

Paper B

Electron microscopy study of γ-Al_2O_3 supported cobalt Fischer-Tropsch catalysts

Øyvind Borg[a], John Charles Walmsley[b], Roya Dehghan[c], Bjørn Steinar Tanem[b], Edd Anders Blekkan[a], Sigrid Eri[d], Erling Rytter[a,d], Anders Holmen[a]

[a]: Department of Chemical Engineering,
Norwegian University of Science and Technology,
NO-7491 Trondheim, Norway

[b]: SINTEF Materials and Chemistry,
NO-7465 Trondheim, Norway

[c]: Department of Physics,
Norwegian University of Science and Technology,
NO-7491 Trondheim, Norway

[d]: Statoil R&D, Research Centre, Postuttak,
NO-7005 Trondheim, Norway

This paper was submitted to *Catal. Lett.*

Paper C

Identification of cobalt species during temperature programmed reduction of Fischer-Tropsch catalysts

Øyvind Borg[a], Magnus Rønning[a], Sølvi Storsæter[a], Wouter van Beek[b], Anders Holmen[a]

[a]: Department of Chemical Engineering,
Norwegian University of Science and Technology,
NO-7491 Trondheim, Norway

[b]: The Swiss-Norwegian Beam Lines at ESRF, SNBL/ESRF, BP 220,
F-38043 Grenoble, Cédex, France

This paper was published in *Stud. Surf. Sci. Catal.*, 163:255-272, 2007.

Paper D

Fischer-Tropsch synthesis over γ-alumina-supported cobalt catalysts: Effect of support variables

Øyvind Borg[a], Sigrid Eri[b], Edd Anders Blekkan[a], Sølvi Storsæter[a], Hanne Wigum[b], Erling Rytter[a,b], Anders Holmen[a]

[a]: Department of Chemical Engineering,
Norwegian University of Science and Technology,
NO-7491 Trondheim, Norway

[b]: Statoil R&D, Research Centre, Postuttak,
NO-7005 Trondheim, Norway

This paper has been accepted for publication in *J. Catal.*

Paper E

Fischer-Tropsch synthesis over different alumina supported cobalt catalysts

Øyvind Borg[a], Sigrid Eri[b], Erling Rytter[b], Anders Holmen[a]

[a]: Department of Chemical Engineering,
Norwegian University of Science and Technology,
NO-7491 Trondheim, Norway

[b]: Statoil R&D, Research Centre, Postuttak,
NO-7005 Trondheim, Norway

This paper was published in *Prepr. Pap. - Am. Chem. Soc., Div. Fuel Chem.*, 51:699-701, 2006.

Paper F

Fischer-Tropsch synthesis over un-promoted and Re-promoted γ-Al_2O_3 supported cobalt catalysts with different pore sizes

Øyvind Borg[a], Nina Hammer[a], Sigrid Eri[b], Odd Asbjørn Lindvåg[c], Rune Myrstad[c], Edd Anders Blekkan[a], Magnus Rønning[a], Erling Rytter[a,b], Anders Holmen[a]

[a]: Department of Chemical Engineering,
Norwegian University of Science and Technology,
NO-7491 Trondheim, Norway

[b]: Statoil R&D, Research Centre, Postuttak,
NO-7005 Trondheim, Norway

[c]: SINTEF Materials and Chemistry,
NO-7465 Trondheim, Norway

This paper was submitted to *Appl. Catal.*

Paper G

The effect of water on the activity and selectivity for γ-alumina supported cobalt Fischer-Tropsch catalysts with different pore sizes

Øyvind Borg[a], Sølvi Storsæter[a], Sigrid Eri[b], Hanne Wigum[b], Erling Rytter[b], Anders Holmen[a]

[a]: Department of Chemical Engineering,
Norwegian University of Science and Technology,
NO-7491 Trondheim, Norway

[b]: Statoil R&D, Research Centre, Postuttak,
NO-7005 Trondheim, Norway

This paper was published in *Catal. Lett.*, 107:95-102, 2006.

Paper H

Fischer-Tropsch synthesis. Recent studies on the relation between the properties of supported cobalt catalysts and the activity and selectivity

Øyvind Borg[a], Vidar Frøseth[a], Sølvi Storsæter[a], Sigrid Eri[b], Erling Rytter[a,b], Anders Holmen[a]

[a]: Department of Chemical Engineering,
Norwegian University of Science and Technology,
NO-7491 Trondheim, Norway

[b]: Statoil R&D, Research Centre, Postuttak,
NO-7005 Trondheim, Norway

This paper has been accepted for publication in *Stud. Surf. Sci. Catal.*

Paper I

Fischer-Tropsch synthesis on cobalt catalysts: the effect of water

Edd Anders Blekkan, Øyvind Borg, Vidar Frøseth, Anders Holmen

Department of Chemical Engineering,
Norwegian University of Science and Technology,
NO-7491 Trondheim, Norway

This paper has been accepted for publication in *Catalysis, Royal Society of Chemistry*, 20, 2007.